Aerospace Report No. ATR-79(9553)-6

STUDIES IN UPPER AND LOWER ATMOSPHERE COUPLING

NASA Headquarters Contract NASW-3120
Final Report

Y. T. Chiu, C. J. Rice and L. R. Sharp
Space Sciences Laboratory
THE AEROSPACE CORPORATION
Los Angeles, California 90009

MARCH 1979

This work is supported by NASA under Contract NASW-3120.

I. INTRODUCTION

This report summarizes the theoretical and data-analytic work on upper and lower atmosphere coupling performed under NASA Headquarters contract NASW-3120 during the period April 1978 to March 1979. As such, this report is primarily devoted to an overview of various studies published and to be published under this contract. Individual study reports are collected in the last section as exhibits.

Work performed under the subject contract are in the following four areas of upper-lower atmosphere coupling:

1. Magnetosphere-ionosphere electrodynamic coupling in the aurora.
2. Troposphere-thermosphere coupling.
3. Ionosphere - neutral - atmosphere coupling.
4. Planetary wave dynamics in the middle atmosphere.

Contract work in the first three areas have been published or are being published. The fourth area is part of a long-term project and a progress report will be given here.

The primary aim of these studies is to examine the detailed dynamics of specific physical phenomena which require or exhibit coupling between components of the upper and lower atmospheres. Thus our approach is to examine physically the relationships between upper and lower atmospheric components, as a means of understanding the dynamical phenomena themselves rather than as a means of providing a "physical mechanism" for some claimed correlative relationship. Thus, for example, in the study of upper and lower atmosphere coupling in the aurora, we prefer to concentrate on the basic understanding of the electrodynamics of the auroral processes. For we believe that unless we understand the mutual influence between the ionosphere and the magneto sphere in the electrodynamics of the auroral process itself, it may be futile to speculate

on the electrodynamical interaction between the auroral currents and other terrestrial current systems. As for data analysis work, we concentrated on finding possible correlations between lower and upper atmospheric data sets which are un-reconstructed, global and are of good statistical coverage. Tropospheric weather maps, for example, do not qualify as a source of data because they are reconstructed from the measurements of a few stations or balloons and because they are usually synoptic rather than global. Using Atmospheric Explorer (and other satellite) measurements of thermospheric density fluctuations and measurements of lightning occurrence frequency by a lightning monitor on board a DMSP satellite, we found a remarkable correlation between the locations of the centers of lightning occurrence and the centers of wave-like density fluctuations of the thermosphere.

Further summaries of work in the above-mentioned four areas are given in the following sections. References to exhibits are made in these sections, but the exhibits are collected in the last section of the report.

II. AURORAL MAGNETOSPHERE - IONOSPHERE COUPLING

Work in this area resulted in the evolution of an electrostatic model of a quiet auroral arc (Exhibit 1: Electrostatic Model of a Quiet Auroral Arc, Y. T. Chiu and J. M. Cornwall, submitted for publication Journal of Geophysical Research). This attempt to understand the spectacular findings of particle and electrostatic field distributions in the auroral arc by instruments of the S3-3 satellite evolves from an earlier study of auroral

particle and field distributions (Exhibit 2: Self-Consistent Particle and Parallel Electrostatic Field Distributions in the Magnetospheric-Ionospheric Auroral Region, Y. T. Chiu and Michael Schulz, J. Geophys. Res. 83, 629, 1978), researches on which were done while this contract was being negotiated. In this new study (Exhibit 1) several approaches to a theory of the auroral arc were unified so as to yield an explanation for the particle and vector electrostatic field signatures seen by S3-3 experiments. In particular, it is shown that the scale size of the auroral arc in the transverse direction (~ 50 km) is a consequence of the electrodynamic coupling between the ionosphere and the magnetosphere. The theory yields a direct relationship between the auroral arc scale size, the magnetospheric parallel electrostatic potential accounting for auroral particle accelerations, and the ionospheric Pedersen conductivity.

As result of these contract researches in the electrodynamics of the auroral arc, and in particular as result of our attempts at assessing the mutual influence of the ionosphere and magnetosphere in the auroral process, we have been invited to participate in the Solar Terrestrial Predictions Workshop in April 1979 in the area of magnetosphere-ionosphere coupling and predictions. Exhibit 3 (Auroral Magnetosphere-Ionosphere Coupling: A Brief Topical Review, Y. T. Chiu, J. M. Cornwall and Michael Schulz) is our contribution to this workshop. Sponsorship of NASA under the subject contract is specifically acknowledged.

III. TROPOSPHERE - THERMOSPHERE COUPLING

Considerable scientific interest has recently been focused upon the possible coupling of dynamical processes between the troposphere and the upper atmosphere.

However, because of numerous limitations in the collection and interpretation of data, there is little, if any, evidence that upper and lower atmospheric processes are coupled in a physically discernible manner. While the major attention to date has been directed toward upper atmospheric influences on tropospheric processes, we would like to point out that the reverse, tropospheric influences upon upper atmospheric phenomena, should also be examined, not just because they may provide clues to understanding atmospheric coupling but also because they might be misinterpreted as a sun-weather signal. Indeed, considering the relative energetics of upper and lower atmospheric processes, it is rather surprising that tropospheric "signals" are not prominent in the thermosphere, although, to be sure, such "signals" cannot be easily identified unless one has globally distributed data sets with extensive statistical coverage.

Contract work in this area (Exhibit 4: A Correlation of Thermospheric Gravity Waves with Tropospheric Lightning, Y. T. Chiu, B. C. Edgar, C. J. Rice and L. R. Sharp, submitted for publication Geophysical Research Letters) resulted in a report on correlative features of two sets of space-based atmospheric measurements, which are globally distributed with good statistical coverage. One set of data, pertaining to tropospheric processes, is lightning occurrence frequency derived from measurements of a lightning detector onboard a Defense Meteorological Satellite Program (DMSP) satellite in a dawn-dusk polar orbit sampling lightning activity worldwide. The second set of data, pertaining to thermospheric phenomena, is the occurrence frequency of wavelike structures in neutral atmospheric density profiles derived from measurements of several cold cathode ion gauges onboard Atmospheric Explorer spacecrafts AE-C and AE-D, and onboard the Air Force spacecraft S3-1. We found a significant correlation between the occurrence patterns of dawn lightning, indicative of massive long-lived tropospheric convective activity, and the occurrence patterns of wave-like structures in

the thermosphere.

In contrast to statistical correlations for which no plausible physical mechanisms are apparent, our search for a correlative connection between the occurrence patterns of thermospheric wave-like structures and lightning distribution at dawn is in fact suggested by the qualitatively-understood mechanism of gravity wave generation by deep convective activity and by wind shears in the upper troposphere. Therefore, we attempt a correlative study of the distributions of lightning activity and of thermospheric wave-like structures not because the two are directly connected but because lightning is a good indicator of tropospheric activities which are thought to be physical generators of gravity waves.

IV. NEUTRAL ATMOSPHERE - IONOSPHERE COUPLING

Included in this research program of upper-lower atmospheric coupling are studies of coupling between the ionized and neutral components of the atmosphere. It is generally understood that coupling between these components is most likely to occur in the lower thermosphere ($\sim$ 100 km) and in the middle atmosphere where minor constituents such as ozone play a major dynamical role.

While this contract is in negotiations, researches were already in progress on the possible mechanisms by which the ozone content of the middle atmosphere may be disturbed. Large perturbations of ozone density may generate large scale "holes" of ozone through which upper atmospheric disturbances may be transmitted to the lower

atmosphere. Studies of ozone density perturbations resulted in the publication of the paper: "The Response of Atmospheric and Lower Ionospheric Layer Structures to Gravity Waves" by Y. T. Chiu and B. K. Ching in Geophysical Research Letters (Exhibit 5).

Coupling between the ionized and neutral components of the atmosphere takes place in many forms, but nowhere is it more manifest than in the case of equatorial spread-F where it is only very recently established that ions of lower thermosphere origin (molecular ions) are found to exist in the upper ionosphere (~ 500 km). To understand spread-F phenomena such as these, we have investigated the role of neutral atmospheric dynamics upon convective ionospheric instabilities. This contract research results in the publication of "Rayleigh-Taylor and Wind-Driven Instabilities of the Nighttime Equatorial Ionosphere" by Y. T. Chiu and J. M. Straus in the Journal of Geophysical Research (Exhibit 6).

V. PLANETARY WAVES IN THE MIDDLE ATMOSPHERE

A long-termed project to study the wave-wave and wave-mean-flow interactions in the middle atmosphere has been started under this contract. Meteorologists have long observed that inter-annual variations in the Northern mid-latitudes, such as the degree of severity of winters in the U.S. are somehow connected with the dominance of planetary wave types in the middle atmosphere varying from year to year. Further, planetary waves (of zonal wave number 1 and 2) interact with the mean middle-

atmospheric zonal flow and with each other. The phenomenon of winter stratospheric warming has, for the past few years, been recognized as the result of planetary wave interactions. The theory of the interaction of a single planetary wave (wave number 1) with the mean zonal wind has been used to interpret stratospheric warming observations. However, these observations indicate, among other effects, that the warming results in wave energy transfer from zonal wave number 1 to zonal wave number 2 as much as it results in changes of mean flow. Thus, to study the phenomenon of wave-wave interaction, as well as to study the reasons for inter-annual variation in the dominance of planetary wave types, we have started a project to study the interactions of two waves with the mean wind in the middle atmosphere. With two waves, wave-wave interaction can be taken into account whereas, with only one wave, only wave-mean-wind interaction is included, as in current models.

Our method is to first study the time-independent problem of two waves in equilibrium with the mean wind to see if we may model the inter-annual variation of wave types. Numerical calculations of this equilibrium problem are being carried out. Our next step is to turn on the time dependence and study wave-wave interactions in the presence of wave-mean-wind interactions.

VI. INTERIM CONCLUSIONS

Studies in the dynamical coupling between the components of the upper and lower atmosphere have been carried out under this contract in the following areas: 1) auroral magnetosphere-ionosphere coupling, 2) troposphere-thermosphere coupling, 3) neutral

atmosphere-ionosphere coupling, and 4) planetary waves in the middle atmosphere. We have not only found that new evidences of such couplings exist but that understanding of the coupling mechanism is fundamental in the understanding of some upper atmospheric phenomenon themselves. The auroral process is found to be such as example.

VII. EXHIBITS

1. Electrostatic Model of a Quiet Auroral Arc, Chiu and Cornwal; submitted to J. Geophys. Res., 1979.

2. Self-consistent Particle and Parallel Electrostatic Field Distributions in the Magnetospheric-Ionospheric Auroral Region, Chiu and Schulz; J. Geophys. Res., 83, 629, 1978.

3. Auroral Magnetosphere-Ionosphere Coupling: A Brief Topical Review, Chiu, Cornwall and Schulz; Solar-Terrestrial Predictions Workshop and Proceedings, 1979.

4. A Correlation of Thermospheric Gravity Waves with Tropospheric Lightning, Chiu, Edgar, Rice and Sharp; submitted to Geophys. Res. Letters, 1979.

5. The Response of Atmospheric and Lower Ionospheric Layer Structures to Gravity Waves, Chiu and Ching, Geophys. Res. Letters, 5, 539, 1978.

6. Rayleigh-Taylor and Wind-Driven Instabilities of the Nighttime Equatorial Ionosphere, Chiu and Straus, accepted for publication J. Geophys. Res., 1979.

ELECTROSTATIC MODEL OF A QUIET AURORAL ARC

Y. T. Chiu and J. M. Cornwall*

Space Sciences Laboratory
The Aerospace Corporation
El Segundo, Calif.

*Permanent address: Department of Physics
University of California, Los Angeles, California

December 1978

Submitted for Publication:
Journal of Geophysical Research

This work is partially supported by NASA under grant NASW-3120
and partially by The Aerospace Corporation-Sponsored Research Program.

ABSTRACT

Given auroral electron and ion distribution functions as observed with satellites in inverted-V events, we construct a self-consistent electrostatic field distribution (both parallel and perpendicular to the earth's magnetic field). This field distribution is determined by: 1) magnetic mirror forces which cause charge separation for species with different pitch angle distributions; 2) Poisson's equation, which gives the electric field in terms of the charge separation; 3) the ionospheric physics of charge and current conservation, coupled with precipitation sources and recombination losses. In a situation where the particle distribution functions have no L-dependence at the equator, these three ingredients combine to produce a self-consistent latitudinal scale length in and above the ionosphere of some tens of km, as typically observed in quiet arcs. A variety of particle and field data are semiquantitatively given correctly by the model. Earlier works left out at least one of the three ingredients, with the result that an ionospheric scale length could only be determined when other physical mechanisms (e.g. polarization currents) involving the equatorial magnetosphere were taken into account. Although these other mechanisms may be important, we do not consider them in this paper.

I. INTRODUCTION

In the theoretical studies of auroral arcs, it is only rather recently that attention has focused on quantitative evaluation of significant parallel electric fields and particle distributions. Most earlier work ignored realistic particle distributions and has been grounded on the MHD approximation [Sato, 1978; and Holzer, 1973; Holzer and Sato, 1973; Ogawa and Sato, 1971; Atkinson, 1970], which is suitable for evaluation of electric fields and currents perpendicular to the Earth's magnetic field, but which cannot completely determine parallel electric fields [Evans, 1974; 1975; Mizera and Fennel, 1977; Croley et al., 1978; Shelley et al., 1976] and currents [Vondrak et al., 1971; Cloutier et al., 1973; Vondrak, 1975; Sesiano and Cloutier, 1976; Frank et al., 1977; Ghielmetti et al., 1978]. Another school of thought has concentrated on turbulence-produced anomalous parallel resistivity [Papadopoulos, 1977; Hudson and Mozer, 1978], with at best inconclusive results: the main problem is that current-driven instabilities [Kindel and Kennel, 1971; Hudson et al., 1978] heat ions to the point where the instability shuts down. More phenomenological models of the relationship between field-aligned currents and perpendicular electric fields have also been considered (Mallinckrodt and Carlson, 1978; Maltsev et al., 1977).

That leaves (at least) two other mechanisms for parallel electric fields: 1) dissipationless electrostatic "shocks" [Kan, 1975, Swift, 1975, 1976; Mozer et al., 1977; Torbert and Mozer, 1978] (static solution to the Vlasov-Poisson equations); 2) electric fields produced in a mirroring magnetic field by differential pitch-angle anisotropies of electrons and ions [Alfvén and Fälthammar, 1963; Lemaire and Scherer, 1971; 1974; Lennartsson, 1977; Whipple, 1977; Chiu and Schulz, 1978]. These mechanisms have been considered separately, but not together (to our knowledge). One sort of electrostatic

shock is known as a double layer, [Block, 1975; Shawhan et al., 1978]; it exists independently of the magnetic field strength and has a length scale of a few Debye lengths. We will not consider it further. Another type is highly oblique to the magnetic field, and in consequence the unit of length is the ion Larmor radius. It has been dealt with by Swift [1975, 1976] for a spatially-constant B field, and without consideration of ionospheric physics.

Electric fields produced by differential pitch-angle anisotropies have been considered by many authors [Lemaire and Scherer, 1974; Lennartsson, 1977; Whipple, 1977; Chiu and Schulz, 1978], but always with a condition of strict charge neutrality; this eliminates shocks of the type emphasized by Swift [1975, 1976].

In this work, we take into account both mechanisms discussed above, as well as some standard simple ionospheric physics of the type usually incorporated into the MHD models. The result is a fairly accurate representation of the particle and field data taken by the auroral satellite S3-3 at some thousands of kilometer altitude. A major new feature is the self-consistent prediction of latitudinal spatial structure in an auroral arc (indeed, that is what the term "arc" refers to) near and above the ionosphere, even if particle distributions at the equatorial regions of the auroral field lines are spatially homogeneous. The predicted scale length for the perpendicular electric field is tens to perhaps one or two hundred kilometers, more or less in agreement with observations of the largest-sized feature of discrete auroral arcs. (We are not trying to explain the small-scale spatial variations, which are undoubtedly connected to rapid cross-field variations in energetic particle fluxes at very high altitudes.)

The reader may recall that the other works referred to earlier either were silent on the question of latitudinal spatial scales [e.g. Swift, 1975, 1976; Kan, 1975], or (for

the MHD models) required time-dependent (feedback current) mechanisms to establish the scale [e.g. Sato, 1978; Atkinson, 1970]. We do not dispute the existence or possible importance of feedback mechanisms, but it seems worthwhile to establish that there is a self-consistent scale length under the static conditions invoked by us.

Actually, it is well-known that such a scale length is determined by the ionospheric physics if, in addition, the relation between parallel electric field and current is describable by a finite parallel conductivity. (This is what is missing from the MHD models which require the use of feedback mechanisms.) The electrostatic shock and mirror-field mechanisms used here do not lead to such a simple field-current relation; rather, the current depends in a complicated non-linear way on potential differences. However, near the ionosphere this relation is approximately linear, which (coupled with a factorizability assumption) allows for the derivation of a simple differential equation governing the latitudinal dependences of $E_\perp$, the perpendicular electric field,and its relation to the parallel potential drop. This differential equation is, unfortunately, unable to predict in a self-consistent way, latitudinal particle and field variations past the point where $E_\perp$ starts to return to ambient ionospheric values; we are able to speak only of particles and fields in the region of the arc where the current is upgoing (i.e., downgoing electrons and upgoing ions). This is enough information to see such general features as the latitudinal scale length. Our inability to make predictions in the region of return (downgoing) current stems from the assumption that particle distributions at the auroral equator are independent of latitude and from breakdown of the factorizability assumption mentioned above, and not from inadequacies in the physics of the model. (Presumably the return current is driven, in part, by the buildup of a negative charge density in the ionosphere; e.g. Vondrak [1975].)

Our work is not, of course, an attempt to "explain" discrete auroral arcs; it is an attempt to generate an internally self-consistent picture of particle distributions and electric fields (perpendicular and parallel) as they vary both along and across the field lines. We therefore parametrize particle distribution functions so that they fit both the S3-3 data and particle events fairly well and at the same time seem reasonable at the equator of the auroral field lines. In the absence of specific equatorial information, we choose equatorial distributions with no explicit L-dependence, thus sacrificing information which is possibly important in the return-current region of the arc [e.g. Rostoker and Bostrom, 1976].

Given these particle distributions, the electric field is computed from Poisson's equation in the Earth's magnetic field, subject to boundary constraints imposed by current and charge-density continuity at the ionosphere. It turns out that the parallel electric field receives contributions of the same order of magnitude from differential pitch-angle anisotropies and from space-charge separation; both contributions scale as $W/e\ell$ where W is a typical particle energy, ℓ is the field line length and e is the positive electronic charge. There are no double layers, or localized regions of abruptly changing electric field; $W/e\ell$ is ~1 mV/m everywhere. This is in strong disagreement with claimed measurements of up to 200 mV/m [Mozer et al., 1977]. On the other hand, predicted values of $E_\perp \approx 100$–400 mV/m are in good agreement with observation [Torbert and Mozer, 1978]. $E_\perp$ has a spatial structure consistent with a small negative charge density in the center of the arc.

The input particle distributions used to generate these electric fields are similar to those used in an earlier study [Chiu and Schulz, 1978], in which strict charge neutrality was imposed. They describe: hot magnetospheric plasma (the electrons being

more anisotropic than the protons); trapped electrons (ions in general are not trapped because the electric force and the mirroring force are in the same direction); ionospheric plasma; and back-scattered electrons. These last two constituents are important in partially short-circuiting the very large parallel electric fields which would be generated by the hot plasma alone. The hot plasma is modeled by bi-Maxwellians truncated so as to insure that the hot-plasma source region is equatorial, not ionospheric. Ionospheric electrons are given by an isotropic Maxwellian, while for cold ionospheric ions the influence of gravity at low altitudes must be taken into account. Details of the trapped and backscattered populations will be given later.

A proper treatment of the ionspheric physics, which would allow us to resolve parallel electric field effects all the way down to the level of ambipolar fields ($\sim 10^{-3}$ mV/m for O^+) is beyond the scope of this paper. (Such a treatment would automatically generate the polar wind.) Instead, all we do is impose current and charge conservation on the ionosphere, balancing auroral sources and sinks against recombination and photoionization. Because of a lack of detailed knowledge of the transition region from ambipolar parallel electric fields to aurorally-supported fields, our results for parallel electric fields are reliable only above an altitude of perhaps 2000 km.

This has one important consequence for higher-altitude phenomena, such as observed by S3-3. The number of upgoing H^+ and O^+ ions which are accelerated to ~keV's of energy is a sensitive function of the transition altitude from ambipolar to auroral electric fields, which in turn depends in a complicated way on all the parameters of the model. One therefore expects the fluxes of upflowing ions, and especially the O^+/H^+ ratio, to vary widely from one arc to another, and this is the case experimentally [Ghielmetti et al., 1978; Frank et al., 1977]. One also expects that the model's

quantitative predictions of upgoing ion fluxes are not very reliable, but that the predicted average single-particle energy, which of course is directly related to the parallel electric field, will be well-modeled at sufficiently high altitudes.

We do, in fact, find well-collimated upward-going ion beams with energies in the keV range, as observed from S3-3 [Croley et al, 1978; Shelley et al., 1976]. Available particle-electric field data correlations [see Figure 6] show that such beams are always spatially coincident with the characteristic perpendicular electric-field signatures (as seen on S3-3) of auroral arcs. There are also large fluxes of down-going electrons which are not as beam-like, because the magnetic mirroring force decollimates down-going streams. (One might expect, because of the conjugacy of many auroral phenomena, to see downward ion beams in the opposite hemisphere, but these are not observed, presumably because they are carried off in the vicinity of the equator. Our model distribution functions take this fact into account.)

There is one very obvious class of effects in the S3-3 data which we do not model, and this consists of plasma turbulence and unstable wave modes [Hudson and Mozer, 1978; Hudson et al., 1978]. These may or may not have much to do with direct generation of parallel electric fields by anomalous resistivity, but they could be imporant as dissipation mechanisms for the shock-like structures we find. As a first step in this direction, we would like to study the linear stability of the particle distribution functions formed here, but we do not take even that modest step here.

The paper is organized as follows: Sec. II summarized briefly the physics and the equations we use; Sec. III gives the procedure for obtaining approximate solutions of Poisson's equation coupled to ionosphere current conservation. A comparison with a specific discrete auroral arc as seen from S3-3 is given in Sec. IV; Sec. V gives a summary and conclusions.

II. FORMULATION OF THE MODEL

There are three separate aspects of the model: 1) the form of Poisson's equation in a mirroring magnetic field; 2) incorporation of ionospheric conservation laws as boundary conditions; 3) specific particle distribution functions used.

1. Poisson's equation in a mirroring field.

The first is a straightforward generalization of, for example, Swift's [1975] equation valid for a homogeneous magnetic field. We begin by ordering various scale lengths and drift velocities. The perpendicular scale $\ell_\perp$ of particles and electric fields in arcs ($\ell_\perp \approx 50$ km) is much less than the scale parallel to the magnetic field $\ell_\parallel$ ($\ell_\parallel \approx 10^4$ km or more). Still smaller is the ion gyroradius $v_\perp / \Omega \approx 1$-5 km. We expect the electric fields to scale as

$$E_\parallel \approx \frac{Mv^2}{e\,\ell_\parallel} \quad , \quad E_\perp \approx \frac{Mv^2}{e\,\ell_\perp} \tag{1}$$

in terms of a characteristic ion mass M and velocity v, which reveals the following scaling for drift velocities:

$$\vec{v}_E = \frac{c\,\vec{E}\times\vec{B}}{B^2} \approx \epsilon_\perp \vec{v}$$

$$\vec{v}_p = \frac{-1}{\Omega^2}(\dot{\vec{v}}_E \times \vec{\Omega}) \approx \epsilon_\perp^2 \vec{v} \tag{2}$$

$$\vec{v}_{G,C} \approx \epsilon_\parallel \vec{v}$$

in terms of the fundamental smallness parameters

$$\epsilon_\perp = \frac{v}{\ell_\perp \Omega} \quad , \quad \epsilon_\parallel = \frac{v}{\ell_\parallel \Omega} \tag{3}$$

In (2), v_p is the polarization drift velocity, and v_G, v_C are the gradient and curvature drifts; we assume the basic time scale for $\dot{v}_E$ is $\approx \ell_\perp / v$. Furthermore, (1) shows that the electric force $eE_\parallel$ is comparable to the mirror force $-\mu$ dB/ds, where $\mu \approx Mv_\perp^2/2B$ and s is an element of length along the magnetic field (s = 0 at the equator).

Note that $\epsilon_\perp^{-1}$ is the horizontal scale size of the arc measured in Larmor radii, perhaps 10-30, while $\epsilon_\parallel^{-1}$ might be several thousand. We thus take it that $\epsilon_\perp^2 \gg \epsilon_\parallel$, and drop curvature and gradient drifts altogether, while saving terms through $O(\epsilon_\perp^2)$. An important dimensionless parameter of this order is $c\, \nabla_\perp \cdot \vec{E}_\perp / \Omega B$, which represents the lowest-order correction to the magnetic moment in the presence of $\vec{E}_\perp$. Even though this correction is small ($\epsilon_\perp^2 \approx 10^{-2}$-$10^{-3}$) it is important in Poisson's equation, for it must be compared to the percentage charge separation $\Delta n/n$ which results from solving this equation.

Our problem now is to separate the equations of motion (at least approximately) so that effects due to finite $\epsilon_\perp$ do not mix with those due to finite $\epsilon_\parallel$. This is conveniently done by decomposing, in a frame of reference drifting with the total drift velocity $\vec{v}_E + \vec{v}_p$, the total perpendicular velocity $\vec{v}_\perp$ into two terms, each linear in a velocity $\dot{\vec{\rho}}$:

$$\vec{v}_\perp = \dot{\vec{\rho}} + \frac{c}{\Omega B} (\dot{\vec{\rho}} \cdot \nabla) \vec{E} \tag{4}$$

In (4), $\vec{\rho}$ is the position of a particle with respect to the guiding center. The second term in (4) is formally the same as a polarization drift (with $d/dt = \dot{\vec{\rho}} \cdot \nabla$), but of course it oscillates and is not actually a drift velocity. The significance of this decomposition of $\vec{v}_\perp$ is that the gyration vector $\vec{\rho}$ oscillates with a frequency ω that differs from Ω in $O(\epsilon_\perp^2)$, but that $\rho \equiv |\vec{\rho}|$ varies only in $O(\epsilon_\parallel)$. (That is, in a constant B field, ρ is constant.)

To see this, observe that $\vec{v}_\perp$ or $\vec{\rho}$ oscillates at a frequency

$$\omega \approx \Omega \left[1 - \frac{c}{2\Omega B} \nabla \cdot \vec{E}_\perp\right] \tag{5}$$

as an elementary calculation shows. Now calculate the canonically-defined first invariant J_1:

$$J_1 = \oint d\vec{\rho} \cdot \left[M \vec{v}_\perp + \frac{e}{c} \vec{A}\right] \tag{6}$$

where the integral goes around a gyration orbit of position element $d\vec{\rho}$, and $\vec{A}$ is the vector potential of the Earth's magnetic field. Clearly the first term in (4) gives a contribution $2\pi M\omega\rho^2$ to J_1, and the second term in (6) contributes $-\pi M \Omega \rho^2$ (the flux through the gyration loop). The second term in (4) is easily calculated by using $d\vec{\rho} = \dot{\vec{\rho}}\, dt$, and $\langle \dot{\rho}_i \dot{\rho}_j \rangle = \frac{1}{2} \Omega^2 \rho^2 \delta_{ij}$ to lowest order in cyclotron-phase averaging as indicated by the brackets; the result is

$$J_1 = 2\pi M \Omega \rho^2 \left[\frac{\omega}{\Omega} + \frac{c}{2B\Omega} \nabla \cdot \vec{E}_\perp - \frac{1}{2}\right] = \pi M \Omega \rho^2 \tag{7}$$

Therefore $\rho \sim B^{-1/2}$, and varies only on the $\epsilon_{||}$ scale, as claimed; the $\epsilon_{\perp}^{2}$ terms have cancelled.

A more useful form of the first invariant involves $|\dot{\rho}| \approx \omega\rho$:

$$J_1 = \frac{\Omega}{\omega^2}\,\dot{\rho}^2 \tag{8}$$

We express this in terms of a modified invariant:

$$\mu \equiv \frac{M\dot{\rho}^2}{2B}\left(1 + \frac{c\,\nabla\cdot\vec{E}_{\perp}}{\Omega B}\right) \tag{9}$$

It is easy to calculate that an alternative form for μ is

$$\mu = \frac{M}{2B}\langle v_{\perp}^2\rangle \tag{10}$$

using (4); therefore, the total energy of a particle (in the drifting reference frame) is

$$\mathcal{E} = \frac{1}{2}Mv_{||}^{\,2} + \mu B + e\phi\,. \tag{11}$$

However, this form does not display the expected separation between longitudinal and transverse motion, since ϕ is the local potential, not the guiding-center potential. Note that the difference between ϕ and the guiding-center potention ϕ_{GC} is, after phase-averaging,

$$e(\phi - \phi_{GC}) \approx -\frac{1}{4}\,e\rho^2\,\nabla\cdot\vec{E}_{\perp}\,. \tag{12}$$

On the other hand, one calculates from (7) and (12) that

$$\frac{J_1\omega}{2\pi} + e\,\phi_{GC} = \mu B + e\phi \tag{13}$$

where $J_1\,\omega/2\pi$ is the canonical expression for the transverse energy, so the left-hand side of (13) expresses the desired separation of the energy into longitudinal ($\frac{1}{2}Mv_{\|}^2$ + $e\phi_{GC}$) and transverse terms.

In practical terms, for particles of energy above a few volts we need not worry about $O(\epsilon_\perp^2)$ corrections in the expression for the energy, and we use the simple expression

$$\mathcal{E} = \tfrac{1}{2}\,Mv_{\|}^2 + \mu B + e\phi_{GC} \tag{14}$$

both in the drift frame and in the Earth-centered reference frame. However, it is important to save the $O(\epsilon_\perp^2)$ terms in (9).

The next step is to write down Poisson's equation, for which we need the charge densities as expressed in terms of the contraints of the motion (9) and (4). For each charged species, we have for the density:

$$n_j = 2\pi \int \dot{\rho} d\dot{\rho} dv_{\|}\; f_j(\mu, \mathcal{E})$$

$$= \frac{2\pi B}{M_j^2}\left[1 - \frac{c\,\nabla\cdot\vec{E}_\perp}{\Omega B}\right] \int d\mu d\mathcal{E}\, f_j(\mu, \mathcal{E})\, \left[\frac{2}{M_j}(\mathcal{E} - \mu B - e\phi)\right]^{-1/2} \tag{15}$$

$$\equiv \left[1 - \frac{c\,\nabla\cdot\vec{E}_\perp}{B\Omega}\right]\; \tilde{n}_j \tag{16}$$

where the integral in (15) runs over positive values of $\mathcal{E}-\mu B-e\phi$. (It is understood that ϕ is evaluated at the guiding center; we have dropped the subscript GC.) The density $\tilde{n}$ is that which would be appropriate in the absence of the perpendicular electric field.

Poisson's equation

$$\nabla\cdot\vec{E}_\perp + B\,\frac{\partial}{\partial s}\,(B^{-1}E_\parallel) = 4\pi\sum_j n_j e_j \tag{17}$$

becomes

$$K\,\nabla\cdot\vec{E}_\perp + B\,\frac{\partial}{\partial s}\,(B^{-1}E_\parallel) = 4\pi\sum_j \tilde{n}_j e_j \tag{18}$$

where K is the plasma dielectric constant:

$$K = 1 + 4\pi\sum_j \frac{\tilde{n}_j M_j c^2}{B^2} \tag{19}$$

Equation (18) generalizes Swifts' work to a non-constant B- field, although it does not quite reduce to his in the limit B = constant, because we have omitted a term $\frac{1}{2}Mv_E^2$ in the energy; in effect, this amounts to setting spatial gradients of K equal to zero. The quasi-neutrality equation of Chiu and Schulz is simply that the right-hand side of (18) vanish. In fact, taking $E_\perp$ from (1) and $\nabla\cdot\vec{E}_\perp \approx E_\perp/\ell_\perp$, one finds that the left-hand side of (18) yields a fractional charge separation $\Delta n/n \approx \epsilon_\perp^2 \approx 10^{-2}$-$10^{-3}$. Or, looked at the other way around, this sort of charge separation can drive perpendicular electric fields of $O(Mv^2/\ell_\perp e) \approx$ 100's of mV/m, as well as parallel fields of $O[(\ell_\perp/\ell_\parallel)E_\perp]$.

It should be noted that the term $B\partial(B^{-1}E_{\parallel})/\partial s$ in (18) is quite negligible; it is of order $\Lambda_D^2/\ell_{\parallel}^2 \approx 10^{-8}$ where Λ_D is the Debye length. This is why ordinary double layers need such small parallel scale lengths in order for there to be appreciable charge separation. From now on, we drop this term.

2. Some simple ionospheric physics.

It is not possible to prescribe separately the currents flowing into the ionosphere and the horizontal electric-field gradients there; they are coupled by the requirement that the ionosphere must be able to balance the current flow (as well as to balance sources and sinks of charge). Two simple equations express these facts: (e.g. Atkinson [1970], whose notation we use; Coroniti and Kennel, 1972) the equation of current continuity

$$J_{\parallel} = \frac{\partial}{\partial x}\left(\Sigma_P \frac{\partial \phi}{\partial x}\right) \tag{20}$$

and of charge balance at the ionosphere

$$0 = \frac{dN}{dt} = S - \alpha(N^2 - N_0^2) \tag{21}$$

In these equations, x is a horizontal north-south coordinate, Σ_P is the height-integrated Pedersen conductivity, N the height-integrated ionospheric electron density, α a recombination coefficient, αN_0^2 represents non-auroral sources, and S represents sources of charge from auroral electron precipitation, or from upward-going ions. These latter are not very important, so it is probably accurate enough to take

$$S = \frac{+(\gamma+1)}{e} J_{\parallel} \tag{22}$$

(where $J_{\parallel}$ is positive for downgoing electrons). Here γ is the number of electron-ion pairs produced at ionospheric altitudes per incoming auroral primary, roughly 30 times the primary's energy in keV, or $\gamma \approx 100$. In equations (20-22), the vertical structure of the ionosphere has been abstracted (or integrated over) in terms of the set of parameters (Σ_P,N,α,γ); therefore, these equations, representing the ionospheric control of the magnetospheric parallel current $J_{\parallel}$, can be evaluated at the top of the ionosphere, defined as the region where significant parallel electric field can be generated by the mechanisms we invoke, or equivalently the baropause level $s \equiv \ell$ (altitude of about 2000 km). We treat an ideal situation in which an auroral arc extends uniformly in the y(east-west) direction, with $E_y = 0$, so there is no Hall current contribution to (20). Finally, we note that

$$\Sigma_P = PN \tag{23}$$

where P is a constant.

As is well-known, equations (20-23) can be combined into a single differential equation given some sort of constitutive relation between $J_{\parallel}$ and the electric field such as $J_{\parallel} = \sigma_{\parallel} E_{\parallel}$. In fact, for the field-generating mechanism considered here, we have no such relation; rather, $J_{\parallel}$ is a complicated function of ϕ (found from (15) by removing the square root factor). As we indicate below in subsection 3, it is possible, at the ionosphere, to linearize this relationship:

$$J_{\parallel} \simeq -Q\,\phi \tag{24}$$

where the zero of potential is chosen so that $J_{\parallel}$ vanishes when there is no potential difference between the magnetosphere and the ionosphere. The electrostatic potential ϕ is negative in the arc, with this convention, reflecting a negatively-charged arc resulting from an electron influx. The constant Q depends in a complicate way on the specific distribution functions used, but by a scaling argument

$$Q \approx \frac{ne^2v}{\mathcal{E}} \tag{25}$$

for a typical auroral-particle density n, velocity v, and energy $\mathcal{E}$. (Later, precise numerical values of Q will be calculated.)

One may now combine equations (20-25) and find

$$\zeta - 1 = -\left(\frac{2}{3}\frac{\Sigma_{P0}}{Q}\right)\frac{\partial^2}{\partial x^2}\,\zeta^{3/2}, \tag{26}$$

where

$$\zeta = 1 + \frac{(\gamma+1)Q|\phi|}{N_0^2 e\alpha}, \quad \Sigma_{P0} = PN_0 . \tag{27}$$

At this point, we note that the scale length in (26) is indeed of typical arc size, if nominal values $\Sigma_{P0} \approx 5$ mho, $Q \approx 0.2$ cm^{-1}sec^{-1}:

$$\Lambda_I = \left(\frac{2}{3}\frac{\Sigma_{P0}}{Q}\right)^{1/2} \approx 40 \text{ km} . \tag{28}$$

A detailed study of the differential equation (26) will be given later; here we note only that $N_0^2 e\alpha/(\gamma+1)Q \approx 30$-$100$ volts, so $\zeta \gg 1$ near the center of the arc. Near the edges of the arc Q varies rapidly as return currents are set up, and the idealized model of (26) breaks down.

The "natural" scale length for horizontal variations is the ion Larmor radius as one sees from (18) by estimating

$$4\pi \sum_j e_j \tilde{n}_j \approx \frac{4\pi e^2 n}{Mv^2} \phi \tag{29}$$

(consistent with (25)). This natural length is stretched by a factor of $\epsilon_\perp^{-1}$ to be of the order of tens of km, as given by (28). This stretching is described by a self-consistent solution of the magnetospheric Poisson's equation (18), with boundary conditions given by the non-linear differential equation (26) (plus equatorial boundary conditions supplied by the distribution functions). Needless to say, this is a highly non-trivial set of equations to master. We are forced to make one rather crude approximation at this point: the electrostatic potential ϕ is written as the product of two factors, one depending only on a horizontal coordinate, the other only on a vertical coordinate. The geometry of the Earth's magnetic field is taken into account by using orthogonal dipolar coordinates, which will be described later when the coupled solutions are discussed.

Next, we turn to the specification of the particle distribution functions.

3. Particle distribution functions.

Since we intend to construct an electrostatic model of a quiet auroral arc which may be compared semi-quantitatively with observations, it is necessary to construct distribution functions representative of the possible particle populations in an auroral flux tube. Such an attempt has been made in Chiu and Schulz [1978], where the following plasma constituent distributions are assumed to be present in the collisionless interval ($0 \leq s \leq \ell$) of the auroral flux tube: hot anisotropic magnetospheric plasma injected by

the substorm, $f_{M\pm}$; cold thermal ionospheric plasma, $f_{I\pm}$; primary and secondary back-scattered electrons, f_{S1} and f_{S2} respectively; and electrons which happened to be scattered into trapped trajectories from the magnetospheric (f_{M-}) and primary back-scattered (f_{S1}) populations, f_T. Electrons on trapped trajectories will hereafter be referred to simply as trapped electrons. The basic forms of these distributions are Maxwellians or bi-Maxwellians where appropriate. The details of constructing the appropriate boundary conditions at s=0, at $s=\ell$ and the phase space boundaries for the various populations have been given; it is not necessary for us to repeat these complicated distribution functions here. The reader may find the expressions listed as equations (9), (11), (13), (25), (26) and (28) in Chiu and Schulz [1978]. The notations for these distribution functions are retained in this paper except for the following: a) the energy variable ϵ in Chiu and Schulz [1978] is changed to $\mathcal{E}$ in this paper and b) the electrostatic potential V(s) in Chiu and Schulz [1978] is to be replaced by the electrostatic potential ϕ which is a function of both s and the latitudinal variable. It should be noted that the parallel energetic particle current at $s=\ell$, consisting of magnetospheric particles and backscattered electrons, calculated from these distribution functions differs slightly from (24) by a term independent of ϕ because the distribution functions are not fully Maxwellians but are cut-off by boundary conditions at s=0 and at $s=\ell$. The constant precipitation current is, however, smaller than (24) by a factor of ($kT/e\phi_\ell$), where kT is a typical magnetospheric particle thermal energy; thus, at the baropause level $s=\ell$, (24) is a good approximation. The full parallel current into the ionosphere at $s=\ell$ is given below:

$$J_{\parallel}(\ell) \simeq -e(2+\frac{A_2}{3})\ N_{M-}\ (T_{\parallel -}/T_{\perp -})\ (kT_{\parallel -}/2\pi M_e)^{1/2}\ (1+e\phi_\ell/kT_{\parallel -}), \qquad (30)$$

$$\equiv -Q_A - Q_B\,(e\phi_\ell/kT_{\parallel -})$$

where $T_{\parallel -}$ and $T_{\perp -}$ are parallel and perpendicular temperatures of magnetospheric electrons respectively and A_2 is a parameter denoting the intensity of secondary backscatter ($A_2 \approx 3$).

In constructing the distribution functions discussed above, a basic simplification, which limits the validity of our construction, has been made, viz. no spatial structure aside from that of the electrostatic potential ϕ has been assumed. As has been discussed previously, the ionospheric boundary condition sets a perpendicular spatial scale for the electrostatic potential ϕ. However, the spatial structure of the inverted-V event, as well as ϕ, need not depend purely on the ionospheric scale. Magnetospheric plasma injected at the equator may also have a perpendicular spatial scale which is determined entirely by the injection process, assumed to be unrelated to our problem. As we shall show later, this simple assumption may be a contributing factor in our not being able to obtain a self-consistent solution in the region of field-aligned return current flow, although the ionospheric problem does prescribe a return current region.

The particle density moments are obtained in the standard way as is described in Appendix B of Chiu and Schulz [1978]. These density moments are denoted as $\tilde{n}_j$ in the Poisson equations (18), whereas they are denoted as n_j in Chiu and Schulz [1978].

III. APPROXIMATE SOLUTION

The electrostatic model of an auroral arc, as formulated in the previous section, consists of obtaining a solution of the Poisson equation

$$\left[1 + \sum_j \frac{4\pi M_j c^2}{B^2} \tilde{n}_j\right] \nabla \cdot \vec{E}_\perp = 4\pi e \sum_j q_j \tilde{n}_j \ , \qquad (31)$$

where q_j is the sign of charged species j and the electrostatic field $\vec{E}$ is given in terms of a potential ϕ such that

$$\vec{E} = -\nabla\phi \ . \qquad (32)$$

In (31), the density moments $\tilde{n}_j$ are given in terms of assumed distribution functions

$$\tilde{n}_j(s) \equiv \int_0^\infty v_{\perp s} dv_{\perp s} \int_{-\infty}^{+\infty} f_j(v_{\parallel s}, v_{\perp s}, \phi)\, dv_{\parallel s} \ . \qquad (33)$$

Equation (33) is the same as (16); we exhibit it here for the sake of easy reference to Chiu and Schulz. A solution for ϕ in the region $\ell \geq s \geq 0$ is to be constructed for (31) under the ionospheric boundary condition,

$$\nabla_\perp \cdot (\Sigma_P \nabla\phi)_{s=\ell} = (\gamma+1) J_\parallel(\ell) \qquad (34)$$

where $J_\parallel(\ell)$, the parallel current into the ionosphere, is related to ϕ by (30). In (34), the parameter γ, introduced by Atkinson [1970], is the total number (≈ 100) of electron-ion pairs produced by the precipitating energetic electrons comprising $J_\parallel(\ell)$.

The density moments $\tilde{n}_j$ involve various related forms of error functions of ϕ; therefore, (31) is a highly non-linear partial differential equation for the electrostatic potential ϕ which depends on two spatial dimensions. Besides the high degree of non-linearity in ϕ the boundary condition (34) is also highly irregular because it is a differential equation for the spatial dependence of ϕ in a direction perpendicular to the magnetic field. Numerical solution of such a problem is not likely to be possible for reasonable resources even with the largest presently available computers, while the probability of obtaining an exact analytic solution is rather remote unless unrealistic assumptions about particle populations are made. We attempt to obtain an approximate solution by a combination of analytic and numerical means.

We first unravel the geometrical properties of the differential operators in (31) and (34) by using orthogonal dipolar coordinates (λ, ν, ψ), defined in terms of spherical coordinates (r, ϑ, ψ) [Cummings et al., 1969].

$$\lambda = \cos\vartheta/r^2 \; ; \quad \nu = \sin^2\vartheta/r \tag{35}$$

In (35), r is the spherical distance from the origin and ϑ is the co-latitude. The structure functions of the dipolar coordinates, in the notation of Morse and Feshbach [1953, pp. 21-30], are summarized by

$$h_\lambda = h_\nu h_\psi = r^3/(1+3\cos^2\vartheta)^{1/2},$$

$$h_\psi = r\sin\vartheta. \tag{36}$$

Note that surfaces of equal ν are L-shells since $\nu = (1/LR_E)$. Thus at a given ν (or L) the ratio of h_λ at two different values of λ (or field line distance s) is just the inverse ratio of the magnetic field strengths at the respective points.

With these coordinates, the differential operators in (31), (32) and (34) are given explicitly by:

$$\vec{E}_\perp = -\frac{\hat{\nu}}{h_\nu}\frac{\partial\phi}{\partial\nu} \tag{37}$$

$$\vec{E}_\parallel = -\frac{\hat{\lambda}}{h_\lambda}\frac{\partial\phi}{\partial\lambda} \tag{38}$$

$$\nabla\cdot\vec{E}_\perp = -\frac{1}{h_\lambda h_\nu h_\psi}\frac{\partial}{\partial\nu}\left(\frac{h_\lambda h_\psi}{h_\nu}\frac{\partial\phi}{\partial\nu}\right). \tag{39}$$

For the ionospheric continuity equation (34), the integrated Pedersen conductivity Σ_P is properly redefined as

$$\Sigma \equiv \int_{\lambda_e}^{\lambda_0} \sigma_P(\lambda)d\lambda \approx \frac{2\lambda_0}{r_0}\,\Sigma_P\ , \tag{40}$$

where σ_P is the Pedersen conductivity, λ_0 is the baropause position (s=ℓ)and λ_e is the bottom of the ionospheric E-layer in dipolar coordinates. The ionospheric boundary condition (34) becomes

$$\frac{\partial}{\partial\nu}\left(\frac{h_\lambda h_\psi}{h_\nu}\frac{\partial\phi}{\partial\nu}\right)\Big|_{\lambda_0} = h_\nu h_\psi(\gamma+1)J_\parallel / \Sigma\Big|_{\lambda_0}, \tag{41}$$

where it is understood that both sides of (41) are to be evaluated at λ_0.

We observe that the use of dipolar coordinates has reduced the differential operators to that of a single variable ν (or L). This is of little help in the treatment of the boundary conditions (41) because it is an equality valid at $\lambda=\lambda_0$ only. However, using mixed coordinates where appropriate we may transform (41), with the use of (30) and (40), into

$$\frac{\partial}{\partial\nu}(r^3\,\nu\,\frac{\partial\phi}{\partial\nu})\Big|_{\lambda_0} \simeq -\left.\frac{r^4}{(1+3\cos^2\vartheta)^{1/2}}\right|_{\lambda_0}\cdot(\gamma+1)\,[Q_A+Q_B(e\phi_\ell/kT_{\parallel -})]/(2\lambda_0\Sigma_P). \qquad (42)$$

For the auroral region at the baropause λ_0 the variation of r as function of ν is negligible, as is the variation of $\cos^2\vartheta$ at small ϑ, viz. large L. Thus, (42) may be approximated by a linear differential equation

$$\frac{\partial}{\partial\nu}(\nu\,\frac{\partial\phi}{\partial\nu})\Big|_{\lambda_0} \simeq -\frac{r_0^3}{2\cos\vartheta_0(1+3\cos^2\vartheta_0)^{1/2}}\cdot(\gamma+1)[Q_A+Q_B(e\phi_\ell/kT_{\parallel -})]/\Sigma_P \qquad (43)$$

where ϑ_0 is evaluated at the center of the auroral arc. The linearity of the dependent variable ϕ_ℓ and the form of the differential operator on the left hand side of (43) suggest that we seek an approximate solution of (31) and (43) in separable form

$$\phi(L,s) = \varphi(s)\,\zeta(L)\ , \qquad (44)$$

where at the center of the auroral arc $L=L_0$, $\zeta(L_0) = 1$. Thus, $\varphi(s)$ is an electrostatic potential distribution along a given field line L and $\zeta(L)$ is a dimensionless shape factor directly related to the latitudinal distribution of the precipitation current.

Under the approximation (44), the problem reduces to the solution of coupled differential and transcendental equations. The structure equation is

$$\frac{\partial}{\partial L}\left(L\,\frac{\partial Y}{\partial L}\right) + \frac{\tilde{L}}{L^2}\,Y = 0 \quad , \tag{45}$$

where

$$Y = 1 + (Q_B/Q_A)\ (e\,\varphi_\ell\ /kT_{\parallel -})\,\zeta_L \tag{46}$$

and $\tilde{L}$, related to the latitudinal structure scale Λ_I by $\Lambda_I = \pi R_E/\tilde{L}^{1/2}$, is defined by

$$\tilde{L} = (\gamma+1)e^2 Q_B R_E^2\ \ /[2kT_{\parallel -}\,\Sigma_P \cos\vartheta_0 (1+3\cos^2\vartheta_0)^{1/2}\ ] \quad . \tag{47}$$

The normalization of the linear equation (45) is given by the requirement that $\zeta(L_0) = 1$ so that the potential drop along the field line at $L=L_0$ is φ_ℓ, indicated by particle data. Poisson's equation (31) becomes a transcendental algebraic equation

$$[(\gamma+1)J_\parallel(\ell)/2\cos\vartheta_0\,\Sigma_P]\ [B^2\,\varphi_s/B_\ell^{\,2}\,\varphi_\ell\ ]\ \ [1+\sum_j \frac{4\pi M_j c^2}{B^2}\ \tilde{n}_j(B/B_\ell\ ,\ \varphi_s\,\zeta_L)]$$

$$= 4\pi e\ \ \sum_j q_j\,\tilde{n}_j(B/B_\ell\ ,\ \varphi_s\,\zeta_L) \tag{48}$$

where, from (30),

$$J_\parallel(\ell) = -Q_A - Q_B\,[e\,\varphi_\ell\ \zeta_L/kT_{\parallel -}] \quad . \tag{49}$$

In the above equations, we have adopted the simplified notation for which the arguments of the functions φ and ζ are denoted as subscripts.

Examination of (45) and (48) indicates that the separable form (44) cannot possibly be a general solution of the problem. It is seen that from (45) and (46) the function ζ_L is uniquely determined in terms of the total central electrostatic potential drop φ_ℓ. This means that φ_s is to be determined from (48); however, (48) depends not only on φ_s but also on ζ_L. Therefore, for ζ_L determined from (45) there is no guarantee that a pure function of s, φ_s, can be found to satisfy (48). It is therefore surprising that such a φ_s can be found for a substantial range of L about $L=L_0$. A detailed numerical example, using particle data for an event observed by the S3-3 satellite as input, will be discussed in the next section.

To summarize our procedure of obtaining an approximate solution in separable form, we list the steps as follows:

a. The major parameters of the model, such as φ_ℓ and L_0, are determined by fitting our assumed form of particle distributions to the observed particle distributions at the center of the inverted -V event, $L=L_0$.

b. The structure equation (45) is solved to obtain ζ_L in the vicinity of L_0.

c. For each value of L in the vicinity of L_0, a solution " φ_s" is obtained from (48).

d. " φ_s" is an acceptable solution φ_s if it is invariant with respect to L in the vicinity of L_0 and if it satisfies the accessibility criteria set forth in Chiu and Schulz. If no such " φ_s" is found, minor parameters of the distribution

functions are adjusted and the procedure is repeated, but the fit to observed distributions in procedure (a) above is always maintained.

In general, such a tedious procedure cannot yield an acceptable φ_s unless L is in the immediate vicinity of L_0, or unless one assumes distribution functions dependent on L. We have not explored the latter alternative with much detail at present. Since the L-dependence of particle distributions at the equator is intimately related to the question of the equatorial structure of injected magnetospheric plasma and the question of auroral current return flows, we consider this to be a suitable subject for a future communication. We have, however, investigated the possibility that some of the parameters of (43), such as the ionospheric integrated Pedersen conductivity Σ_P, may be functions of L. Although we have solved the structure function equation for several of these cases, the complications that they induce in the procedure for obtaining a self-consistent φ_s severely limit their applicability without significant compensatory increase of the range of validity of the solution. It is not clear to us at this point whether this is due to the limited validity of the separable form or of uniform distribution functions, or both.

IV. EXAMPLE OF A QUIET ARC

Before we proceed to consider the available data for the modeling of a quiet arc, we shall set forth the practical approximations to the formal Bessel function solutions to the structure equation (45).

$$Y(L) \propto J_0 (2 \ (\tilde{L}/L)^{1/2}) , \tag{50}$$

where J_0 is the Bessel function of zero order and the constant of proportionality is to be determined by $\zeta(L_0) = 1$ at the center of the arc $L = L_0$. Examination of the numerical values of L reveals that $\tilde{L} \sim 10^4$ whereas $L_0 \sim 10$, therefore, the argument of J_0 in (50) is sufficiently large for a typical arc that the sinusoidal approximation for Y and dY/dL is valid in the vicinity L_0.

We obtain, for practical purposes, the electrostatic potential

$$\phi(L,s) = \varphi(s)\, \zeta(L) , \tag{51}$$

where

$$\zeta(L) \simeq [1 + c_Q] \cos [\frac{L-L_0}{L_0} \ (\tilde{L}/L_0)^{1/2}] - c_Q . \tag{52}$$

The constant c_Q is given by

$$c_Q = (Q_A/Q_B)\, (kT_{\parallel -}/e\, \varphi_l) . \tag{52}$$

The perpendicular electric field is

$$\vec{E}_{\perp} = - \frac{\hat{\nu}}{h_{\nu}} R_E(\tilde{L}L_0)^{1/2} [1 + c_Q] \varphi(s) \sin\left(\frac{L-L_0}{L_0} (\tilde{L}/L_0)^{1/2}\right), \quad (53)$$

where $\hat{\nu}$ is a unit vector in the ν-coordinate direction. The parallel electric field in dipolar measure is

$$E_{\parallel}^{\lambda} = - \frac{\hat{\lambda}}{h_{\lambda}} \left(\frac{\partial s}{\partial \lambda}\right) \zeta(L) \frac{\partial \varphi}{\partial s} , \quad (54)$$

although one usually uses the conventional parallel electric field in s-coordinate measure, in which case,

$$E_{\parallel}^{s} = - \hat{s} \zeta(L) \frac{\partial \varphi}{\partial s} . \quad (55)$$

Both (54) and (55) are computed from our numerical approximate solution $\varphi(s)$. Henceforth, we shall follow the conventional s-coordinate measure and refer to (55) as the parallel electric field with the s superscript suppressed.

For an example of modeling the electrostatic structure of a quiet auroral arc, we choose an event for which particle distributions were observed with satellites at high and low altitudes about an hour apart [Mizera and Fennell, 1977; Croley et al., 1978]. With data from two measurements we not only have a consistency check of the data but also obtain an idea of the adequacy of the particle distributions assumed in our model to fully account for the observations. In Figure 1 we show the electron energy flux data observed at 7300 km over the northern auroral region for different pitch angles by the S3-3 satellite on August 12, 1976. Figure 2 shows electron energy flux data for essentially the same event observed at 275 km over the southern auroral region by the

same satellite. The solid (0^{o} pitch-angle) and dashed (180^{o} pitch-angle) curves show a fit of the low-altitude data set with our model distribution functions, assuming that there is a total potential drop of 3 kV between the equator and the baropause at L_0=8.35 (invariant latitude of 69.75^{o}). The assumptions of arc location and dipolar field lines are at slight variance with the actual location (70.6^{o}) and with the fact that the Earth's magnetic field is not a dipole, but these factors are not crucial to the physics of the model. A self-consistent solution for $\varphi(s)$ at L_0 is obtained and the structures of $\phi(s,L_0)$ and $E_{\parallel}(s, L_0)$ are shown in Figure 3. The electron distributions at pitch-angles of 0^{o}, 90^{o}, and 180^{o} at 7300 km are shown as solid, dotted and dashed curves, respectively on Figure 1. In effect, the particle distributions on Figure 1 are "predicted" by our model at L_0 for which the inputs consist of the data on Figure 2 and assumptions about the shape and existence of particle populations. From Figure 1, it is seen that the structures of particles at 0^{o} and 180^{o} pitch-angles are consistent with our model. Note that because of the higher altitude, the parallel potential drop is only about 0.85 keV, in agreement with the data. The distribution of electrons at 90^{o} pitch-angle include trapped electrons, indicated by the spike in the dotted curve, as well as the regular magnetospheric and backscattered electrons. The data for 90^{o} pitch-angle (crosses) do not show a spike as in the model; however, the data clearly show evidence of a trapped electron population since there is no signature of a break at 0.85 kV for the 90^{o} pitch-angle distribution, which would be required if only magnetospheric and backscattered electrons are involved. Evidently, our assumed trapped electron distribution is not a good representation of the data. It must be noted however, that the total number of trapped electrons required to produce the solution of Figure 3, the integrated flux under the spike, is in good agreement with the 90^{o} pitch-angle data below 0.85 kV. In other words, our assumed trapped electron distribution is too narrow in energy spectrum. We

have not experimented with other distributions for the trapped electrons; however, this is an area which may need further development. A similar situation also exists for ions at 180° pitch-angle (upward moving) observed at 7300 km, whose distribution is shown on Figure 4. In this case, the data clearly show a sharp peak at ~2.2 kV, although the width of the peak is clearly too broad to be in agreement with a Maxwellian with ionospheric temperatures. In our model, which is collisionless, ions may be accelerated from the ionosphere by the parallel electric field, but they may not change their temperatures. Consequently, the model prediction is a sharp spike with a temperature of ~0.1 eV at the position of the arrow on Figure 4. Unlike the case of trapped electrons, the integrated ion flux in the model seems to be too large also. If we take the two discrepant features discussed above seriously, we may argue that these are indications that particles orginating fom the baropause, the upward moving ion beam and trapped electrons, may have undergone dynamical processes not included in our collisionless model. Interactions with a region of plasma turbulence, always observed to be associated with arcs, may be a good candidate. Perhaps the turbulence is generated by the ion beam itself. Such considerations are beyond the scope of this paper.

Having obtained a semi-quantitative description of the observed signatures of particle distributions in the center of an inverted -V event, we may now proceed with steps b, c, d and their iterations in order to obtain an approximate solution $\phi(s,L)$. Prior to discussing our results, let us recapitulate that the model results at L_0 (Figs. 1, 3, and 4) are obtained with the input shown on Figure 2.

Figure 5 shows the distributions of the electrostatic potential $\phi(\ell,L)$ and the north-south perpendicular electrostatic field $E_\perp(\ell,L)$ as functions of L (or invariant latitude, or linear distance from L_0=8.35) at the baropause $s=\ell$. A separable form (51)

of the approximate solution has been shown to be self-consistent by the solution steps b, c and d and their iterations over the range of L-values from L_0 to L_4. The potential and perpendicular electric fields from L_0 to L_4 are indicated as solid and dashed curves respectively on Figure 5. Outside of L_4, we have not been able to verify the self-consistency of the solutions to the structure equation (52). These regions are marked with cross hatches on Figure 5. Aside from this imperfection, there are three physical features of the electrostatic potential structure on Figure 5 which we consider to be significant. First, the structure of the verified portions of the electrostatic potential $\phi(\ell, L)$ clearly indicates an electrostatic field scale length of ~50 km in the quiet auroral arc, in agreement with observations. It is of crucial importance to note that this auroral scale as manifested in the parameter $\tilde{L}$ (47) depends on the auroral current $J_{\parallel}(\ell)$ (49) through the parameter Q_B and on the ionospheric conductivity Σ_P. This is quite unlike Swift's shock solution for which the auroral scale length is assumed at the outset. Second, the magnitude of the perpendicular electric field (53) is also dynamically related to the parallel potential drop $\varphi(\ell)$ and the auroral current through the parameter c_Q. The numerical value of ~100 V/km is in good agreement with observations. Third, the structure of the perpendicular electric field indicates a field reversal at the center of the arc L_0. This feature is again in agreement with observations.

The electrostatic structure shown on Figure 5 is calculated for the event of August 12, 1976. Unfortunately, there were no electrostatic field observations for this event, which was rich in particle observations. Observed electrostatic structures for other typical quiet arcs exhibiting similar particle distribution features described in the foregoing are available. Figure 6 shows a simultaneous observation of electron, proton and electrostatic structures as the S3-3 satellite crosses several arc structures. (It is

possible that there was only one arc structure but there were multiple crossings.) Figure 7 shows an expand view of the electrostatic structure for the period indicated by the brace in the middle of Figure 6. It is evident that the perpendicular electrostatic field structure corresponding to the proton beam and electron inverted -V events on Figure 6 are similar to that shown on Figure 5.

Figure 8 shows the altitude dependence of electrostatic potentials at the field lines L_0, L_1 L_2 and L_3, defined on Figure 5. The altitude dependences of the perpendicular electric fields for the reconstructed event of August 12, 1976 at L_1, L_2 and L_4 are shown on Figure 9. It should be noted that at 7000 km the magnitude of the north-south perpendicular electric field is ~30 V/km, considerably below that shown on Figures 6 and 7. However, the parallel potential drops for the events of July 29, 1976 (Figure 7) are considerably higher than 3 kV, ranging from 10 kV to above 30 kV. Thus, we would expect larger perpendicular electric fields for the July 29, 1976 event from our model. Finally, Figure 10 shows the altitude dependence of the parallel electric field for the event of August 12, 1976 at the locations L_0, $L_2$and L_4. The parallel electric field maximizes at higher altitudes as one moves away from the center of the arc. The strength of the parallel electric field in our model is well below 1 V/km.

V. CONCLUSIONS

In this paper we have attempted to unify, formally and in a semiquantitative model of a quiet auroral arc, several elements of auroral physics, which have been separately recognized but have never been joined together into a coherent mechanism to study the physical scales and properties of auroral features. We use the collisionless time-independent Poisson equation to approximate the relationship between particle and electrostatic field (both perpendicular and parallel components) distributions in a quiet auroral arc. This element of our work is a generalization of Swift's [1975, 1976] work in that the structure of an inhomogeneous magnetic field and the semiquantitative characterisites of various particle populations [Chiu and Schulz, 1978] in an auroral flux tube are included. The physics of charge balance in the high-altitude auroral region (the Poisson equation) is coupled to the field-aligned current, which is related to the high-altitude particle and electrostatic field distributions on the one hand and is controlled by the ionospheric conductivity on the other. In this way, we have coupled the bulk ionospheric properties, usually discussed in MHD models of auroral currents, to the particle and field properties of auroral arcs. The result is a fairly accurate representation of the particle and field data taken by the auroral satellite S3-3 at some thousands of kilometer altitude. These include the relationships between the signatures of the parallel electrostatic potential drop in the auroral arc and the magnitude and signatures of the perpendicular electrostatic field. In particular, a major new feature is the self-consistent prediction of latitudinal spatial structure in an auroral arc near and above the ionosphere, even if the particle distributions at equatorial regions of the auroral field lines are assumed spatially homogeneous. The predicted scale length for the perpendicular electric field is tens to perhaps one or two hundred kilometers, more or less in agreement with observations of

the largest-sized features of discrete auroral arcs. This scale length, related to the parallel electrostatic potential drop and the ionospheric conductivity, arises as result of the coupling between the magnetospherically-driven field-aligned current and the ionosphere; it is quite distinct from the assumed ion Larmor radius transverse scale of Swift, who did not couple ionospheric physics into his model. The scale length of the parallel electric field distribution, however, is of order of thousands of kilometers, yielding parallel electrostatic fields below 1 V/km, while the total potential drop along the flux tube is in agreement with particle observations. Because of these features of our electrostatic potential structure, our model may be considered to be a shock solution with a large parallel scale length and a small perpendicular scale length. It is to be distinguished from shocks of the double layer type which have extremely short (Debye length) parallel scale lengths and undetermined perpendicular scale lengths.

Needless to say, the foregoing calculations do not settle the question of auroral arc structure; we have left out such possibly important physics as wave turbulence and anomalous resistivity, feedback currents, and most particularly we cannot yet model the return current. This is in part a mathematical problem and in part a problem of physics. The mathematical difficulty is breakdown of the self-consistency of the factorizability assumption in the return-current region, while in the physics we have left out a treatment of return current paths in the magnetosphere as well as buildup of negative charge in the ionosphere, which must be an important driving force for the return current. We hope to return to these problems later.

ACKNOWLEDGMENT

We appreciate fruitful discussions with J. Lemaire, E. C. Whipple, M. Schulz, P. F. Mizera, J. F. Fennell and D. R. Croley. Further, we thank F. S. Mozer and R. B. Torbert for the use of their electric field data.

REFERENCES

Alfvén, H., and C.-G. Fälthammar, Cosmical Electrodynamics, pp. 163-167, Clarendon, Oxford, 1963.

Atkinson, G., Auroral Arcs: Result of the Interaction of a Dynamic Magnetosphere with the Ionosphere, J. Geophys. Res., 75, 4796, 1970.

Block, L. P., Double Layers, in Physics of the Hot Plasma in the Magnetosphere, ed. B. Hultqvist and L. Stenflo, Plenum Press, N.Y., 1975.

Chiu, Y. T., and M. Schulz, Self-Consistent Particle and Parallel Electrostatic Field Discontinuities in the Magnetospheric-Ionospheric Aurroral Region, J. Geophys. Res., 83, 629, 1978.

Cloutier, P. A., B. R. Sandel, H. R. Anderson, P. M. Pazich, and R. J. Spiger, Measurement of Auroral Birkeland Currents and Energetic Particles, J. Geophys. Res., 78, 640, 1973.

Coroniti, F. V., and C. F. Kennel, Polarization of the Auroral Electrojet, J. Geophys. Res., 77, 2835, 1972.

Croley, D. R., Jr., P. F. Mizera, and J. F. Fennell, Signature of a Parallel Electric Field in Ion and Electron Distributions in Velocity Space, J. Geophy. Res., 83, 2701, 1978.

Cummings, W. D., R. J. O'Sullivan, and P. J. Coleman, Jr., Standing Alfvén Waves in the Magnetosphere, J. Geophys. Res., 74, 778, 1969.

Evans, D. S., Precipitating Electron Fluxes Formed by a Magnetic Field-aligned Potential Difference, J. Geophys. Res., 79, 2853, 1974.

Evans, D. S., Evidence for Low Altitude Acceleration of Auroral Particles, in Physics of Hot Plasmas in the Magnetosphere, ed. B. Hultqvist and L. Stenflo, pp. 319-340, Plenum Press, N. Y., 1975.

Frank, L. A., K. L. Ackerson, and D. M. Yeager, Observations of Atomic Oxygen (O^+) in the Earth's Magnetotail, J. Geophys. Res., 82, 129, 1977.

Ghielmetti, A. G., R. G. Johnson, R. D. Sharp, and E. G. Shelley, The Latitudinal, Diurnal and Altitudinal Distributions of Upward Flowing Energetic Ions of Ionospheric Origin, Geophys. Res. Letters, 5, 59, 1978.

Holzer, T. E., and T. Sato, Quiet Auroral Arcs and Electrodynamic Coupling Between the Ionosphere and the Magnetosphere, 2, J. Geophys. Res., 78, 7330, 1973.

Hudson, M. K., R. L. Lynch, and F. S. Mozer, Magnetic Field-aligned Potential Drops due to Electrostatic Ion Cyclotron Turbulence, Geophys. Res. Letters, 5, 143, 1978.

Hudson, M. K., and F. S. Mozer, Electrostatic Shocks, Double Layers, and Anomalous Resistivity in the Magnetosphere, Geophys. Res. Letters, 5, 131, 1978.

Kan, J. R., Energization of Auroral Electrons by Electrostatic Shock Waves, J. Geophys. Res., 80, 2089, 1975.

Kindel, J. M., and C. F. Kennel, Topside Current Instabilities, J. Geophys. Res., 76, 3055, 1971.

Lemaire, J., and M. Scherer, Simple Model for an Ion-Exosphere in an Open Magnetic Field, Phys. Fluids, 14, 1683, 1971.

Lemaire, J., and M. Scherer, Ionosphere-Plasmasheet Field-aligned Currents and Parallel Electric Fields, Planet. Space Sci., 22, 1485, 1974.

Lennartsson, W., On High-latitude Convection Field Inhomogeneities, Parallel Electric Fields and Inverted-V Precipitation Events, Planet. Space Sci., 25, 89, 1977.

Mallinckrodt, A. J., and C. W. Carlson, Relations Between Transverse Electric Fields and Field-aligned Currents, J. Geophys. Res., 83, 1426, 1978

Maltsev, Y. P., W. B. Lyatsky, and A. M. Lyatskaya, Currents over the Auroral Arc, Planet. Space Sci., 25, 53. 1977.

Mizera, P. F., and J. F. Fennell, Signatures of Electric Fields from High and Low Altitude Particle Distributions, Geophys. Res. Letters, 4, 311, 1977.

Morse, P. M., and Feshbach, H., Methods of Theoretical Physics, Vol. 1, P. 21, McGraw-Hill, N. Y., 1953.

Mozer, F. S., C. W. Carlson, M. K. Hudson, R. B. Torbert, B. Paraday, J. Yatteau, and M. C. Kelley, Observations of Paired Electrostatic Shocks in the Polar Magnetosphere, Phys. Rev. Letters, 38, 292, 1977.

Ogawa, T., and T. Sato, New Mechanism of Auroral Arcs, Planet. Space Sci., 19, 1393, 1971

Papadopoulos, K., A Review of Anomalous Resistivity for the Ionosphere, Rev. Geophys. Space Phys., 15, 113, 1977.

Rostoker, G., and R. Bostrom, A Mechanism for Driving the Gross Birkeland Current Configuration in the Auroral Oval, J. Geophys. Res., 81, 235, 1976.

Sato, T., A Theory of Quiet Auroral Arcs, J. Geophys. Res., 83, 1042, 1978.

Sesiano, J., and P. A. Cloutier, Measurements of Field-aligned Currents in a Multiple Auroral-Arc System, J. Geophys. Res., 81, 116, 1976.

Shelley, E. G., R. D. Sharp, and R. G. Johnson, Satellite Observations of an Ionospheric Acceleration Mechanism, Geophys. Res. Letters, 6, 54, 1976.

Shawhan, S. D., C. G. Fälthammar, and L. P. Block, On the Nature of Large Auroral Zone Electric Fields at 1-R_E Altitude, J. Geophys. Res., 83, 1049, 1978.

Sato, T., and T. E. Holzer, Quiet Auroral Arcs and Electrodynamic Coupling Between the Ionosphere and the Magnetosphere, 1, J. Geophys. Res., 78, 7314, 1973.

Swift, D. W., On the Formation of Auroral Arcs and Acceleration of Auroral Electrons, J. Geophys. Res., 80, 2096, 1975.

Swift, D. W., An Equipotential Model for Auroral Arcs, 2, Numerical Solutions, J. Geophys. Res., 81, 3935, 1976.

Torbert, R. B., and F. S. Mozer, Electrostatic Shocks as the Source of Discrete Auroral Arcs, Geophys. Res. Letters, 5, 135, 1978.

Vondrak, R. R., Model of Birkeland Currents Associated with an Auroral Arc, J. Geophys. Res., 80, 4011, 1975.

Vondrak, R. R., H. R. Anderson, and R. J. Spiger, Rocket-based Measurements of Particle Fluxes and Currents in an Auroral Arc, J. Geophys. Res., 76, 7701, 1971.

Whipple, E. C., Jr., The Signature of Parallel Electric Fields in a Collisionless Plasma, J. Geophys. Res., 82, 1525, 1977.

Figure Captions

Figure 1. Electron energy flux data observed at 7300 km over the northern auroral region by the S3-3 satellite on August 12, 1976.

Figure 2. Electron energy flux data for essentially the event of Figure 1 but observed at 275 km over the southern auroral region by the S3-3 satellite.

Figure 3. Self-consistent solution for the structures of the electrostatic potential ϕ and parallel electric field $E_{\parallel}$ at the center of the arc L_0.

Figure 4. Upward moving ion energy flux observed at 7300 km over the northern auroral region by the S3-3 satellite on August 12, 1976.

Figure 5. Distributions of the electrostatic potential ϕ and the north-south perpendicular electrostatic field $E_{\perp}$ as functions of L at the baropause $s=\ell$.

Figure 6. Simultaneous observations of electron energy spectrum (E_e), ion energy spectrum (E_I) and perpendicular electrostatic field ($\mathcal{E}_y$) structures on July 29, 1976 by the S3-3 satellite. The brace in the middle of the figure shows the time period for which the electrostatic structure is shown as an expanded view on Figure 7.

Figure 7. Expanded view of the two perpendicular components of the electrostatic field for the period indicated by the brace in the middle of Figure 6. Day 211 is July 29, 1976.

Figure 8. Altitude dependence of electrostatic potentials at the field lines L_0, L_1, L_2 and L_3.

Figure 9. Altitude dependence of the perpendicular electric field for the reconstructed event of August 12, 1976 at L_1, L_2 and L_4.

Figure 10. Altitude dependence of the parallel electric field for the event of August 12, 1976 at the locations L_0, L_2 and L_4.

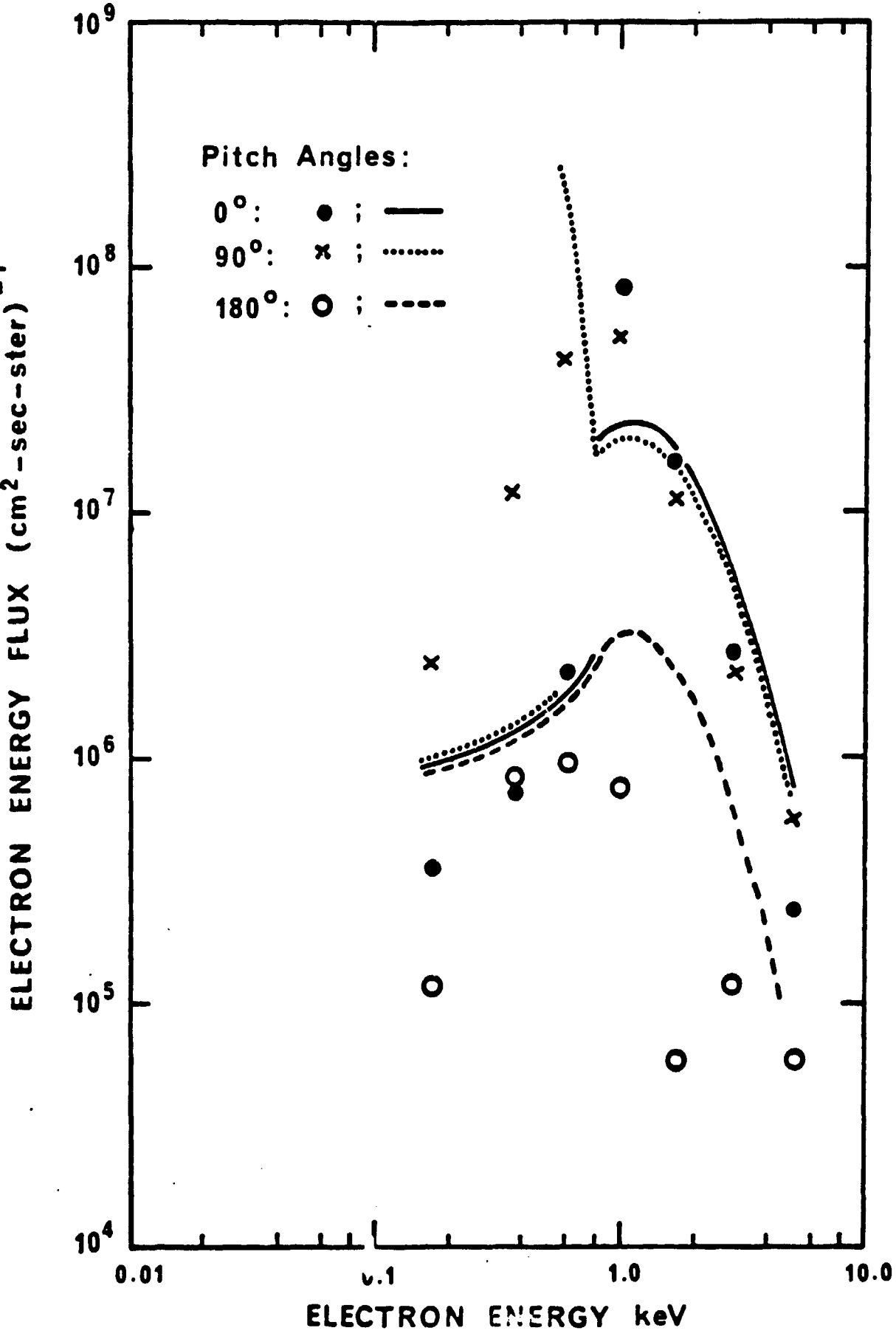
Pitch Angles:
0°: ● ; ——
90°: × ; ·····
180°: O ; - - -
ELECTRON ENERGY FLUX (cm²-sec-ster)⁻¹
10⁹
10⁸
10⁷
10⁶
10⁵
10⁴
0.01
0.1
1.0
10.0
ELECTRON ENERGY keV

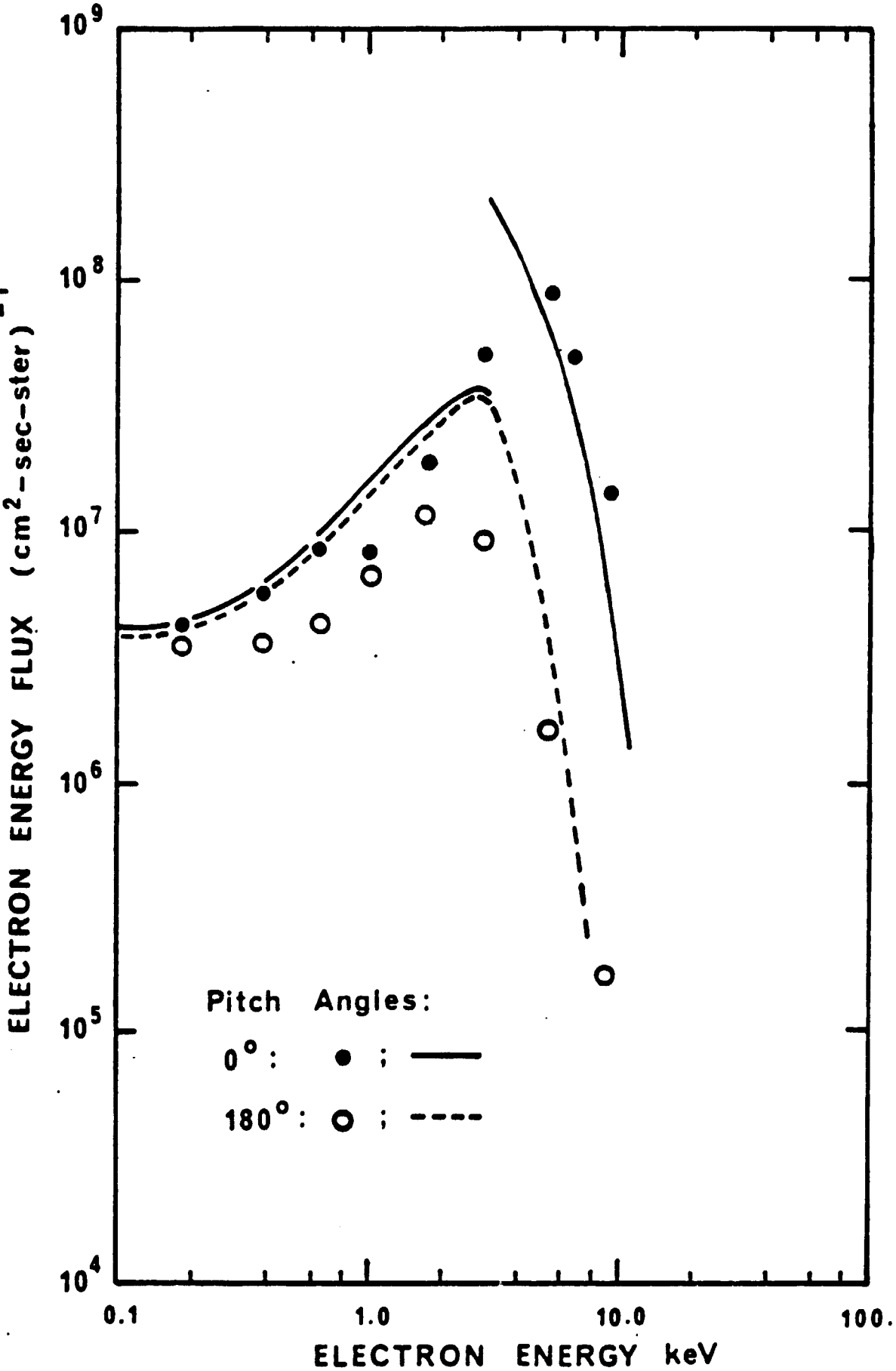
10^9
10^8
10^7
10^6
10^5
10^4
ELECTRON ENERGY FLUX (cm^2-sec-ster)$^{-1}$
Pitch Angles:
0°: ● ; ——
180°: ○ ; ----
0.1
1.0
10.0
100.
ELECTRON ENERGY keV

Fig. 2

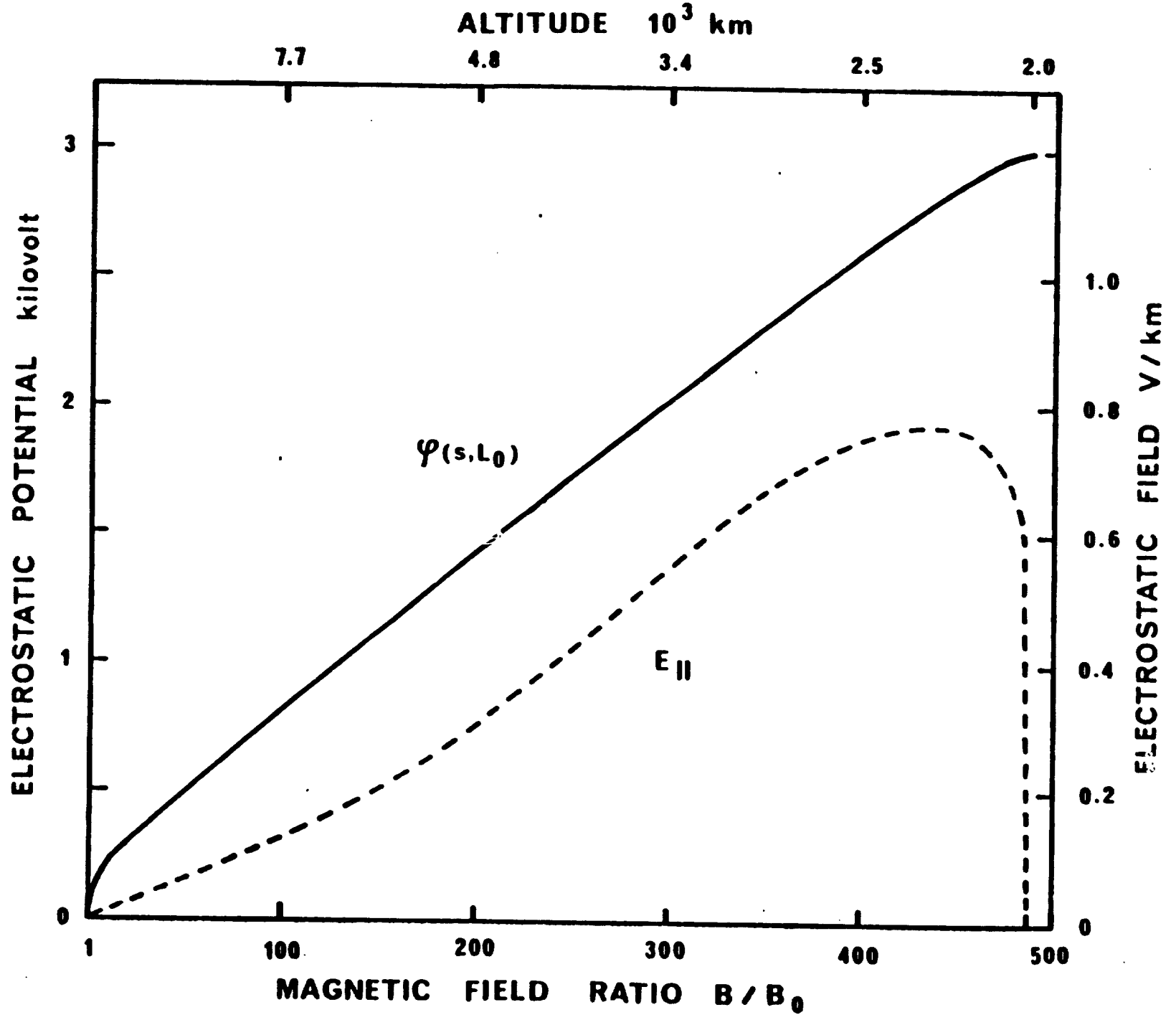
ALTITUDE 10^3 km
7.7
4.8
3.4
2.5
2.0
ELECTROSTATIC POTENTIAL kilovolt
ELECTROSTATIC FIELD V/km
$\varphi(s,L_0)$
E_{II}
0
1
2
3
0
0.2
0.4
0.6
0.8
1.0
1
100
200
300
400
500
MAGNETIC FIELD RATIO B/B_0

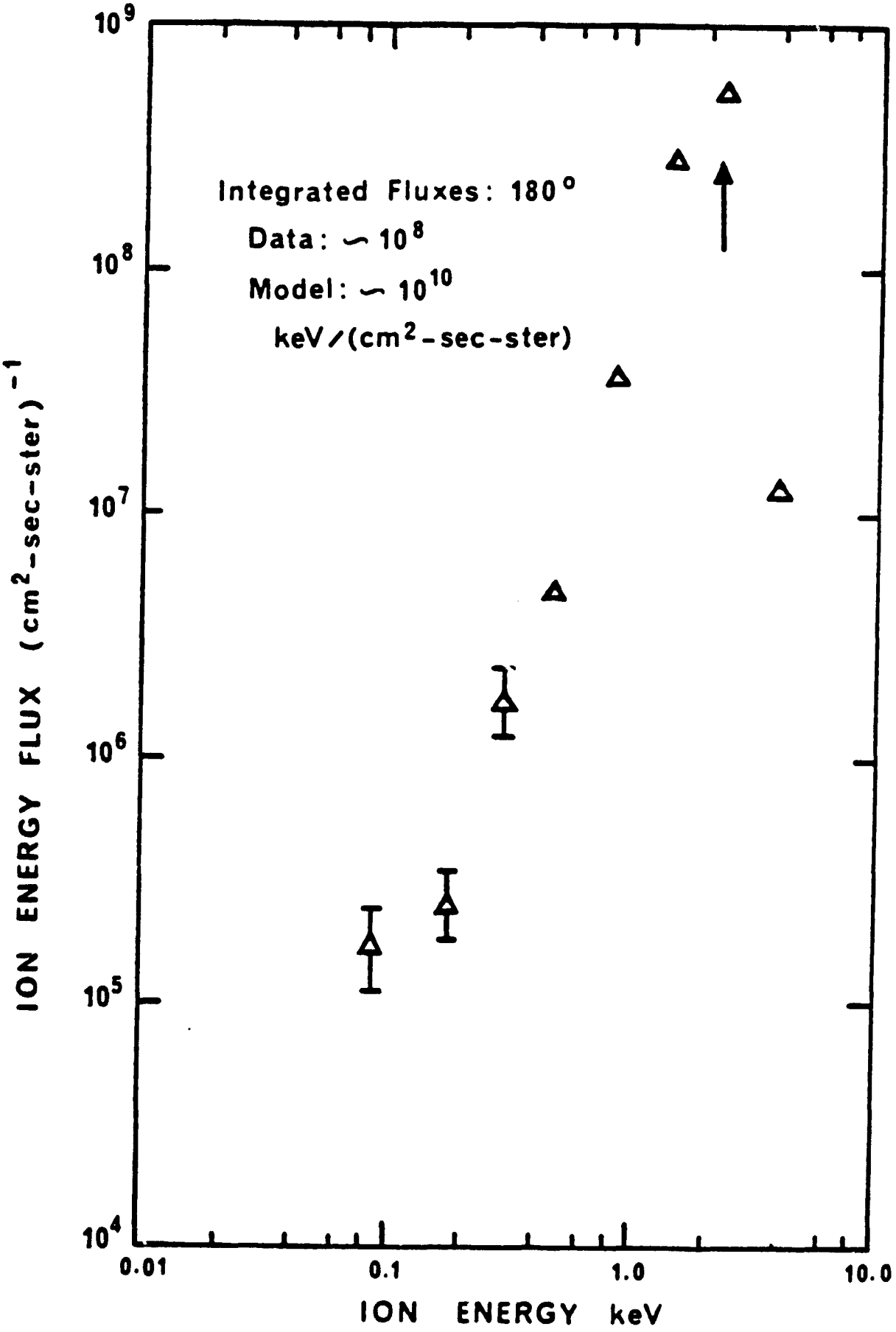
Integrated Fluxes: 180°
Data: ~ 10^8
Model: ~ 10^10
keV/(cm^2-sec-ster)
ION ENERGY FLUX (cm^2-sec-ster)^-1
10^9
10^8
10^7
10^6
10^5
10^4
0.01
0.1
1.0
10.0
ION ENERGY keV

Fig 4

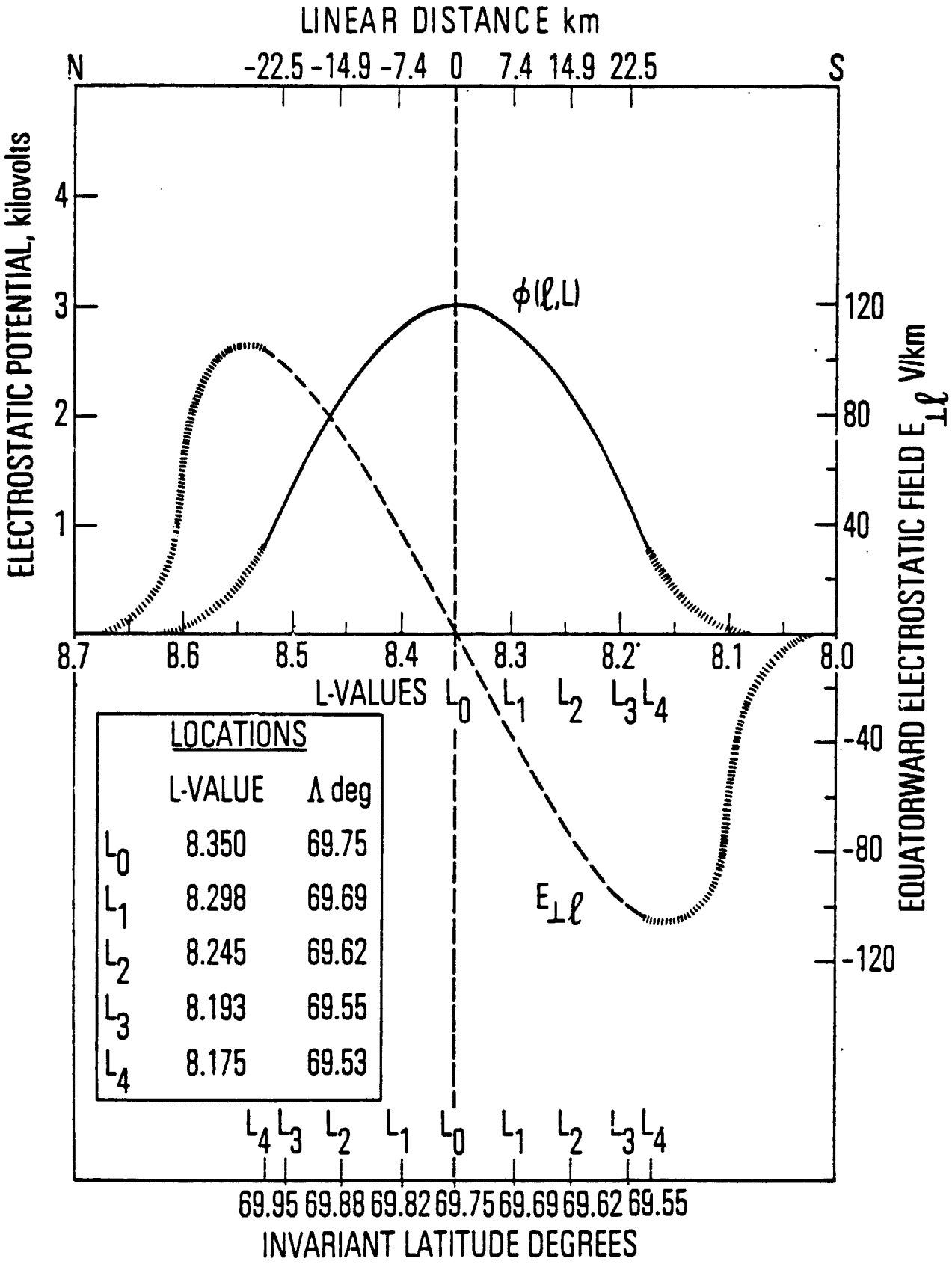
LINEAR DISTANCE km
N
-22.5 -14.9 -7.4 0 7.4 14.9 22.5
S
ELECTROSTATIC POTENTIAL, kilovolts
EQUATORWARD ELECTROSTATIC FIELD E⊥ℓ V/km
φ(ℓ,L)
E⊥ℓ
8.7 8.6 8.5 8.4 8.3 8.2 8.1 8.0
L-VALUES L0 L1 L2 L3 L4
LOCATIONS
L-VALUE Λ deg
L0 8.350 69.75
L1 8.298 69.69
L2 8.245 69.62
L3 8.193 69.55
L4 8.175 69.53
L4 L3 L2 L1 L0 L1 L2 L3 L4
69.95 69.88 69.82 69.75 69.69 69.62 69.55
INVARIANT LATITUDE DEGREES

Fig. 5

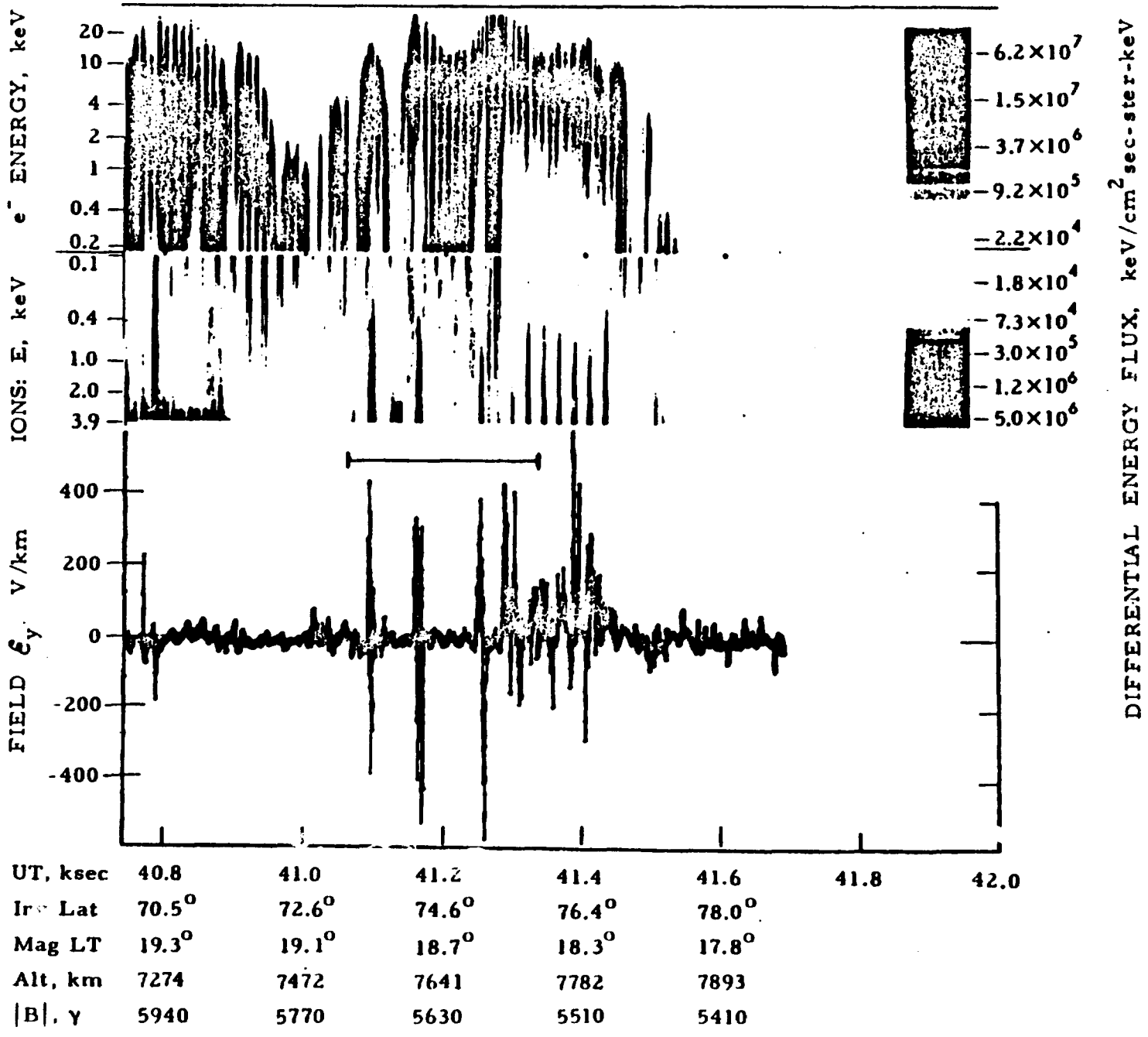
S3-3, 29 JULY 1976
e⁻ ENERGY, keV
20
10
4
2
1
0.4
0.2
0.1
IONS: E, keV
0.4
1.0
2.0
3.9
FIELD $\mathcal{E}_y$ V/km
400
200
0
-200
-400
6.2×10⁷
1.5×10⁷
3.7×10⁶
9.2×10⁵
2.2×10⁴
1.8×10⁴
7.3×10⁴
3.0×10⁵
1.2×10⁶
5.0×10⁶
DIFFERENTIAL ENERGY FLUX, keV/cm²sec-ster-keV
UT, ksec 40.8 41.0 41.2 41.4 41.6 41.8 42.0
Inv Lat 70.5° 72.6° 74.6° 76.4° 78.0°
Mag LT 19.3° 19.1° 18.7° 18.3° 17.8°
Alt, km 7274 7472 7641 7782 7893
|B|, γ 5940 5770 5630 5510 5410

Fig. 6

PERPENDICULAR ELECTROSTATIC FIELD COMPONENTS V/km
$E_{\perp Y}$
320
160
0
-160
-320
$E_{\perp X}$
340
180
0
-180
-340
SCALE: 50 km
40
100
160
220
280
340
S3-3 TIME sec FROM 41,000 sec OF DAY 211

Fig 7

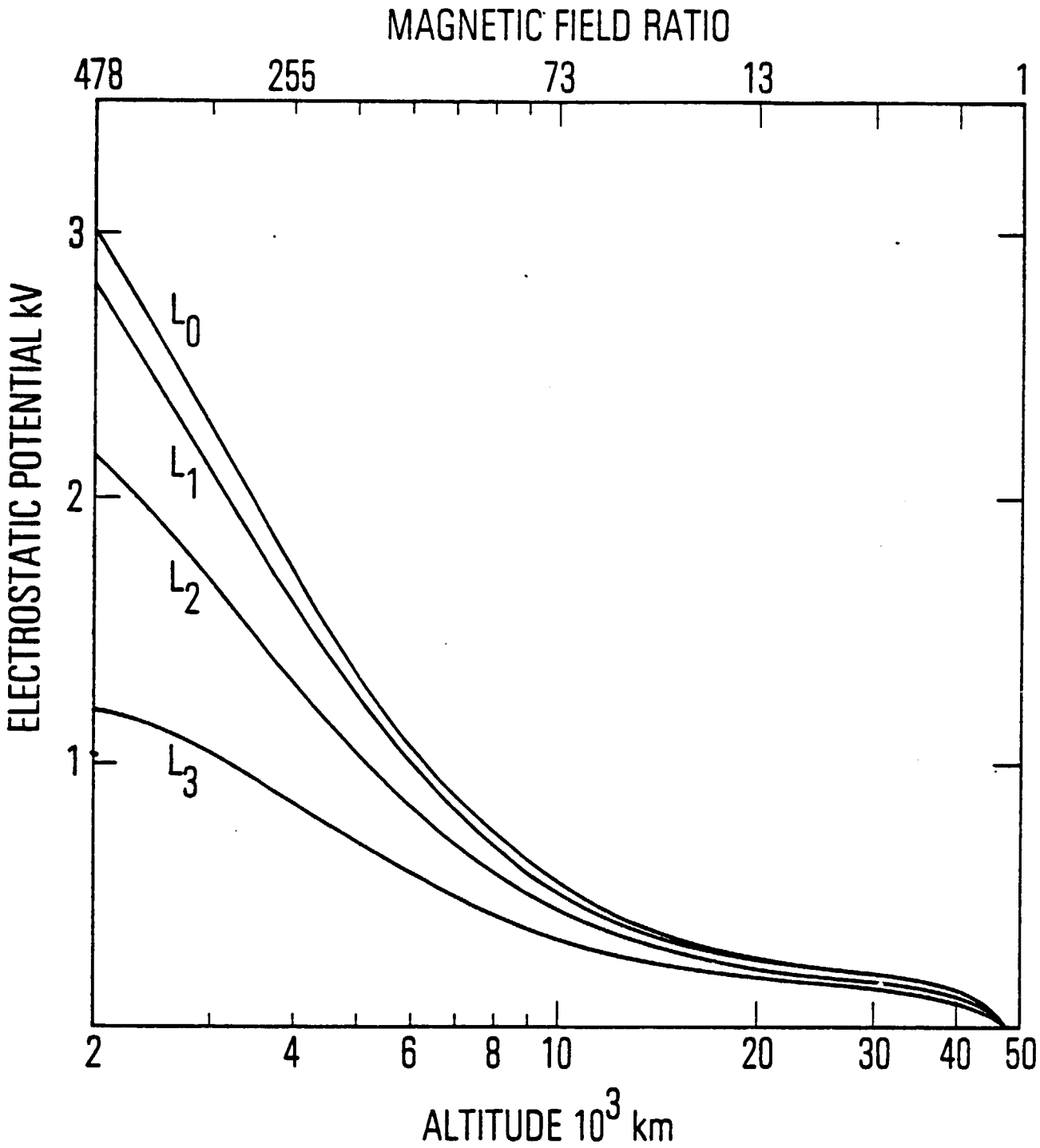
MAGNETIC FIELD RATIO
478
255
73
13
1
3
2
1
ELECTROSTATIC POTENTIAL kV
L_0
L_1
L_2
L_3
2
4
6
8
10
20
30
40
50
ALTITUDE 10^3 km

Fig. 8

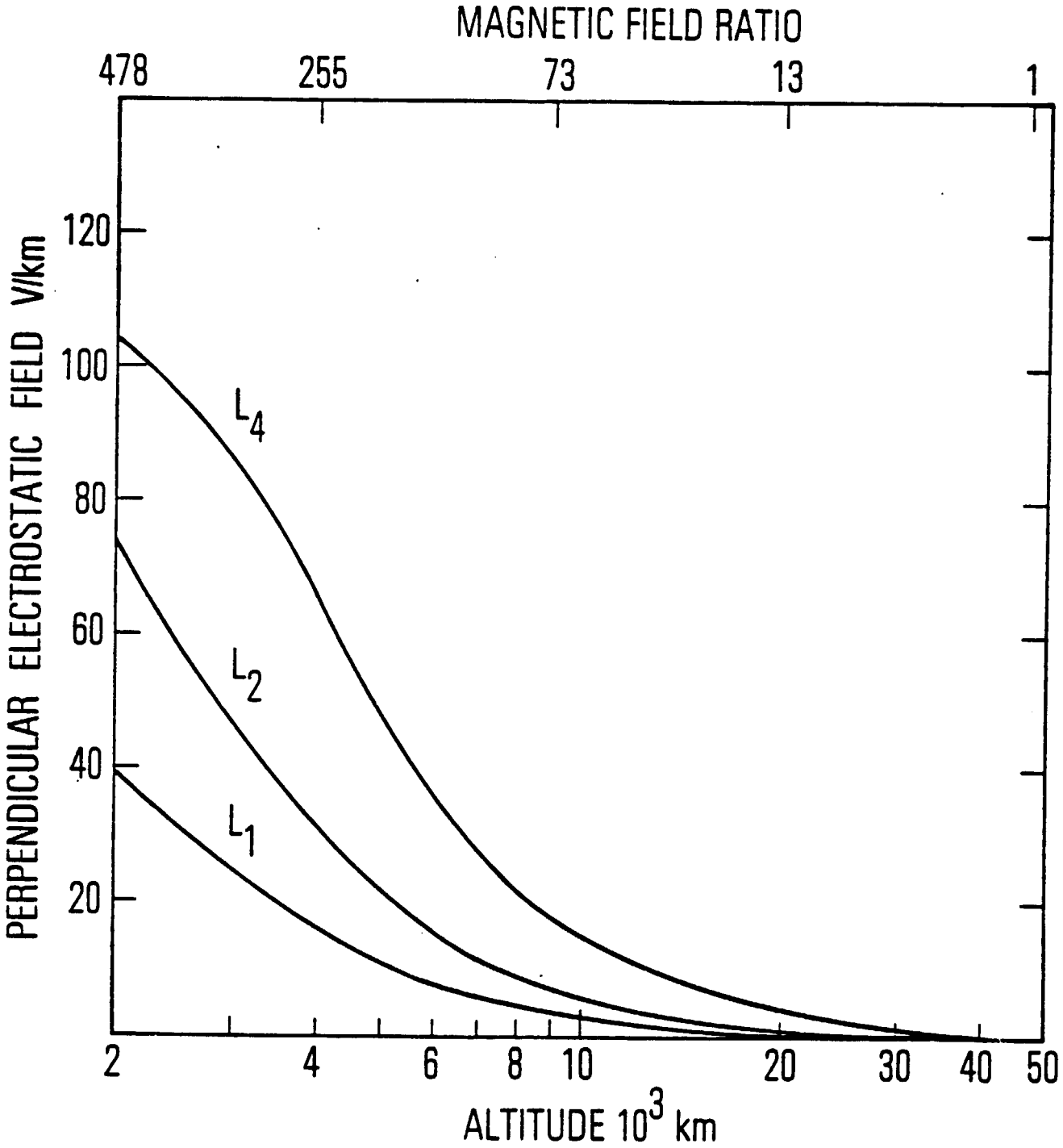
MAGNETIC FIELD RATIO
478
255
73
13
1
PERPENDICULAR ELECTROSTATIC FIELD V/km
120
100
80
60
40
20
L_4
L_2
L_1
2
4
6
8
10
20
30
40
50
ALTITUDE 10^3 km

Fig.9

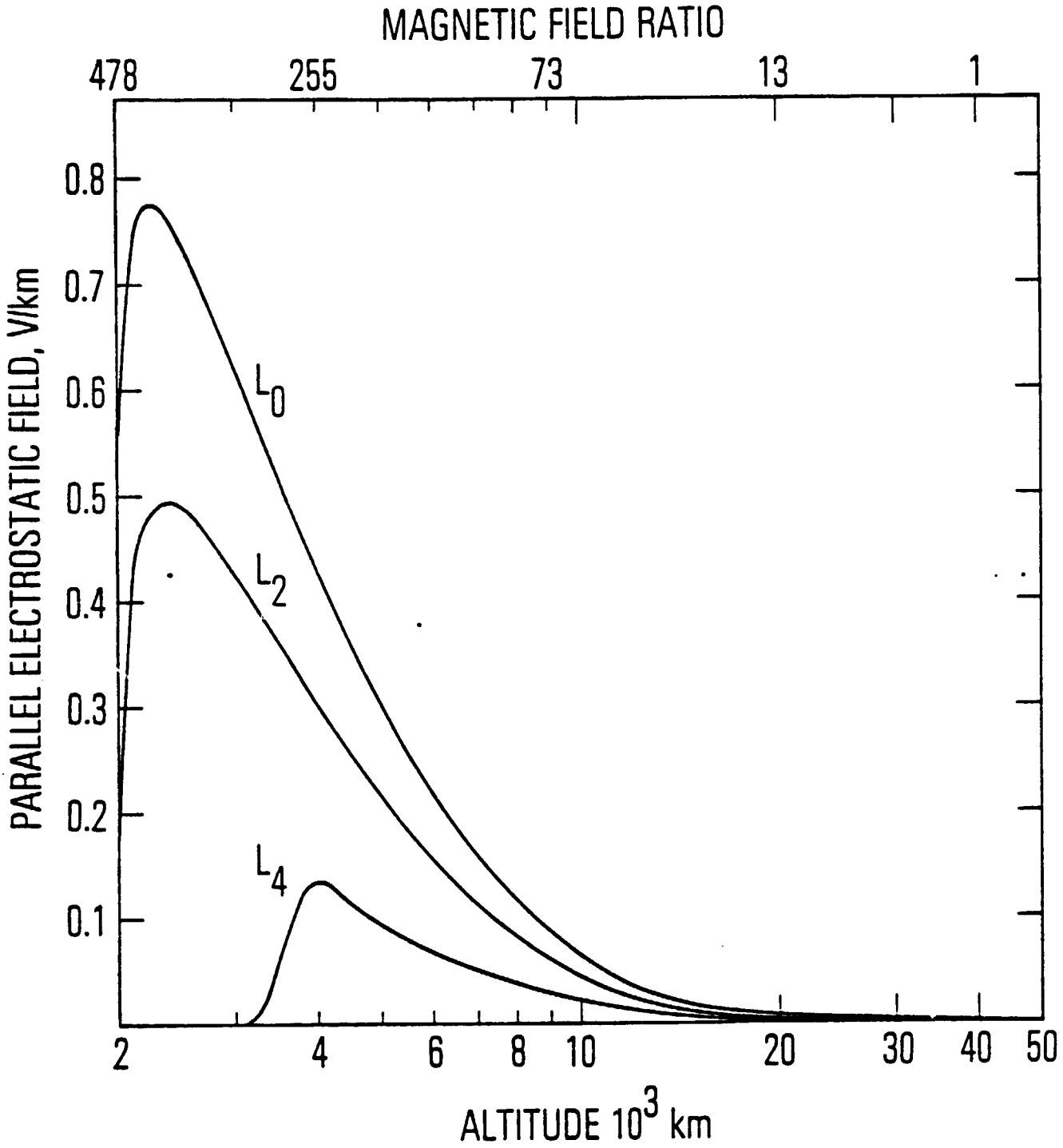
MAGNETIC FIELD RATIO
478
255
73
13
1
0.8
0.7
0.6
0.5
0.4
0.3
0.2
0.1
PARALLEL ELECTROSTATIC FIELD, V/km
L_0
L_2
L_4
2
4
6
8
10
20
30
40
50
ALTITUDE 10^3 km

Fig. 10

Space Sciences Laboratory
Report No. SSL-77(2960)-2

SELF-CONSISTENT PARTICLE AND PARALLEL ELECTROSTATIC FIELD DISTRIBUTIONS IN THE MAGNETOSPHERIC-IONOSPHERIC AURORAL REGION

by

Y. T. Chiu and Michael Schulz
Space Sciences Laboratory

The Ivan A. Getting Laboratories
THE AEROSPACE CORPORATION
Los Angeles, California 90009

MAY 1977

Published in:
Journal of Geophysical Research

This work is supported under U. S. Air Force SAMSO
Contract No. F04701-76-C-0077
and by The Aerospace Corporation Company Financed Research Program

SELF-CONSISTENT PARTICLE AND PARALLEL ELECTROSTATIC FIELD DISTRIBUTIONS IN THE MAGNETOSPHERIC-IONOSPHERIC AURORAL REGION

by

Y. T. Chiu and Michael Schulz
Space Sciences Laboratory
Ivan A. Getting Laboratories
The Aerospace Corporation
El Segundo, California 90245

ABSTRACT

The variation of the self-consistent electrostatic potential along the magnetic field is calculated by application of the principle of quasi-neutrality to the plasma components distributed along an auroral field line. The equilibrium plasma consists of hot anisotropic magnetospheric plasma, ionospheric plasma evaporated or extracted upwards by the parallel electrostatic field, and backscattered electrons. It is shown that the above charged-particle populations can support a potential difference of up to several kilovolts between the equator and the ionosphere along an auroral field line. Moreover, the corresponding parallel electric field has the proper signature to account for electron precipitation characteristics. Comparisons between theoretical and observed electron precipitation fluxes lead to estimates for the various physical parameters in the model.

INTRODUCTION

Nearly two decades of magnetospheric research have established that charged particles from the solar wind are energized inside the magnetosphere, although the mechanism of their energization is not yet precisely determined. Hot magnetospheric plasma are often observed (DeForest and McIlwain, 1971; and references therein) in the equatorial region on auroral field lines. Observations of energetic electrons at low altitudes on the same auroral field lines (Evans, 1975; and references therein) and, more recently, observations of energetic ions of ionospheric orgin (Hultqvist et al., 1971; Shelley et al., 1976; Mizera et al., 1976) confirm that magnetospheric and ionospheric plasmas interact strongly in the auroral region. In particular, beam-like pitch-angle and energy distributions are often observed and seem to indicate that such energetic particles have been accelerated or retarded by an electric field $\vec{E}$ parallel to the magnetic field $\vec{B}$. Moreover, it has been pointed out (Evans, 1975) that the characteristics of such energetic electron events may perhaps be roughly classified into two categories: (a) transient events for which the flux distributions indicate diffusive energy gain, and (b) quiescent quasi-static events for which the pitch-angle and flux distributions show a beam-like behavior. Since the magnetospheric plasma during a substorm event is highly disturbed, the existence of the first category of event is not at all surprising; the diffusive energy gain might be associated with the anomalous resistance that can occur along a magnetic field line as consequence of several instability mechanisms (e.g., Perkins, 1968; Kindel and Kennel, 1971; Papadopoulos and Coffey, 1974). The

second category of event, which does not show diffusive energy gain, seems to require a quasi-static electric potential difference of up to several kilovolts between the ionosphere and the equator in order to account for the beam-like behavior of electron flux distributions. Although a parallel electric field can arise as the result of mapping perpendicular electric fields downward into the ionosphere, where collisional resistance along and collisional conductance across the magnetic field may become important (Chiu, 1974), such a process is limited to the lower ionosphere and cannot account for the beam-like characteristics of energetic-electron precipitation. In regions of open field lines, charge-separation effects related to the polar wind also give rise to a parallel electric field (Banks and Holzer, 1968); however, the magnitude of such a total potential drop is far less than the potential differences of up to several kilovolts that are inferred to occur between the ionosphere and the equator along certain (presumably closed) auroral field lines. Thus, the evident existence of quasi-static parallel electric fields in the auroral region remains a puzzle in auroral physics. In this paper we propose to consider the origin of such parallel electrostatic fields and their mutual consistency with auroral plasma.

Basically, there are two mechanisms by which a quasi-static electric potential difference V_{ℓ} can be established along a magnetic field line in a collisionless plasma. On the one hand, one can appeal to quasi-stable double layers that have been produced in bounded laboratory plasmas (Quon and Wong, 1976) in which there are interpenetrating plasma streams involving ions and

electrons reflected from the walls. Although it has been conjectured (Block, 1975) that such double layers may also exist in the magnetosphere, where plasma boundaries are somewhat amorphous, we shall temporarily defer consideration of the double-layer mechanism until its existence and stability can be verified for magnetospheric plasma. On the other hand, Alfvén and Fälthammar (1963, pp. 163-167) have pointed out that an anisotropic collisionless plasma in a magnetic field can be in quasi-neutral equilibrium without a parallel electric field only if the magnetic field is homogeneous or if the pitch-angle anisotropy is the same for both electrons and ions. Otherwise, in the case of a dipolar magnetic field such as the earth's, the absence of a parallel electric field would result in different distributions of ions and electrons along the field line if the equatorial anisotropies of the particles were different. Conversely, charge neutrality of the plasma along the magnetic field line demands that an electrostatic field be established parallel to the magnetic field line. The electrostatic potential energy difference $|e|V_{\ell}$ between the ionosphere (where $B = B_{\ell}$) and the equator (where $B = B_0$) is estimated to be of the order of the mirror ratio B_{ℓ}/B_0 multiplied by the mean perpendicular particle energy (Alfvén and Fälthammar, 1963; Persson, 1966), i.e., to be of the order of hundreds of keV for plasma in an auroral flux tube. However, the magnetospheric-ionospheric flux tube along an auroral field line contains not only anisotropic magnetospheric plasma, but also thermal plasma extracted or evaporated from the ionosphere and back-scattered electrons of intermediate energy. Since the various components

of colder plasma (here assumed isotropic at the foot of the field line) are expected to participate in the maintenance of charge neutrality, we would expect the above estimates of electrostatic potential difference along an auroral field line (Alfvén and Fälthammar, 1963; Persson, 1966) to be unrealistically large. Indeed, calculations of the parallel electric field by application of the principle of quasi-neutrality (Lemaire and Scherer, 1973) yielded electrostatic potential differences of only a few volts between the ionosphere and the equator, although the effects of backscattered electrons and of pitch-angle anisotropy for magnetospheric plasma were ignored in those calculations. In view of the importance of the question, we have undertaken to re-examine the conditions which define quasi-neutrality for auroral plasma, especially for flux tubes in the high latitude trough region of the ionosphere, poleward of the plasmapause, where the energetic electron observations have been made.

In this paper, we apply the principle of quasi-neutrality to calculate the mutually consistent electrostatic potential and particle distributions along an auroral field line which is populated by collisionless anisotropic magnetospheric plasma and by plasma extracted or backscattered from the ionosphere. It is shown that a potential difference of up to several kilovolts between the equator and the ionosphere may thus be maintained along an auroral field line. While the parallel electric field has the proper signature to account for electron precipitation characteristics (Evans, 1975), it also may self-consistently account for the presence of O^+ ions with keV energies at the upper reaches of auroral field lines (Shelley et al., 1976).

Even though our calculation is similar to that of Lemaire and Scherer (1973, 1977), there are a number of crucial differences which combine to yield a larger potential drop along the field line in our work than in theirs. Among these, three essential factors peculiar to auroral field lines in the trough region are most important in accounting for the differences; indeed these may also explain why the beam-like characteristics of energetic particles are not observed elsewhere. First, as has been pointed out by Alfvén and Fälthammar (1963), different anisotropies for electrons and protons are crucial to the maintenance of a large potential drop along the field line. Since ring-current particles injected onto the auroral field line are expected to be anisotropic in pitch angle, we preserve such a feature in our calculation. Second, copious backscattered electrons are observed and must be considered in a quasi-neutrality calculation. Third, the number density of thermal ions at the ionosphere is an important boundary condition on the problem, since the ions are accelerated upward by the same parallel electric field that accounts for downward acceleration of electrons. Since the trough region of the ionosphere is considerably depleted relative to the average ionosphere, it is expected that the effect of the ionospheric plasma, which has a tendency to reduce the potential difference along a magnetic field line, is correspondingly minimized.

We shall show that in our model the energetic electron flux and pitch-angle distributions at the foot of the field line are essentially similar to those found in the previous model (Evans, 1975) for electron precipitation under the influence of arbitrarily postulated parallel electric fields.

In our calculation, however, we require that the electrostatic potential be a solution to the quasi-neutrality equation, and this requirement is found to be an important constraint on the admissibility of the electrostatic potential, otherwise postulated, for the problem. It should be noted that our approach, though yielding similar flux distributions at the foot of the field line, is basically different from Evans' approach. In Evans' model, the beam-like characteristics of precipitating electrons are attributed to the collimation of an isotropic electron population by an arbitrarily imposed parallel electric field. In our model, the parallel electric field arises naturally as a consequence of the quasi-neutrality requirement imposed on the various particle populations, some of which are assumed to be anisotropic at the equator. Thus, the mapping relationships between electron anisotropy and parallel electric field for the two models are different.

QUASI-NEUTRALITY

The principle of quasi-neutrality is commonly employed in problems of the present type (e.g., Lemaire and Scherer, 1973). One considers a dipolar magnetic flux tube in which the magnitude of $\vec{B}$ varies monotonically from B_0 at the equator to B_ℓ at the foot, which is located at an appropriate altitude to be discussed below. We construct a kinetic model in which the ion and electron distribution functions, f_+ and f_-, are expressed analytically in terms of the velocity components $v_\perp$ and $v_\parallel$ relative to $\vec{B}$, in terms of the local electrostatic potential $V_s \equiv V(s)$, and in terms of the local magnetic intensity $B_s \equiv B(s)$, where s is the coordinate that measures arc length of the field line from the equator. The principle of quasi-neutrality asserts that

$$\int_0^\infty v_\perp \, dv_\perp \int_{-\infty}^{+\infty} [\, f_+(v_\parallel, v_\perp; V_s) - f_-(v_\parallel, v_\perp; V_s) \,] \, dv_\parallel = 0 \,. \tag{1}$$

For our model, in which f_+ and f_- are explicitly constructed, we interpret (1) as an equation for the value of V_s at any point s along the field line ($0 \le s \le \ell$) under the convention that V vanishes at the equator (i.e., $V_0 = 0$). Persson (1966) has shown that a necessary and sufficient condition for V to vanish at all points along the field line is for f_+ and f_- to have the same anisotropy, i.e., the same equatorial pitch-angle distribution. Since ring-current electrons and protons are believed to be

scattered in pitch angle by different wave modes (Kennel and Petschek, 1966; Cornwall, 1966), we expect that their pitch-angle distributions are not the same. Thus, an electrostatic potential $V_s \neq 0$ is required in order to satisfy the quasi-neutrality condition expressed by (1).

Since our model is intended for application in the topside ionosphere and the magnetosphere, the plasma is assumed to be collisionless in the interval $0 \leq s \leq \ell$. This assumption of collisionless plasma in the flux tube entails at least two consequences which require consideration at the outset. On the one hand, the distribution functions f_+ and f_- are required to be mapped along the field line in accordance with Liouville's theorem, the detailed consequences of which will be discussed below. On the other hand, we are obligated to select ℓ so that all the charged-particle populations are indeed collisionless throughout the interval $0 \leq s \leq \ell$. For the magnetospheric proton population, which is obviously collisionless in the equatorial region of the auroral field line, the dominant collisional process in the ionosphere, where the neutral-particle density greatly exceeds the plasma density, is ion-neutral, charge exchange. The collision time for this process is given by $t = 1/n_0 \sigma v$, where n_0 is the neutral-particle density, σ is the ion-neutral charge-exchange cross section, and v is the magnitude of the relative impact velocity. For hot magnetospheric plasma one identifies v with the speed of the charged particle and requires that the particle

be relatively free of collisions over its full bounce period $2\pi / \Omega_2 \sim 5LR_E/v$. Thus, the level corresponding to $s = \ell$ is to be determined from the condition that

$$\Omega_2 t \sim 2\pi/[5 n_0(\ell)\, \sigma L R_E] \sim 1 . \qquad (2)$$

Using an average CIRA (1972) model of the neutral atmosphere and a representative value ($\approx 10^{-15}$ cm^2) for the proton-neutral charge-exchange cross section σ, we determine that the location $s = \ell$ corresponds to an altitude ~2000 km. The corresponding thermal plasma density at $s = \ell$ in the auroral region is extremely variable, since sharp ionospheric troughs are not limited to the plasmapause region (Hoffman et al., 1974). At high invariant latitudes ($> 65^\circ$), the trough ionospheric densities may be as low as 10^2-10^3 cm^{-3} in the nightside ionosphere and as high as 10^4 cm^{-3} in the dayside ionosphere at the 1400 km altitude (Hoffman et al., 1974). While the criterion (2) assures us that magnetospheric ions will be relatively free of charge-exchange collisions on their bounce time scale in the interval $0 \leq s \leq \ell$, charge-exchange collisions near the foot of the field line may exert sufficient frictional force on H^+ ions of ionospheric origin to modify their density distribution along the field line. We acknowledge that most energetic eletrons, as well as ions with energies $\geq$ 50 keV, remain collisionless to much lower altitudes than 2000 km. It is a shortcoming

of our model that all particles going beyond $s = \ell$ are considered lost. This shortcoming could be remedied only by allowing ℓ to depend upon particle species and energy, but such a remedy would render the present model entirely intractable.

Having defined the interval $0 \le s \le \ell$ for which our model applies, we next consider the consequences of Liouville's theorem. Since the plasma is considered to be collisionless throughout the interval $0 \le s \le \ell$, the time-independent distribution function for either species must depend only on the constants of the motion, namely

$$W \equiv (m_q/2)(v_{\parallel s}^2 + v_{\perp s}^2) + q|e|V_s \tag{3}$$

and

$$\mu \equiv m_q v_{\perp s}^2 / 2B_s , \tag{4}$$

where m_q is the particle mass and $q(= \pm 1)$ is the particle charge in units of the electronic charge $|e|$. Liouville's theorem asserts that

$$f_\pm(v_{\parallel s}, v_{\perp s}; V_s) = f_\pm(v_{\parallel s'}, v_{\perp s'}; V_{s'}) \tag{5}$$

if the points $(v_{\parallel s}, v_{\perp s}; s)$ and $(v_{\parallel s'}, v_{\perp s'}; s')$ are connected by a dynamical trajectory in phase space. The conservation laws expressed by (3) and (4) imply that

$$v_{\parallel s'}^2 = v_{\parallel s}^2 + [1 - (B_{s'}/B_s)]v_{\perp s}^2 + (2q|e|/m_q)(V_{s'} - V_s) \qquad (6)$$

for any such pair of points on the same dynamical trajectory in phase space. Thus, we say that the point $(v_{\parallel s}, v_{\perp s}; s)$ is accessible from the source point, defined as $(v_{\parallel s*}, v_{\perp s*}, s^*)$, if $v_{\parallel s'}$ is real (i.e., if $v_{\parallel s'}^2 > 0$) for all s' between s and s^*. An obviously necessary condition for particle accessibility to s from a source point s^* is that $v_{\parallel s^*}^2$, as given by (6), be positive or zero. The sufficiency of this condition, namely $v_{\parallel s^*}^2 \geq 0$, depends on the functional form of V_s. It can be shown (see Appendix A) that the condition $v_{\parallel s^*}^2 \geq 0$ is sufficient for accessibility to any source point s^* for both species of particle ($q = \pm 1$) if $dV_{s'}/dB_{s'} > 0$ and

$$(d^2V_{s'}/dB_{s'}^2) \leq 0 \qquad (7)$$

for all points s' between s and s^*. In our model, we use the criterion $v_{\parallel s^*}^2 \geq 0$ to determine particle accessibility to their respective source points s^*; thus, we require, in accordance with (7), that V_s increase monotonically with B_s and appear concave downward when plotted as a function of B_s throughout the entire interval $B_0 \leq B_s \leq B_\ell$. Since the functional form of V_s becomes evident only

upon solution of (1), we have to assume that the above requirements on dV_s/dB_s and d^2V_s/dB_s^2 are satisfied in specifying analytical forms for $f_\pm (v_{\parallel s}, v_{\perp s}; V_s)$ in our model. Only after "evaluation" of the density moment and "solution" of (1) for V_s are the derivatives dV_s/dB_s and d^2V_s/dB_s^2 available to be tested for sign. These conditions thus turn out to be very restrictive constraints (applied a posteriori) on the acceptability of "solutions" to (1). In theory, any "solution" of (1) not satisfying these constraints has to be discarded, since it would have been based on a false mapping of $f_\pm$ in (1). In practice, however, a slight violation of (7) comparable to the limit of numerical resolution in computing the density moments may have to be tolerated.

A proper consideration of constraints upon V_s, based on accessibility of a particle to its source point in phase space, should include not only the electrostatic potential, as in (7), but also the gravitational potential. We have chosen to neglect the effects of gravity in (7) because we seek solutions for which $|e|V_\ell \sim 1$ keV. For O^+ ions, the gravitational escape energy from the 2000 km altitude is ~ 8.2eV; therefore, we should have included the gravitational potential in the consideration of phase-space accessibility of cold ions near the foot of the field line where $|e|(V_\ell - V_s) \lesssim 10$ eV. We have properly included the gravitational potential in the treatment of the dynamics of cold ions, as was done in the works of Eviatar et al. (1964) and Lemaire and Scherer (1973). However, the enforcement of (7) as a constraint upon V_s near the foot

of the field line may not be sufficient, i.e., may constitute an erroneous allocation of points $(v_{\parallel}, v_{\perp}; s)$ in phase space with respect to accessibility of cold ions from their source point $s^* = \ell$. We have been able to show that, even if gravity is taken into consideration, cold ions satisfying $v_{\parallel s^*}^2 > 0$ in (6) are accessible to their source at the foot of the field line if V_s satisfies (7) and if dV_s/dB_s is sufficiently large near the foot of the field line (see Appendix A).

In the foregoing, we have concentrated on discussing the properties of V_s imposed by the requirement that the particles in phase space be accessible along dynamical trajectories to their sources, which are assumed to be either at the equator ($s^* = 0$) or at the foot of the field line ($s^* = \ell$). Among the possible particle populations supporting V_s, there may be populations which are not accessible to any source points in the interval $0 \leq s \leq \ell$ (Lemaire and Scherer, 1971 a; b). Such particles execute dynamical trajectories with two turning points in the interval $0 < s < \ell$, and are therefore trapped by the electrostatic potential on the one hand and by the effective magnetic mirroring potential on the other. For a potential V_s ($0 \leq V_s \leq V_\ell$) satisfying the constraint imposed by (7), only electrons may execute such trapped trajectories. We assume that the phase-space trajectories available for such trapped electrons are defined by the requirements that $v_{\parallel 0}^2 < 0$ and $v_{\parallel \ell}^2 < 0$.

Details on the construction of the model particle distribution functions for the various populations are given in the next section.

PARTICLE POPULATIONS

In the present model, the following plasma-constituent distributions are assumed to be present in the collisionless interval ($0 \leq s \leq \ell$) of the auroral flux tube: hot anisotropic magnetospheric plasma, $f_{Mq}\ (v_{\|s}, v_{\perp s}; V_s)$; cold thermal ionospheric plasma, $f_{Iq}\ (v_{\|s}, v_{\perp s}; V_s)$; two populations of backscattered electrons, $f_{Si}\ (v_{\|s}, v_{\perp s}; V_s)$ with ($i = 1, 2$); and trapped electrons, $f_T\ (v_{\|s}, v_{\perp s}; V_s)$. The magnetospheric distributions f_{Mq} are considered to arise from an equatorial source ($s^* = 0$) while the ionospheric distribution f_{Iq} and the backscattered distributions f_{Si} are considered to be injected at $s = \ell$. The trapped electrons f_T are considered to have been scattered into their trapped trajectories and do not require an accessible source.

Particles belonging to f_{Mq} are classified as precipitating ($v_{\|\ell}^2 > 0$) or mirroring ($v_{\|\ell}^2 < 0$) according to their respective values of

$$v_{\|\ell}^2 = v_{\|s}^2 + [1 - (B_\ell / B_s)]\, v_{\perp s}^2 + (2q|e|/m_q)(V_s - V_\ell), \qquad (8)$$

which determines accessiblity to $s = \ell$. Since $v_\|$ is positive for downgoing particles in our convention, and since all magnetospheric particles going beyond $s = \ell$ are considered to be absorbed, we require that $f_{M\pm} = 0$ for trajectories that obey both the condition $v_\| < 0$ and the condition $v_{\|\ell}^2 > 0$. Further, since the source of the $f_{M\pm}$ is located at $s = 0$, we require that

all trajectories of $f_{M\pm}$ be accessible to $s = 0$ by the criterion discussed in the previous section, i.e., that $v_{\|0}^2 > 0$. Noting that magnetospheric particles may be anisotropic, we postulate an otherwise bi-Maxwellian form for $f_{M\pm}$ at the equator, so that

$$f_{Mq}(v_{\|s}, v_{\perp s}; V_s) = C_{Mq}[\theta(-v_{\|\ell}^2) + \theta(v_{\|s})\theta(v_{\|\ell}^2)]\theta(v_{\|0}^2) \times \exp\{-(m_q v_{\|s}^2/2\kappa T_{\|q}) - (q/e)V_s/\kappa T_{\|q}) - (m_q v_{\perp s}^2/2\kappa T_{\|q})[1 - (B_0/B_s)] - (m_q v_{\perp s}^2/2\kappa T_{\perp q})(B_0/B_s)\}, \quad (9)$$

where κ is the Boltzmann constant and C_{Mq} is a normalization constant defined in such a way that the equatorial number density is given by

$$N_{Mq} = 2\pi \int_{-\infty}^{+\infty} dv_{\|} \int_0^{\infty} v_{\perp}\, dv_{\perp}\, f_{Mq}(v_{\|}, v_{\perp}; 0^+) . \quad (10)$$

The unit step function $\theta(x)$ is defined as $+1$ for $x \geq 0$ and vanishes for $x < 0$.

For ionospheric electrons, we require accessibility from the source at $s = \ell$, i.e., we require that $v_{\|\ell}^2 > 0$. The condition $v_{\|0}^2 \gtrless 0$ distingushes between electrons that mirror before reaching the equator ($v_{\|0}^2 < 0$) and those that cross the equator ($v_{\|0}^2 > 0$) to be lost in the conjugate ionosphere. However, the "loss cone" is assumed to be completely filled in either case, and the distribution function is not complicated by this distinction. All cold electrons that enter the ionosphere are assumed to be

replenished immediately and the ionosphere is considered completely symmetrical between north and south. Thus, we postulate an ionospheric electron distribution function, which is taken to be an isotropic Maxwellian distribution of temperature T_{I-}, at $s = \ell$:

$$f_{I-}(v_{\parallel s}, v_{\perp s}; V_s) = (m_-/2\pi\kappa T_{I-})^{3/2} N_{I-}\, \theta(v_{\parallel \ell}^2)$$

$$\times \exp\left\{ - (m_- v_s^2/2\kappa T_{I-}) - (q|e|/\kappa T_{I-})(V_s - V_\ell) \right\}, \quad (11)$$

where N_{I-} is the cold ionospheric electron density at $s = \ell$.

For cold ions, the effect of gravity must be taken into account. Thus, the mapping relationship between the source point $(v_{\parallel \ell}, v_{\perp \ell}; \ell)$ and the point $(v_{\parallel s}, v_{\perp s}; s)$, analogous to (6), is

$$v_{\parallel \ell}^2 = v_{\parallel s}^2 + [1 - (B_\ell/B_s)] v_{\perp s}^2 + (2|e|/m_q)(V_s - V_\ell)$$

$$+ 2GM_E[(1/r_\ell) - (1/r_s)], \quad (12)$$

where G is the gravitational constant, M_E is the mass of the earth, and r_s is the radial distance between the center of the earth and the point s. The quantity $GM_E m_{O+}/R_E$ is approximately 10.53 eV; therefore, the influence of gravity upon the distributions of cold ion-density and parallel electrostatic potential is important near the foot of the field line, where $|e|(V_\ell - V_s)$ is of comparable magnitude.

The dominant ionic species in the topside ionosphere are O^+ and H^+. The mass difference between the two species influences their relative distributions along the field line and creates an additional charge-separation electric field, as in the polar wind (Banks and Holzer, 1968), although we are dealing with closed field lines. While such an effect may be important in connection with the distribution of O^+ and H^+ ions at the foct of the field line, we note again that such a charge-separation electric potential is orders of magnitude smaller than V_ℓ, which is of the order of kilovolts. Thus, for the sake of simplicity in exposing what are possibly the major factors in the maintainence of V_ℓ, we assume that the ionosphere consists of H^+ ions only. A treatment of the mutual consistency between the large auroral parallel electrostatic potential and the distributions of O^+ and H^+ ions in the trough region of the ionosphere will be given in subsequent work on the formation of the ionospheric trough. For the present paper, we use the cold ion distribution

$$f_{I+}(v_{\parallel s}, v_{\perp s}; V_s) = (m_+/2\pi\kappa T_{I+})^{3/2} N_{I+} \theta(v_{\parallel \ell}^2)\, \theta(-v_{\parallel s}) \times \exp\left\{ -(m_+ v_s^2/2\kappa T_{I+}) - (|e|/\kappa T_{I+})(V_s - V_\ell) - (GM_E m_+/\kappa T_{I+})[(1/r_\ell) - (1/r_s)] \right\}, \quad (13a)$$

which is the mapping of a simple Maxwellian distribution in accordance with (12). This distribution is similar to that postulated by Lemaire and

Scherer (1973): we assume that upward-moving ions are lost as they cross the equator so that there are no downward-moving ions in the interval $0 < s \leq \ell$.

For the sake of completeness, we have also experimented with forms for which the ion stream has speed u (>0) at $s = \ell$, as in the polar wind:

$$f_{I+}(v_{\parallel s}, v_{\perp s}; V_s) = (m_+/2\pi\kappa T_{I+})\, N_{I+}\, \theta(-v_{\parallel s})\, \delta(v_{\parallel \ell} + u) \times \exp(-m_+ v_{\perp s}^2 B_\ell / 2\kappa T_{I+} B_s) , \quad (13b)$$

and

$$f_{I+}(v_{\parallel s}, v_{\perp s}; V_s) = (m_+/4\pi\kappa T_{I+})\, N_{I+} \exp(-m_+ v_{\perp s}^2 B_\ell / 2\kappa T_{I+} B_s) \times [\delta(v_{\parallel \ell} + u)\theta(-v_{\parallel s}) + \delta(v_{\parallel \ell} - u)\theta(v_{\parallel s})] . \quad (13c)$$

The form (13b) resembles (13a) and that used by Lemaire and Scherer (1973) in that upward-moving ions are considered to be lost as they cross the equator. The form given by (13c) resembles that postulated by Schulz and Koons (1972) in that it consists of two oppositely directed streams at all points along the field line. The mapping of (13b) and (13c) is in accordance with (12); therefore, we have to make sure that the ion stream will be accessible to $s = \ell$. We have shown that ions are not trapped (so as to be inaccessible to both $s = 0$ and $s = \ell$) by the combined electrostatic and gravitational potential if V_s varies sufficiently with B_s near the foot of the field line. In a proper treatment, utilizing the form (13a) for the O^+ and H^+ species separately, the artificial modeling of an upward flow at the foot of the field line is unnecessary.

In the construction of ion distributions above, we have ignored the important effect of the magnetospheric convection electric field upon the cold ions in the auroral flux tube. Under the action of the perpendicular convection electric field, the particles begin to drift across $\vec{B}$. Electron drift is negligible on the bounce time scale, but cold-ion drift is not. The net result is a loss of cold ions from the flux tube. Whereas Lemaire and Scherer (1973) postulated the loss process to have occurred entirely at the equator, we have attempted to model the depletion of ions along the flux tube by assuming that the convection electric field causes a constant probability of cold-ion depletion per unit field-line length. Thus, the distributions (13) are to be multiplied by a depletion factor

$$D = \exp\left\{ -\int_s^{s_l} \frac{ds'}{\tau} \frac{[\theta(-v_{\parallel s}) - \theta(v_{\parallel s})]}{|v_{\parallel s'}|} - 2\int_0^{s_l} \frac{ds'}{\tau} \frac{\theta(v_{\parallel s})}{|v_{\parallel s'}|} \right\}, \quad (14)$$

where τ, the time constant for the process, need not be very long in comparison with the cold-ion bounce period. In the present model, we assume τ to be an adjustable parameter, and τ is generally found to be of the order of 20 minutes. Since the inclusion of (14) in the distribution function (13) of cold ions renders the density moment integrations entirely intractable, we assume $v_{\parallel s'}$ in (14) to be given by the parallel velocity of a cold ion stream free of the influence of the magnetic field, i.e., by

$$v_{\parallel s'} = \{ u^2 + (2|e|/m_+)(V_\ell - V_{s'}) + 2GM_E[(1/r_{s'}) - (1/r_\ell)] \}^{1/2} , \qquad (15)$$

where u, assumed to be approximately one half of the cold-ion thermal speed, is the upward flow speed at the foot of the field line. With the use of a trial model of $V_{s'}$, the depletion factor D is thus made independent of the phase-space integrations and the cold-ion density is given by the product of the density moment obtained from (13a) and the depletion factor D.

Backscattered electrons are assumed to be produced at altitudes below $s = \ell$ in a manner that yields isotropic distributions at $s = \ell$, but $s = \ell$ is regarded as the source of backscattered electrons in the sense that accessibility to $s = s^*$ requires $v_{\parallel\ell}^2 > 0$. As in the model of Evans (1974), which is based on the abstracted results of a detailed calculation by Banks et al. (1974), we distinguish two populations of backscattered electrons: the primary backscattered electron distribution $f_{S1}(v_{\parallel s}, v_{\perp s}; V_s)$ and the secondary distribution $f_{S2}(v_{\parallel s}, v_{\perp s}; V_s)$. Both distributions of backscattered electrons are related to the precipitating magnetospheric electron flux per unit kinetic energy ϵ_ℓ at $s = \ell$, namely

$$dJ_{M\downarrow}/d\epsilon_\ell = 2\pi \int_0^1 (2\epsilon_\ell/m_-^2) \cos\alpha_\ell \; f_{M-}(v_{\parallel\ell}, v_{\perp\ell}; V_\ell)\, \theta(v_{\parallel\ell}^2)\, d(\cos\alpha_\ell)$$

$$\approx 2\pi (\epsilon_\ell/m_-^2) C_{M-} \; \theta(\epsilon_\ell - |e|V_\ell)$$

$$\times \exp[-(\epsilon_\ell/\kappa T_{\parallel -}) + (|e|V_\ell/\kappa T_{\parallel -})] \,. \qquad (16)$$

We estimate the relationship between the upward primary backscatter flux $dJ_{S1\uparrow}/d\epsilon_\ell$ and the total precipitating flux $dJ_\downarrow/d\epsilon_\ell$ of energetic electrons by means of a transfer function $S(\epsilon_\ell, \epsilon_\ell')$ in the integral equation

$$dJ_{S1\uparrow}/d\epsilon_\ell \equiv \int_0^\infty S(\epsilon_\ell, \epsilon_\ell')\, (dJ_\downarrow/d\epsilon_\ell')\, d\epsilon_\ell' \,. \qquad (17)$$

The total precipitating flux $dJ_\downarrow/d\epsilon_\ell'$ in (17) is given by the sum of the magnetospheric precipitating flux, $dJ_{M\downarrow}/d\epsilon_\ell'$ in (16), and the precipitating flux of the primary backscattered electrons, $dJ_{S1\downarrow}/d\epsilon_\ell'$. Kinematical considerations require that $J_{S1\downarrow} = J_{S1\uparrow}$, since the discussion on thermal electrons applies equally well to backscattered electrons: whatever goes up must come down. For the primary-backscatter transfer function $S(\epsilon_\ell, \epsilon_\ell')$, we choose a form given by

$$S(\epsilon_\ell, \epsilon_\ell') = [\epsilon_\ell/(\epsilon_\ell')^2]\, \theta(\epsilon_\ell' - \epsilon_\ell) \,. \qquad (18)$$

This represents an analytically convenient fit to the transfer function deduced by Evans (1974) from a detailed calculation by Banks et al. (1974). The normalization of (18) yields an integrated probability of 0.5 for an incident electron to be backscattered with energy ϵ_ℓ between 0 and ϵ_ℓ'. This agrees well with the estimate by Evans (1974) that 46% of the incident electron flux is backscattered. Thus, we obtain the relationship

$$dJ_{S1\uparrow}/d\epsilon_\ell = \int_{\epsilon_\ell}^{\infty} [\epsilon_\ell/(\epsilon_\ell')^2][(dJ_{M\downarrow}/d\epsilon_\ell') + (dJ_{S1\uparrow}/d\epsilon_\ell')]\, d\epsilon_\ell' \quad , \qquad (19)$$

where we have expressed $J_\downarrow = J_{M\downarrow} + J_{S1\downarrow} = J_{M\downarrow} + J_{S1\uparrow}$. The solution of (19) for $dJ_{S1\uparrow}/d\epsilon_\ell$ in terms of $dJ_{M\downarrow}/d\epsilon_\ell$ is effected by multiplication of both sides by $1/\epsilon_\ell$ and differentiation with respect to ϵ_ℓ. These steps yield

$$\frac{1}{\epsilon_\ell}\frac{d}{d\epsilon_\ell}\left[\frac{dJ_{S1\uparrow}}{d\epsilon_\ell}\right] = -\frac{1}{\epsilon_\ell^2}\frac{dJ_{M\downarrow}}{d\epsilon_\ell} \quad . \qquad (20)$$

The solution of (20) is given by

$$dJ_{S1\uparrow}/d\epsilon_\ell = \int_{\epsilon_\ell}^{\infty} (d\epsilon_\ell'/\epsilon_\ell')(dJ_{M\downarrow}/d\epsilon_\ell')$$

$$\approx (2\pi\kappa T_{\parallel -}/m_-^2)\, C_{M-} \{\theta(|e|V_\perp - \varepsilon_\perp) + \theta(\varepsilon_\perp - |e|V_\perp) \exp[(|e|V_\perp - \varepsilon_\perp)/\kappa T_{\parallel -}]\} \quad (21)$$

upon insertion of (16) above. The integration of (16) and (21) with respect to $\varepsilon_\perp$ reveals a total precipitation flux

$$J_\downarrow \equiv J_{M\downarrow} + J_{S1\downarrow} \approx 2J_{M\downarrow} \approx 2J_{S1\downarrow}$$
$$\approx 4\pi(\kappa T_{\parallel -}/m_-)^2 C_{M-}[1 + (|e|V_\perp/\kappa T_{\parallel -})] \quad . \quad (22)$$

Thus, we find that half of the precipitating energetic electron flux is magnetospheric, while the other half consists of electrons previously backscattered.

The secondary backscatter is characterized (Banks et al., 1974; Evans, 1974) by a "universal" spectrum having an intensity proportional to the total flux $J_\downarrow$ of incident energetic electrons. The secondary flux is negligible ($\leq 1\%$ of maximum) at energies $\varepsilon_\perp \geq 200$ eV, and so we obtain a fit in simple analytic form of the lower-energy portion of the "universal" secondary backscatter spectrum given by Banks et al. (1974):

$$dJ_{S2\uparrow}/d\varepsilon_\perp \approx (\varepsilon_\perp/\varepsilon_2^2) A_2 [1 + (\varepsilon_\perp/\varepsilon_2)]^{-4} J_\downarrow \quad , \quad (23)$$

where $A_2 \approx 3.0$, $\epsilon_2 \approx 15$ eV, and $J_\uparrow$ is given by (22). In the application of the present model to various observations to be considered in the next section, we found it necessary to vary A_2 somewhat in order to fit the low-energy portions of observed electron spectra; therefore, A_2 will be considered an adjustable parameter of the model.

It remains necessary to convert the upward differential fluxes given by (21) and (23) into distribution functions $f_{Si}(v_{\parallel s}, v_{\perp s}; V_s)$, where $i = 1, 2$. We do this by assuming that the backscatter distributions are isotropic (cf. Banks et al., 1974; Evans, 1974) at $s = \ell$. One then obtains the relationship

$$dJ_{Si\uparrow}/d\epsilon_\ell = (2\pi\epsilon_\ell/m_-^2)\, f_{Si}(v_\ell; V_\ell) \quad , \tag{24}$$

from which we derive the following backscattered electron distribution functions:

$$\begin{aligned} f_{S1}(v_{\parallel s}, v_{\perp s}; V_s) \approx\ & (2\kappa T_{\parallel -}/m_-)\, C_{M-}\, \theta(v_{\parallel \ell}^2)\{\theta(2|e|V_\ell - m_- v_s^2) \\ & + \theta(m_- v_s^2 - 2|e|V_\ell)\exp[(2|e|V_s - m_- v_s^2)/2\kappa T_{\parallel -}]\} \\ & \div [v_s^2 + (2|e|/m_-)(V_\ell - V_s)] \end{aligned} \tag{25}$$

and

$$f_{S2}(v_{\parallel s}, v_{\perp s}; V_s) \approx 2(\kappa T_{\parallel -}/\epsilon_2)^2 C_{M-} A_2 [1 + (|e| V_\ell / \kappa T_{\parallel -})] \theta(v_{\parallel \ell}^2) \div [1 + (|e|/\epsilon_2)(V_\ell - V_s) + (m_- v_s^2/2\epsilon_2)]^4 \quad (26)$$

For electrons on trapped trajectories, we construct their distribution $f_T(v_{\parallel s}, v_{\perp s}; V_s)$ by assuming it to be a Maxwellian distribution in equilibrium with the "source", from which the trapped electrons had been scattered onto their present trajectories (Lemaire and Scherer, 1971b). In our model, there are two such possible "sources", namely those at $s = 0$ and at $s = \ell$. Thus, for each "source" j, we construct a trapped electron distribution

$$f_{Tj}(v_{\parallel s}, v_{\perp s}; V_s) = (m_-/2\pi\kappa T_j)^{3/2} N_j(s_j^*) \theta(-v_{\parallel 0}^2) \theta(-v_{\parallel \ell}^2) \times \exp\{ - (m_- v_s^2/2\kappa T_j) + (|e|/\kappa T_j)(V_s - V_{s_j}^*) \}, \quad (27)$$

where s_j^* is the location of the "source" and T_j is an adjustable temperature for the trapped population. For $j = 1$, we identify f_{T1} with the distribution scattered into trapped trajectories from f_{M-}, and so we take $N_1(s_1^*) = N_{M-}$. For $j = 2$ we identify f_{T2} with the distribution of electrons that have been scattered into trapped trajectories from distributions whose sources are at $s = \ell$. There are several such "source"

distributions, but calculations reveal that the density moments of low-temperature trapped particles originally injected at $s = \ell$ are negligible due to phase-space limitations if $V_\ell \sim 1$ kilovolt. Therefore, we identify f_{T2} with electrons scattered into trapped trajectories from f_{S1}. Since the primary backscattered electron distribution has temperature $T_{\parallel -}$, we assume both trapped distributions to have the same temperature $T \equiv T_{\parallel -}$, forming a single distribution

$$f_T(v_{\parallel s}, v_{\perp s}; V_s) = (m_-/2\pi\kappa T)^{3/2} N_T \, \theta(-v_{\parallel 0}^2) \, \theta(-v_{\parallel \ell}^2) \times \exp\left[- (m_- v_s^2/2\kappa T) + (|e| V_\ell/\kappa T) \right] , \quad (28)$$

where

$$N_T = N_{M-} + N_{S1} \exp(- |e| V_\ell/\kappa T) , \quad (29)$$

N_{S1} being the density derived from f_{S1} at $s = \ell$. The existence of trapped electrons had been assumed in previous exospheric models of the solar wind (Lemaire and Scherer, 1971b), but not in the magnetosphere (Eviatar et al., 1964; Lemaire and Scherer, 1973). Observational evidence for or against their existence would be welcome. Perhaps one may argue that certain regions of phase space would be empty if trapped electrons do not exist (see Figure 1b). Evidence suggesting the filling of all regions of phase space in auroral electron-precipitation events is given by Kaufmann et al. (1976).

Figure 1 summarizes the regions of phase space occupied by the various particle populations discussed above. The left panel indicates velocity-space demarcations that characterize the various portions of the magnetospheric and ionospheric populations of ions. The right panel illustrates the corresponding velocity-space demarcations for electrons.

THE MODEL

In the previous two sections we have summarized the manner in which charge neutrality is to be enforced on the constructed particle distributions in an auroral flux tube. The general features of the model dealt with in the previous sections are quite akin to those of the exosphere and plasma-sheet models of Lemaire and Scherer (1971b, 1973, 1977), although considerations such as accessibility of sources, anisotropy of magnetospheric particles, and the inclusion of backscattered electrons characterize the greater generality of the present formulation. However, it is mainly the area of model usage which distinguishes the present model from previous exospheric models, since the major purpose of the present model is to explore the factors that may contribute to the maintainence of a large auroral potential difference between the equator and the ionosphere. Therefore, we apply our model to specific electron-precipitation events for which distinctly beam-like energetic electrons are observed.

A second feature involving the usage of our model has to do with the geometry of the assumed magnetic field. In the construction of particle distributions in the previous section, we have tacitly assumed that the model is to be applied to particle and electric-field distributions in a closed dipolar flux tube. While we shall continue to assume so in the rest of this work, we wish to note that the physical processes discussed in this work are also applicable to regions of open field lines. For regions of open field lines, it would be necessary to reconstruct

the particle distributions discussed in the previous section. Although magnetospheric particles in such open-field-line regions are likely to be isotropic, a large electrostatic potential difference may still be maintained by virtue of electron backscatter. Applications of our model of particle and electric field distributions for open field-line regions will be considered in a subsequent work.

In typical observations, either the electron flux distribution(at a given pitch angle) $dJ_-/d\varepsilon\, d\Omega$ or the electron energy flux(at a given pitch angle) $\varepsilon\, dJ_-/d\varepsilon\, d\Omega$ is observed at an altitude below 2000 km. As a first step in the usage of our model, we require that the theoretical flux distribution at the foot of the field line, i.e.,

$$(dJ_-/d\varepsilon_\ell\, d\Omega) = (2\varepsilon_\ell/m_-^2)\,[\, f_{M-}(\varepsilon_\ell, \alpha; V_\ell) + f_{S1}(\varepsilon_\ell, \alpha; V_\ell) + f_{S2}(\varepsilon_\ell, \alpha; V_\ell) + f_{I-}(\varepsilon_\ell, \alpha; V_\ell)\,] , \quad (30)$$

where α is the pitch angle and $d\Omega$ the corresponding element of solid angle, be fitted to the observed flux distribution. Except for events in which diffusive energy gain is evident (Evans, 1975), good fits are usually obtained. The parameters V_ℓ, $T_{\parallel -}$, $(N_{M-}/T_{\perp -})$, and A_2 are stringently constrained by the fitting. Specific examples of fits to observed particle-flux and observed energy-flux distributions are shown in Figures 2 and 3, respectively. Detailed discussions of the cases will be given in the next section. In the usual situation, only the electron-flux distribution

for a specific event is available for comparison with the theoretical flux; therefore, we assume the ion parameters to be variable in the search for a self-consistent parallel electrostatic potential V_s. Should energetic ion distributions be available, a self-consistency check of our model can be made immediately since V_ℓ is a common parameter for both electron and ion distributions. In the usage of our model, the field-aligned current

$$J_\parallel \equiv |e| \int_0^\infty v_{\perp s}\, dv_{\perp s} \int_{-\infty}^{+\infty} [\, f_+(v_{\parallel s}, v_{\perp s}; V_s) - f_-(v_{\parallel s}, v_{\perp s}; V_s)\,]\, v_{\parallel s}\, dv_{\parallel s} \qquad (31)$$

is neither made to vanish nor assigned any particular numerical value, as is done in Lemaire and Scherer (1973). If $J_\parallel$ is measured for a specific event to which we apply our model, then an additional consistency ckeck can be made on the model since V_ℓ is again a common parameter in (30) and (31). In general, because of the assumed magnetospheric particle anisotropy, and because of the loss of cold ions to the magnetospheric convection pattern, $J_\parallel$ is nonvanishing in our model. Further, the loss of cold ions from the flux tube implies that a perpendicular current $J_\perp$ also exists. Such considerations raise the question of how to complete the electrical circuit in the auroral region. This presumably occurs via other field lines than the one under consideration and presumably involves perpendicular electric fields which co-exist with the parallel electric field. It is not our intention to explore here the mechanisms by which

any such magnetospheric circuits are closed. In subsequent work, such questions will be addressed in connection with the so-called "inverted-V" structures.

Having obtained the parameters V_ℓ, $T_{\parallel -}$, $(N_{M-}/T_{\perp -})$ and A_2 from a comparison of (28) with data for a specific event, we next proceed to implement the quasi-neutrality condition (1). Since we have assumed specific forms for the distribution functions, we calculate the density moments of $f_{M\pm}$, $f_{I\pm}$, f_{Si} and f_T (in closed form) as functions of V_s, B_s, and the particle parameters ($N_{M\pm}$, $N_{I\pm}$, $T_{\parallel\pm}$, $T_{\perp\pm}$, $T_{I\pm}$, T, A_2, and τ). Examples of the required velocity-space integrations, some of which are quite tedious, are given in Appendix B. Not all of the above particle parameters are entirely independent, since the limits of (1) as $s \to 0$ and as $s \to \ell$ constitute two constraints among the above particle parameters and the potential difference V_ℓ. Thus, only the parameters N_{I+}, $T_{\parallel +}$, $T_{\perp\pm}$, $T_{I\pm}$, T, and τ may be considered free parameters of the model, although the known conditions of the ionosphere in the auroral region impose additional bounds on N_{I+} and $T_{I\pm}$. A summary of the parameters of the model is given in Table 1.

Once the particle parameters are specified, subject to the constraints discussed above, we consider (1), the quasi-neutrality equation in integrated form, as a transcendental equation to be solved for V_s as a function of B_s.

This is done on the CDC 7600 computer, since a large number of transcendental functions are involved. The "solution" so obtained is, however, not necessarily the required solution of the model, since an acceptable V_s must be a monotonic function of B_s and it must satisfy (7). If V_s does not satisfy these tests, the particle parameters are adjusted and the solution process is repeated until a satisfactory solution is obtained.

RESULTS

Since the primary purpose of the present model is to determine circumstances under which a large electrostatic potential difference may be maintained along an auroral field line, we have applied the model to a number of specific cases, two of which will be discussed in this section.

Figure 2 shows the unidirectional electron flux at 45° pitch angle for an event observed in the dayside cusp region on 11 January 1975 (Winningham et al., 1977). The electron-flux data have been compared with the model (solid curve) of Evans (1974), and the figure is taken from Evans (1975). The data suggest that a monoenergetic beam of particles at an energy ~600 eV may be present in the electron spectrum. Figure 3 shows electron energy-flux data at two pitch angles obtained in an "inverted-V" structure (Mizera et al., 1976). This example is particularly interesting not only because of its occurrence in the auroral region (invariant latitude 69.7°) but also because it clearly shows the beam-like character of precipitating high-energy electrons, as is evidenced by the great difference between the unidirectional energy flux at 0° and that at 180° pitch angles. The parameters which determine the model fits shown in Figure 2 (Case W) and in Figure 3 (Case M) are summarized in Table 2.

Although the parameters shown in Table 2 are not uniquely determined from the data, the comparison between the present model parameters and those of Evans' model for Case W illustrates some differences between the two models. In Evans' model, the number density of the electron beam was taken to be 0.85 cm^{-3} and the temperature was taken to be 0.143 keV. While his electron temperature, which determines the slope of the flux distribution at energies above $|e|V_\ell$, is approximately the same as our parallel temperature $\varkappa T_{\parallel -}$, the electron beam density required in Evans' model is considerably smaller than the N_{M-} of our model, primarily because of the fact that in our model only those magnetospheric electrons that would mirror at $s > \ell$ contribute to the energetic electron flux. Further, because of differences in the pitch-angle distributions of the energetic electrons for the two models, the total flux (integrated over pitch angle) is larger in Evans' model than in ours; hence, the low-energy electron fluxes for the two models are also different. For Case M (Figure 3), the required electrostatic potential difference and the required magnetospheric electron temperatures are considerably higher than in Case W (Figure 2). In many respects, Case M is a more stringent test of the model since the electron energy fluxes at two pitch angles are available. In particular, the low-energy portion of the electron spectrum shown in Figure 3 requires considerably lower secondary backscatter than in Figure 2.

With the use of the parameters determined in Table 2, searches for self-consistent electrostatic potentials V_s were made in accordance with the formulation given in the previous two sections. In the solution process,

the model parameters not yet determined in Table 2 are varied in the manner described in Table 1. For Case M, the L value of the field line is 8.35 . For Case W, the observations were made at very high invariant latitudes (77.5° N) where the rocket was possibly on open field lines in the cusp region. In this respect, our model is probably not fully applicable, since we assume the magnetospheric particles to be partially trapped by a dipolar field. However, if the precipitating magnetospheric particles were to have the anisotropies determined in the fitting of Figure 2, the application of the model is not substantially changed even though the solution V_s, as a function of B/B_0, may not be an accurate description of the "true" potential distribution. Since the requirement of the total potential drop V_ℓ remains the same whether one considers open or closed field lines, we attempted an application of our model to Case W by assuming an L value of 8.54 for this event. For this reason, our results for Case W are rather to be viewed as an illustration of our model than as reconstructions of actual particle and potential distributions. The electrostatic potential solutions of (1) satisfying the accessibility criterion (7) for Cases W and M are shown in Figure 4 (Case W) and Figure 5 (Case M) respectively. In Figure 4, it is seen that the potential distribution V_s is concave downward when plotted against the magnetic-field ratio B/B_0. In Figure 5, the potential distribution V_s is also concave downward although it may not appear so because the magnetic-field ratio is plotted on a logarithmic scale. For Case W (Figure 4), the major part of the potential drop is confined to the region above ~ 10000 km altitude, with parallel electric field intensities

of up to 40 μV/m. The potential difference V_ℓ for Case M is considerably larger than that for Case W, hence, the parallel electric field intensity in Figure 5 (up to 140 μV/m) is considerably larger than that in Figure 4. Quite interestingly, the region of major potential drop (above ~12 000 km) in Case M is not drastically different from that in Case W, even though the magnitudes of the potential drops are quite different. The self-consistent electrostatic potential distributions for both cases are consistent with Evans' model, where it is assumed that the region of electron acceleration by parallel electric fields is well above the region of electron flux observation. In both cases, the field lines below 10 000 km altitude are essentially equipotentials. This common feature may be a weak point in the model, since there is some observational evidence that particle acceleration occurs mainly below the 7000 km altitude (J. F. Fennell and P. F. Mizera, personal communications, 1977). To counterbalance the point, however, there also is some evidence of parallel electric fields above 7000 km from barium-release experiments (Haerendel et al., 1976). Evidently, the observational situation is probably quite variable. On the other hand, the location of intense parallel electric field in our model may be somewhat dependent on the assumed location of the ionospheric boundary. Presumably, if we were able to handle the proper ionospheric boundary condition, which depends on particle species and particle energy, the distribution of V_s might be somewhat different. Moreover, the inclusion of an intense perpendicular electrostatic field in the consideration of charge neutrality would also affect the location of the major parallel

electrostatic potential drop. Evidence for the important influence of very intense perpendicular electric fields upon energetic particle accelerations in the auroral region has recently been reported (Mozer et al., 1977). Perpendicular electrostatic fields, moreover, may play a major role in defining "inverted-V" structures (e.g., Swift, 1975).

The critical model parameters required for the solution of (1), satisfying the accessibility criterion (7), are shown in Table 3. All other model parameters are either fixed or determined by charge-neutrality constraints at $s = 0$ and $s = \ell$, in accordance with the summary in Table 1. Comparison of magnetospheric ion temperatures in Table 3 with magnetospheric electron temperatures in Table 2, for both cases, indicates that the solutions require highly anisotropic electrons ($T_{\perp -}/T_{\parallel -} = 4.1$ for Case W and $T_{\perp -}/T_{\parallel -} = 3.8$ for Case M) and isotropic ions ($T_{\perp +}/T_{\parallel +} = 1$), even though the potential differences and particle densities in the two cases are quite different. Although this peculiar feature, common to both cases, may be a coincidence, we are inclined toward the view that the difference between the pitch-angle anisotropies of electrons and ions required by the model is not accidental. For field lines just poleward of the plasmapause, where the magnetospheric particle populations are probably of ring-current origin, the ion population is susceptible to cyclotron instability at lower pitch-angle anisotropies than the corresponding process for the electrons (Cornwall et al., 1971). Thus, one would expect the equilibrium population to be much more nearly isotropic

for protons than for electrons. For field lines nearer to the cusp, where the magnetic field is very weak, the pitch-angle anisotropy of an ion population is more likely to be destroyed by scattering off magnetic-field inhomogeneities of a given scale size than is the anisotropy of an electron population. Even without consideration of scattering by random magnetic-field inhomogeneities, the motion of ions at a given energy is less likely to be adiabatic than that of electrons at the same energy. Thus, considerations of possible wave-particle interactions and of non-adiabaticity of particle motion in the earth's magnetic field seem to favor a tendency for auroral-zone ions to be more nearly isotropic in pitch-angle distribution than electrons. Such a tendency is consistent with the temperature parameters required for self-consistent solutions in our model.

An important feature of our model concerns the relationship between the magnitude of the parallel potential drop V_ℓ and the ionospheric dnesity N_{I+} required to obtain a self-consistent solution. Comparison of Case W with Case M in Tables 2 and 3 shows that V_ℓ and N_{I+} are inversely related, i.e., to maintain V_ℓ = 0.59 kV in Case W requires N_{I+} = 1200 cm^{-3}, whereas to maintain V_ℓ = 1.76 kV in Case M requires N_{I+} = 90 cm^{-3}. The sensitivity of our model to the ionospheric density N_{I+} and (in particular) the above inverse relationship are expected, since V_ℓ is essentially maintained by charge separation caused by the difference between magnetospheric particle pitch-angle anisotropies and by the inevitability of electron backscatter. The existence of a parallel potential distribution V_s implies that ions from the ionosphere will be

accelerated up the field line to neutralize the electron excess. Thus, the higher the ion density N_{I+}, the more difficult it is for the model to maintain a large equilibrium potential difference V_ℓ. Although local-time dependence of the ionospheric density is not introduced into the model, the values of N_{I+} required for both cases in Table 3 are consistent with the local time of observation for the two cases. Since Case W was observed in the dayside cusp region and Case M was observed at a local time of 2024 hours, the anticipated day-night difference in ionospheric densities at 2000 km is consistent with the order-of-magnitude difference between N_{I+} for the two cases. It should be noted that N_{I+} was solely determined by the requirement of obtaining a self-consistent solution. The density N_{I+} determined for Case M is consistent with the winter nighttime trough-region ionosphere (Hoffman et al., 1974). The density N_{I+} determined for Case W is also consistent with the winter dayside high-latitude ionosphere, since the event was observed in January 1975 (Winningham et al., 1977). As is discussed above, the maintenance of a kilovolt-magnitude parallel electrostatic potential requires rather low ionospheric densities, which correspond to winter conditions of the polar F-region. Conversely, only very small parallel potential differences may be maintained if the F-region ionospheric densities N_{I+} at 2000 km were $\sim 10^4$ cm^{-3}, corresponding to summer daytime conditions. These considerations are applicable only to the general dependence on the ionospheric boundary conditions of our model since the dayside north-south asymmetry

of the ionosphere is neglected in our consideration. Quite interestingly, statistical analysis of OGO-4 data indicated that field-aligned electron precipitation events were more likely to occur during winter (Berko and Hoffman, 1974). Since our model requires ion densities at the lower boundary which are consistent with F-region trough densities only, and further, since energetic O^+ and H^+ ions in the keV range (moving upward along auroral field lines) have been reported (Shelley et al., 1976), we may perhaps invoke the self-consistent parallel electric field as a possible mechanism for the formation of the ionospheric trough. A detailed consideration of such a mechanism will be made in a subsequent work.

The density distributions n_j of particles of various species (j = M- , M+ , S1, S2, T, I-, and I+) for Case W are shown in Figures 6 and 7. From Figure 6, it is seen that roughly 1/3 of the magnetospheric electrons are precipitating, so as to yield a precipitating electron beam of density 0.9 cm^{-3}, in agreement with the density required in the model of Evans (1975). The density distribution n_{S1} of primary backscattered electrons shows a peculiar kink near the magnetic-field ratio $B/B_0 \approx 300$. The formation of the kink is quite easily understood if one recalls that, according to (21), the primary backscattered electron distribution consists of a low-energy component ($\varepsilon_\ell < |e|V_\ell$) and a high-energy component ($\varepsilon_\ell > |e|V_\ell$). The high-energy component of primary backscattered electrons has a density distribution similar to n_{M-} near the foot of the field line, whereas the low-energy component has a distribution similar to the n_{S2} of secondary backscattered electrons,

shown in Figure 7. The sum of two such curves produces the shape of n_{S1} shown in Figure 6. Comparison of magnetospheric ion density n_{M+} in Figure 6 with ionospheric ion density n_{I+} in Figure 7 in the region just above the intense parallel electric field indicates that the densities of the two species are comparable there. Since the ionospheric ions in this region have been accelerated by the electric field, we would expect substantial numbers of energetic ions in the region, in agreement with Shelley et al. (1976).

CONCLUSION

We have demonstrated in this model that parallel electrostatic potential differences of the order of one kilovolt may be self-consistently maintained along an auroral field line by the magnetospheric and ionospheric particle populations in the flux tube. Our model attempts to abstract the characteristics of magnetospheric and ionospheric particle distributions and to incorporate the very important process of electron backscatter in a magnetic field. By application of the principle of quasi-neutrality, a self-consistent parallel electrostatic potential distribution, in equilibrium with the particle distributions along the auroral field line, is obtained. Application of the model to two typical events of field-aligned electron precipitation have yielded particle parameters which are consistent with the conditions of the ionosphere and the magnetosphere at the time and place of observation of the events. The difference in the pitch-angle anisotropies of magnetospheric ions and electrons and the inclusion of backscattered electrons are the key factors which self-consistently support a parallel potential difference of kilovolt range. Our model suggests that such large parallel potential differences between the ionosphere and the magnetospheric equator can be maintained only if the ion density at the lower boundary (2000 km altitude) is comparable to that in the F-region trough. We are inclined to view the generation of a large parallel electrostatic potential drop as a self-consistent mechanism by which the F-region ionospheric trough is formed by extraction of cold ions from the ionosphere. These cold ions are accelerated upward into the magnetosphere where their energies will be $\sim|e|V_{\ell}$, i.e., in the keV range.

As we have stated in the introduction, our model is not intended to be applicable to all types of field-aligned electron precipitation events in which beam-like characteristics are evident. In particular, our model is incapable of explaining events in which diffusive energy gain is evident. Further, our model is not intended to exclude the possible existence of double layers or electrostatic shocks. Indeed, it is quite easy to obtain in our model a "solution" which has the characteristics of a double layer similar to that obtained by Lemaire and Scherer (1977). However, such a potential distribution does not satisfy our accessibility criterion imposed by (7). We do not know how to treat the velocity-space integration for particles that are accessible to the source point s^* only under conditions more stringent than the simple criterion on $v_{\|s^*}^2$. Therefore, we are unable to generate "double layer" solutions that are acceptable within the framework of our model.

In a simple model such as ours, there are obviously a number of features which require improvement. Clearly, our assumption of an ionospheric boundary independent of particle species and energy is not justified. The exclusion of perpendicular electric fields in our consideration of quasi-neutrality is clearly not realistic, since auroral events are invariably accompanied by intense perpendicular electric fields (Mozer et al., 1977). We have ignored these crucial features primarily for the sake of simplicity and for the sake of concentrating on the implications of pitch-angle anisotropy, electron backscatter, and ionospheric conditions. We hope to remove these shortcomings of our model in subsequent works.

Finally, we take note of some very recent studies by Lennartsson (1976, 1977) and Whipple (1977), which have some features in common with the present work. We became aware of these studies only after completion of the present numerical calculations, but we do not view the present work as a duplication of their efforts. The problem of calculating parallel electric fields and charged-particle distributions in the auroral zone is a complicated one, and different investigators are likely to approach the problem in somewhat different ways.

APPENDIX A: ACCESSIBILITY

We have used the simple criterion $v_{\|s*}^2 \gtrless 0$ in order to determine whether a phase-space point ($v_{\|s}$, $v_{\perp s}$; s) is connected to a source point ($v_{\|s*}$, $v_{\perp s*}$; s^*) under the laws of adiabatic charged-particle motion. Strictly speaking, however, the necessary and sufficient condition for accessibility is that $v_{\|s'}^2 > 0$ for all s' between s and s^*. The equivalence of this seemingly more stringent criterion to the simple criterion on $v_{\|s*}^2$ is contingent on the functional form of $V_s(B_s)$, as will be shown here.

We wish to determine some (preferably minimal) constraints on the form of V_s that will assure the truth of the following statement for all particles of interest: if $v_{\|s}^2 > 0$ and $v_{\|s*}^2 > 0$, then $v_{\|s'}^2 > 0$ for all s' between s and s^*. The statement will obviously hold true if $v_{\|s'}^2$ is a montonic function of $B_{s'}$ for $0 \le s' \le \ell$. It will also hold true if $v_{\|s'}^2$ is concave downward when plotted as a function of $B_{s'}$ between $s' = 0$ and $s' = \ell$. The presence of $q = \pm 1$ in (12) would make it difficult for both ions and electrons to have a monotonic (or both to have a concave-downward) $v_{\|s'}^2$ for all values of $v_{\|s}^2$ and $v_{\perp s}^2$. We shall therefore try to make $v_{\|s'}^2$ monotonic for ions and concave downward for electrons.

Monotonicity of $v_{\|s'}^2$ for ions ($q = +1$) would require that

$$d(v_{\|s'}^2)/dB_{s'} = -(v_{\perp s}^2/B_s) - (2/m_+)|e|(dV_{s'}/dB_{s'}) + \frac{4GM_E}{3R_E B_0}\left[\frac{B_0}{B_{s'}}\right]^{2/3}\frac{[\,4 - 3(r_{s'}/LR_E)\,]^{5/6}}{[\,8 - 5(r_{s'}/LR_E)\,]} \le 0, \tag{A1}$$

as can be shown by differentiating (12) with respect to $B_{s'}$, using a centered-dipole model for the magnetic field ($r_{s'}$ = altitude + R_E). The inequality in (A1) is imposed by the leading term, which would dominate in the limit of large $v_{\perp s}^2$. For the same inequality to hold in the limit of small $v_{\perp s}^2$, however, one must have $dV_{s'}/dB_{s'} > 0$ at least. The stronger condition

$$|e|(dV_{s'}/dB_{s'}) > (GM_E m_+/3R_E B_0)(B_0/B_{s'})^{2/3} \qquad (A2)$$

for $0 \le s' \le \ell$ would enable the electric-field term to overcome gravity, as is required for the unconditional monotonicity of $v_{\parallel s'}^2$.

Gravity is negligible for electrons ($q = -1$), but the appearance of $q < 0$ in (6) necessitates a further functional constraint on V_s. We require (see above) that $v_{\parallel s'}^2$ for electrons be concave downward when plotted against $B_{s'}$. In other words, we require that

$$d^2(v_{\parallel s'}^2)/dB_{s'}^2 = (2/m_-)|e|(d^2V_{s'}/dB_{s'}^2) \le 0 \qquad (A3)$$

for $0 \le s' \le \ell$, which is to say that $V_{s'}$ must be concave downward when plotted against $B_{s'}$.

For electrostatic potentials $V_{s'}$ that fail to satisfy (A2) and (A3), there is a serious danger that a "barrier" in the "effective" potential defined (e.g., Whipple, 1977) by

$$\Phi_{s'} = q|e|V_{s'} + (m_q v_{\perp s}^2/2B_s)B_{s'} - (m_q GM_E/r_{s'}) \qquad (A4)$$

would prevent the access of a particle from s^* to s, despite the fact that both $v_{\parallel s}^2 > 0$ and $v_{\parallel s^*}^2 > 0$ were satisfied for the particle in question. It is to preclude such a danger of improper mapping that we require (A2) and (A3) as constraints (imposed a posteriori) on the admissibility of "solutions" V_s that are found to satisfy (1) for $0 \leq s \leq \ell$.

We have carefully checked to be sure that our solutions $V_s(B_s)$ shown in Figures 4 and 5 satisfy (A3), which is equivalent to (7). We have also verified that our solutions satisfy (A2) for hydrogen ions. However, we find that our solutions fail to satisfy (A2) at $B_s \sim B_\ell$ for heavier ions such as O^+. This is not a serious drawback in the present context. Since we have considered only one species of ionospheric ion, we may logically identify the I^+ population in (13) with H^+ and consider all the O^+ to reside beyond $s = \ell$, i.e., below the base of collisionless medium. Alternatively, we may regard the I^+ population as consisting of ions having a mass equal to the density-weighted mean of m_H and m_O at $s = \ell$.

Either of the above alternatives can be supported by an appeal to the H^+/O^+ density ratio observed at altitudes below 2000 km in high-latitude trough regions (Hoffman et al., 1974), but neither alternative is

strictly acceptable in the context of accounting for the upward fluxes of energetic O^+ that are observed (Shelley et al., 1976) at high altitudes. We presume that a more realistic treatment of the ionosphere (beyond the scope of the present work) would alleviate this dilemma. Thus, in a more sophisticated study, one might treat the several ionospheric constituents separately and also take account somehow of the smooth transition between the collision-dominated lower ionosphere and the collision-free upper ionosphere. Such a study is in progress.

The only O^+ ions that would have been treated improperly in the present work are some of those found equatorward of the maximum in the effective potential Φ_s, which is defined by (A4). Those found earthward of the maximum in Φ_s would have been mapped in precise accordance with Liouville's theorem, except of course for the depletion factor D given by (14). It is not likely that the more sophisticated treatment of the ionosphere described above will alter the prsent form of $V_s(B_s)$ severely, so as to let O^+ ions satisfy (A2), for in that case the ionosphere would rapidly be depleted of O^+. However, a more realistic treatment of the ionosphere would better account for the relative distribution of H^+ and O^+ along the field line and might (by treating the effect of gravity on O^+ in a fully consistent way) enable one to increase the convective sweeping time τ that appears in (14). This would be desirable.

APPENDIX B: DENSITY MOMENT

In this appendix we shall show a sample calculation of the charge-density moment of magnetospheric electrons, which is required for implementing quasi-neutrality. With the use of the distribution function (9) for magnetospheric electrons f_{M-}, we obtain the magnetospheric electron density moment

$$n_{M-}(s) \equiv \int_0^{\infty} v_{\perp s}\, dv_{\perp s} \int_{-\infty}^{+\infty} f_{M-}(v_{\parallel s}, v_{\perp s}; V_s)\, dv_{\parallel s}$$

$$\equiv 2\pi C_{M-} (2\pi T_{\parallel -}/m_-)^{3/2} Q_{M-}(s) \qquad \text{(B1)}$$

In our model, the density of magnetospheric electrons $n_{M-}(0)$ at the equator is the input parameter N_{M-}; therefore, (B1) is normalized so that

$$n_{M-}(s) = N_{M-} [Q_{M-}(s)/Q_{M-}(0)] , \qquad \text{(B2)}$$

where the function $Q_{M-}(0)$ is defined as the limit of $Q_{M-}(s)$ as $s \to 0^+$. The function $Q_{M-}(s)$ is given in terms of functions related to error functions and Dawson integrals (Abramowitz and Stegun, 1974). It is convenient to define

$$E_1(x) = \exp(x^2) \int_0^x dy\, \exp(-y^2) \qquad \text{(B3)}$$

$$E_2(x) = \exp(x^2)\int_x^\infty dy\ \exp(-y^2) \tag{B4}$$

$$E_3(x) = \exp(-x^2)\int_0^x dy\ \exp(y^2) \tag{B5}$$

together with the simplifying relations

$$h_s = B_s - [\,1 - (T_{\parallel -}/T_{\perp -})\,]B_0 \tag{B6}$$

$$\lambda_s = (\,|e|\,V_s/\varkappa T_{\parallel -})^{1/2} \tag{B7}$$

$$\mu_s = [\,(B_s - B_0)\,T_{\perp -}/(B_0 T_{\parallel -})\,]^{1/2} \tag{B8}$$

$$\nu_s = [\,(B_\ell - B_s)/h_\ell\,]^{1/2} \tag{B9}$$

$$\xi_s = \lambda_s^2 - [\,(B_s - B_0)/(B_\ell - B_0)\,]\,\lambda_\ell^2\ . \tag{B10}$$

The function $Q_{M-}(s)$ is given by

$$Q_{M-}(s) = (B_\ell/2h_s)\{(\nu_s\pi^{1/2}/2)\exp[|e|(V_s h_\ell - V_\ell h_s)/(B_\ell - B_s)\kappa T_{\|-}]$$

$$+ E_2(\lambda_s) + \mu_s E_3(\lambda_s/\mu_s)$$

$$+ \theta(\xi_s)\exp[-(\lambda_\ell/\mu_\ell)^2]\,[\mu_s E_3(\xi_s^{1/2}/\mu_s) - \nu_s E_1(\xi_s^{1/2}/\nu_s)]\}\,. \tag{B11}$$

The evaluations of the charge densities are independently checked by three methods: (a) the charge-density integrals for the mirroring and precipitating components are evaluated separately and the sum is checked against (B11); (b) if we set $\theta(v_{\|s})$ equal to unity in (9), then there are no phase-space restrictions due to the functions $\theta(v_{\|\ell}^2)$ and the total charge-density integral is easy to compute, and we have checked that the total charge-density integral is equal to the sum of the mirroring component plus twice the precipitating component; (c) finally, the arguments of the θ functions in (9) simplify in the limit $s \to 0^+$, and the evaluation of (B11) in the limit $s \to 0^+$ has been checked against the $s \to 0^+$ limit of the charge-density integral independently evaluated before the limit is taken.

ACKNOWLEDGMENT

We appreciate communications and/or discussions with Drs. J. M. Cornwall, D. S. Evans, J. F. Fennell, J. H. Hoffman , J. Lemaire, J. M. Luhmann, P. F. Mizera, A. L. Vampola, and J. D. Winningham.

The work was conducted in part under the Company-Financed Research Program of The Aerospace Corporation and in part under U. S. Air Force Space and Missile Systems Organization (SAMSO) contract F04701-76-C-0077.

REFERENCES

Abramowitz, M., and I. A. Stegun , Handbook of Mathematical Functions, 1046 pp., U. S. Dept. of Commerce, Washington, 1964.

Alfvén, H., and C.-G. Fälthammar, Cosmical Electrodynamics, pp. 163-167, Clarendon Press, Oxford, 1963.

Banks, P. M., C. R. Chappell, and A. F. Nagy, A new model for the interaction of auroral electrons with the atmosphere : spectral degradation, backscatter, optical emission, and ionization, J. Geophys. Res., 79, 1459, 1974.

Banks, P. M., and T. E. Holzer, The polar wind, J. Geophys. Res., 73, 6846, 1968.

Berko, F. W., and R. A. Hoffman, Dependence of field-aligned electron precipitation occurrence on season and altitude, J. Geophys. Res., 79, 3749, 1974.

Block, L. P., Double layers, in Physics of the Hot Plasma in the Magentosphere, pp.229-249, edited by B. Hultqvist and L. Stenflo, Plenum Press, N. Y., 1975.

Chiu, Y. T., Self-consistent electrostatic field mapping in the high-latitude ionosphere, J. Geophys. Res., 79, 2790, 1974.

CIRA, COSPAR International Reference Atmosphere, COSPAR Working Group 4, Akademie-Verlag, Berlin, 1972.

Cornwall, J. M., Micropulsations and the outer radiation zone, J. Geophys. Res., 71, 2185, 1966.

Cornwall, J. M., F. V. Coroniti, and R. M. Thorne, Unified theory of SAR arc formation at the plasmapause, J. Geophys. Res., 76, 4428, 1971.

DeForest, S. E., and C. E. McIlwain, Plasma clouds in the magnetosphere, J. Geophys. Res., 76, 3587, 1971.

Evans, D. S., Precipitating electron fluxes formed by a magnetic field-aligned potential difference, J. Geophys. Res., 79, 2853, 1974.

Evans, D. S., Evidence for the low altitude acceleration of auroral particles, in Physics of the Hot Plasma in the Magnetosphere, pp. 319-340, edited by B. Hultqvist and L. Stenflo, Plenum Press, N. Y., 1975.

Evans, D. S., The acceleration of charged particles at low altitudes, in Physics of Solar Planetary Environments, pp. 730-739, edited by D. J. Williams, Am. Geophys. Union, Washington, 1976.

Eviatar, A., A. M. Lenchek, and S. F. Singer, Distribution of density in an ion-exosphere of a non-rotating planet, Phys. Fluids, 7, 1775, 1964.

Haerendel, G., E. Rieger, A. Valenzuela, H. Föppl, and H. Stenbaek-Nielsen, First observation of electrostatic acceleration of barium ions into the magnetosphere, preprint, Max Planck Institute for Physics and Astrophysics, Garching, 1976.

Hoffman, J. H., W. H. Dodson, C. R. Lippincott, and H. D. Hammack, Initial ion composition results from the ISIS-2 satellite, J. Geophys. Res., 79, 4246, 1974.

Hultqvist, B., H. Borg, W. Riedler, and P. Christopherson, Observation of a magnetic field-aligned anisotropy for 1 and 6 keV positive ions in the upper ionosphere, Planet. Space Sci., 19, 279, 1971.

Kaufmann, R. L., D. N. Walker, and R. L. Arnoldy, Acceleration of auroral electrons in parallel electric fields, J. Geophys. Res., 81, 1673, 1976.

Kennel, C. F., and H. E. Petschek, Limit on stably trapped particle fluxes, J. Geophys. Res., 71, 1, 1966.

Kindel, J. M., and C. F. Kennel, Topside current instabilities, J. Geophys. Res., 76, 3055, 1971.

Lemaire, J., and M. Scherer, Simple model for an ion-exosphere in an open magnetic field, Phys. Fluids, 14, 1683, 1971a.

Lemaire, J., and M. Scherer, Kinetic models of the solar wind, J. Geophys. Res., 76, 7479, 1971b.

Lemaire, J., and M. Scherer, Ionosphere-plasmasheet field-aligned currents and parallel electric fields, Planet. Space Sci., 22, 1485, 1974.

Lemaire, J., and M. Scherer, Field-aligned distribution of plasma mantle and ionospheric plasmas, J. Atm. Terr. Phys., to be published, 1977.

Lennartsson, W., On the magnetic mirroring as the basic cause of parallel electric fields, J. Geophys. Res., 81, 5583, 1976.

Lennartsson, W., On high-latitude convection field inhomogeneities, parallel electric fields and inverted-V precipitation events, Planet. Space Sci., 25, 89, 1977.

Mizera, P. F., D. R. Croley, Jr., and J. F. Fennell, Electron pitch-angle distributions in an inverted-'V' structure, Geophys. Res. Letters, 3, 149, 1976.

Mozer, F. S., C. W. Carlson, M. K. Hudson, R. B. Torbert, B. Parady, J. Yatteau, and M. C. Kelley, Observation of paired electrostatic shocks in the polar magnetosphere, Phys. Rev. Letters, 38, 292, 1977.

Papadopoulous, K., and T. Coffey, Nonthermal features of the auroral plasma due to precipitating electrons, J. Geophys. Res., 79, 674, 1974.

Perkins, F. W., Plasma-wave instabilities in the ionosphere over the aurora, J. Geophys. Res., 73, 6631, 1968.

Persson, H., Electric field along a magnetic line of force in a low-density plasma, Phys. Fluids, 6, 1756, 1963.

Quon, B. H., and A. Y. Wong, Formation of potential double layers in plasmas, Phys. Rev. Letters, 37, 1393, 1976.

Schulz, M., and H. C. Koons, Thermalization of colliding ion streams beyond the plasmapause, J. Geophys. Res., 77, 248, 1972.

Shelley, E. G., R. D. Sharp, and R. G. Johnson, Satellite observation of an ionospheric acceleration mechanism, Geophys. Res. Letters, 3, 645, 1976.

Swift, D. W., On the formation of auroral arcs and acceleration of auroral electrons, J. Geophys. Res., 80, 2096, 1975.

Winningham, J. D., T. W. Speiser, E. W. Hones, Jr., R. A. Jeffries, W. H. Roach, D. S. Evans, and H. C. Stenbaek-Nielsen, Rocket-borne measurements of the dayside cleft plasma: The Tordo experiments, J. Geophys. Res., 82, in press, 1977.

Whipple, E. C., Jr., The signature of parallel electric fields in a collisionless plasma. J. Geophys. Res., 82, 1525, 1977.

Table 1. Parameters of the Model

Parameters	Symbols	Remarks
Total Potential Difference	V_ℓ	Determined from observed electron flux
Magnetospheric Electron Density at $s = 0$	N_{M-}	$N_{M-}/T_{\perp-}$ determined from observed electron flux
Magnetospheric Electron Temperatures	$T_{\parallel-}, T_{\perp-}$	$T_{\parallel-}$ and $N_{M-}/T_{\perp-}$ determined from observed electron flux
Magnetospheric Ion Density at $s = 0$	N_{M+}	Determined by charge-neutrality constraint at $s = 0$
Magnetospheric Ion Temperatures	$T_{\parallel+}, T_{\perp+}$	Adjustable, constrained by $T_{\perp+} \geq T_{\parallel+}$ and $T_+ \sim 4T_-$
Ionospheric Electron Density	N_{I-}	Determined by charge-neutrality constraint at $s = \ell$
Ionospheric Electron Temperature	T_{I-}	Adjustable, but fixed at $T_{I-} = 1$ eV here; unimportant
Ionospheric Ion Density	N_{I+}	Adjustable, but constrained to trough-region densities
Ionospheric Ion Temperature	T_{I+}	Adjustable, but fixed at $T_{I-}/32$; unimportant
Secondary Backscatter Intensity	A_2	Determined from observed electron flux
Trapped Electron Temperature	T	Adjustable, but fixed at $T = T_{\parallel-}$
Cold Ion Depletion Time Constant	τ	Adjustable, but usually turns out to be ~20 min

Table 2: Parameters of the Fit

Parameter	Case W (Figure 2)	Case M (Figure 3)
V_ℓ	0.59 kV	1.76 kV
N_{M-}	3 cm^{-3}	0.6 cm^{-3}
$\varkappa T_{\parallel -}$	0.189 keV	1.23 keV
$\varkappa T_{\perp -}$	0.775 keV	4.67 keV
A_2	4.8	3.2

Table 3: Parameters Yielding Solutions

Parameter	Case W (Figure 4)	Case M (Figure 5)
N_{I+}	1200 cm^{-3}	90 cm^{-3}
$\varkappa T_{\parallel +}$	2.0 keV	8.0 keV
$\varkappa T_{\perp +}$	2.0 keV	8.0 keV
t	17 min	19 min

FIGURE CAPTIONS

Figure 1. The regions of phase space occupied by the various particle populations are shown schematically for (a) ions and for (b) electrons. The solid curves are demarcations in phase space for the various populations of particles identified by labels in circles or in cartouches: M for particles of magnetospheric origin, I for particles of ionospheric origin, S for backscattered electrons, and T for electrons trapped between mirror points that both lie on the same half of the field line. The ionic label I in parentheses refers to the population given by (13c), as distinguished from those given in (13a) and (13b). The electronic labels I in parentheses indicate phase space regions occupied by electrons in the extreme tail of the cold ionospheric energy distribution. The dashed diagonal lines are the asymptotes $v_{\parallel} = \pm[(B_I/B) - 1]^{1/2} v_{\perp}$ of the hyperbolic phase space demarcations between $v_{\parallel I}^2 > 0$ and $v_{\parallel I}^2 < 0$.

Figure 2. Electron flux at 45° pitch angle observed in the dayside cusp region on 11 January 1975 on board the Tordo Dos rocket (Winningham et al., 1977) is shown as function of electron energy. The data points and the fit (solid curve) corresponding to Evans' model are taken from Evans (1974).

Figure 3. Electron energy fluxes at 0° and at 180° pitch angles observed in an "inverted-V" structure (Mizera et al., 1976) are shown

as functions of electron energy. The difference between the downgoing and upgoing fluxes at 1.76 keV indicates the presence of a "monoenergetic" beam of precipitating energetic electrons.

Figure 4. The self-consistent electrostatic potential computed for the case corresponding to the observed electron flux of Figure 2 (Case W) is shown as function of magnetic-field ratio and altitude. The magnitude of the parallel electrostatic field is also shown.

Figure 5. The self-consistent electrostatic potential computed for the case corresponding to the observed electron flux of Figure 3 (Case M) is shown as function of magnetic-field ratio and altitude. The curve for the potential V has the same property of downward concavity as that shown in Figure 4. The difference in appearance between this figure and Figure 4 is due to the logarithmic scale used in plotting the magnetic-field ratio here. The magnitude of the parallel electrostatic field computed for this case is considerably larger than that of Figure 4.

Figure 6. Distributions of the various energetic particles along the field line, computed for Case W, are shown as functions of magnetic-field ratio. The subscripts identify the various particle populations: M* for magnetospheric protons and electrons, S1 for primary backscattered electrons, and T for electrons trapped between mirror points that both lie on the same half of the field line.

Figure 7. Distributions of the various "low-energy" particles along the field line, computed for Case W, are shown as functions of magnetic-field ratio. The subscripts I± refer to ionospheric particles, and the subscript S2 refers to secondary backscattered electrons. At the upper reaches of the field line ($B/B_0 \lesssim 10$) the ions are not truly of low energy since they have been accelerated by the parallel electric field.

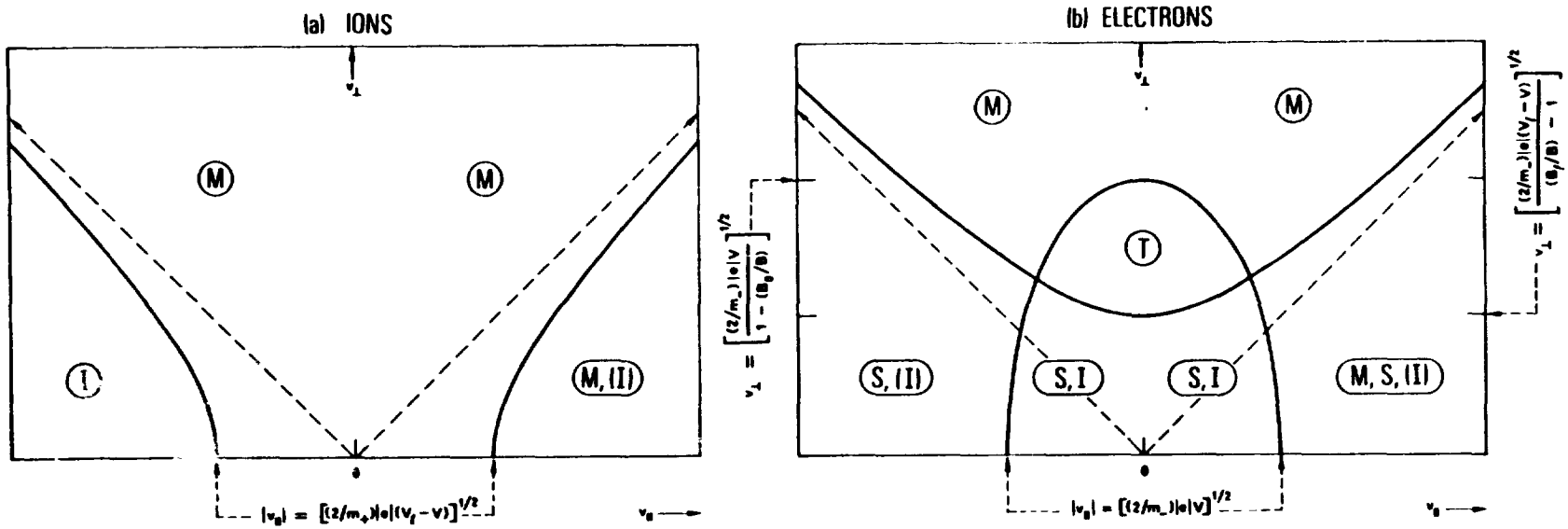
(a) IONS
M
M
I
M, (II)
$v_\perp$
$v_\parallel$
$|v_\parallel| = [(2/m_+)e|(V_f - V)]^{1/2}$
(b) ELECTRONS
M
M
T
S, (II)
S, I
S, I
M, S, (II)
$v_\perp = \left[\frac{(2/m_-)|e|V}{1 - (\Omega_e/\omega)}\right]^{1/2}$
$v_\perp = \left[\frac{(2/m_-)|e|(V_f - V)}{(\Omega_e/\omega) - 1}\right]^{1/2}$
$|v_\parallel| = [(2/m_-)|e|V]^{1/2}$

Fig. 1

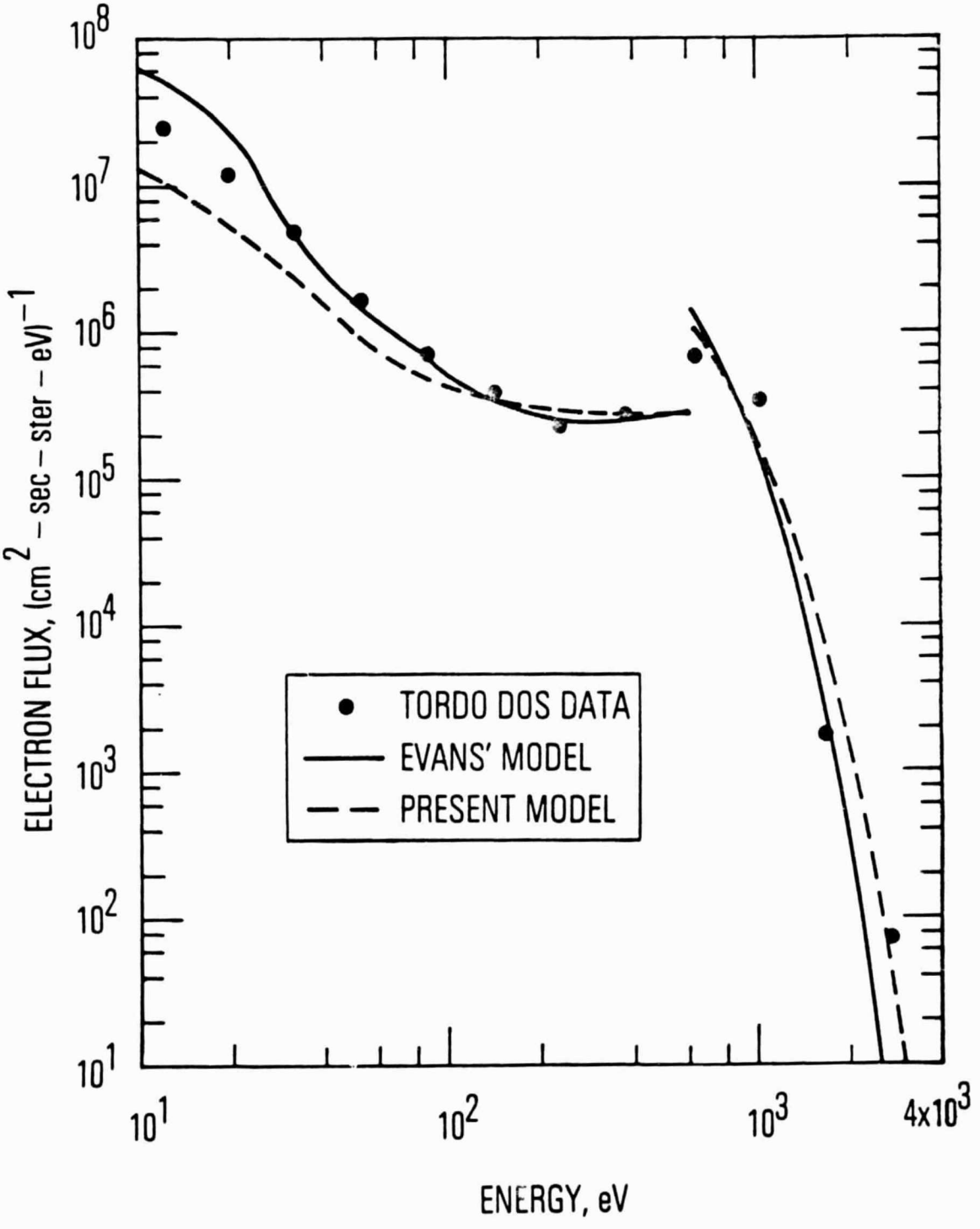
ELECTRON FLUX, (cm^2 – sec – ster – eV)$^{-1}$
10^8
10^7
10^6
10^5
10^4
10^3
10^2
10^1
10^1
10^2
10^3
$4x10^3$
ENERGY, eV
TORDO DOS DATA
EVANS' MODEL
PRESENT MODEL

Fig. 2

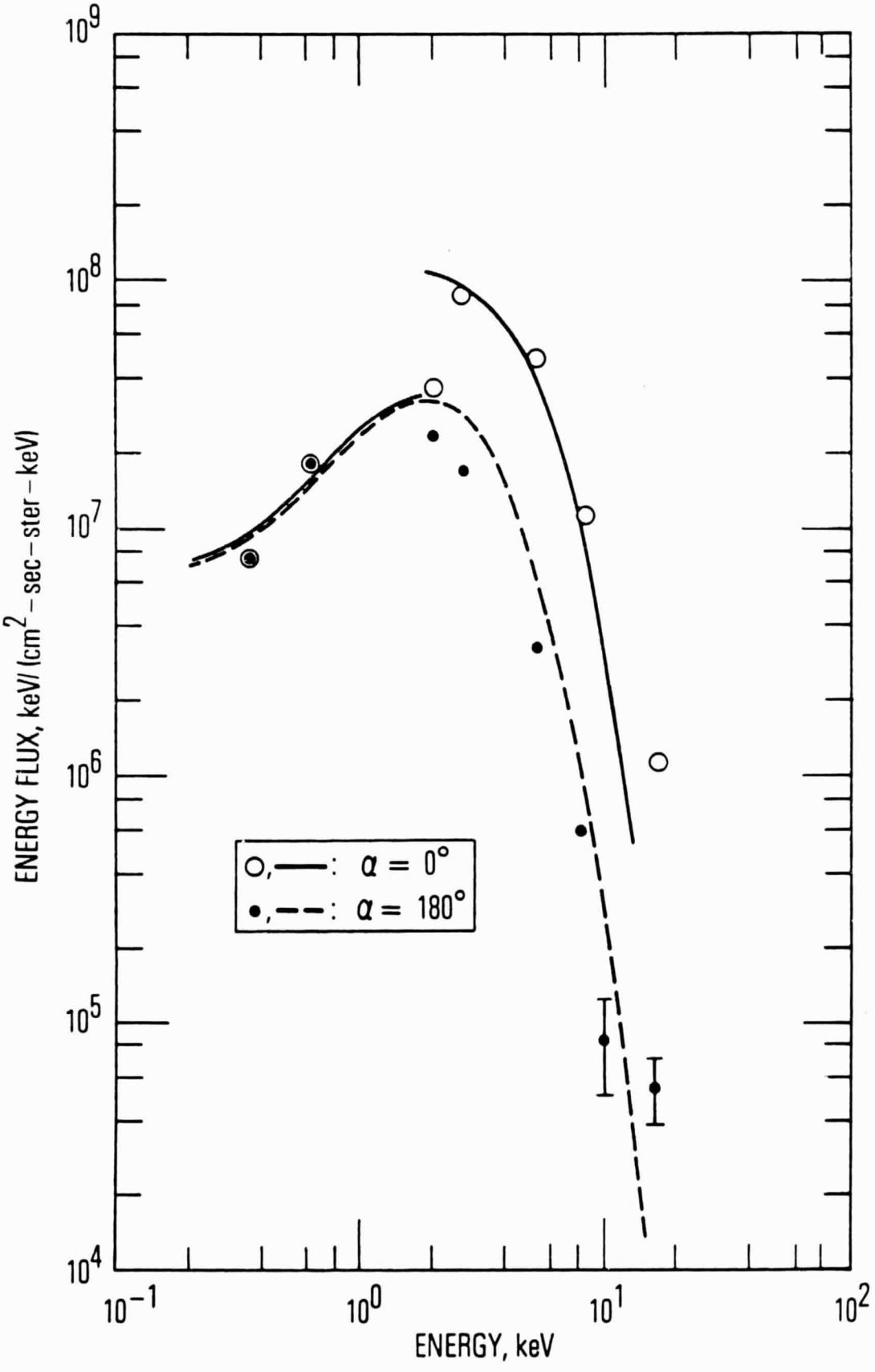
10^9
10^8
10^7
10^6
10^5
10^4
ENERGY FLUX, keV/(cm^2 – sec – ster – keV)
○, ——: α = 0°
●, – – –: α = 180°
10^{-1}
10^0
10^1
10^2
ENERGY, keV

Fig. 3

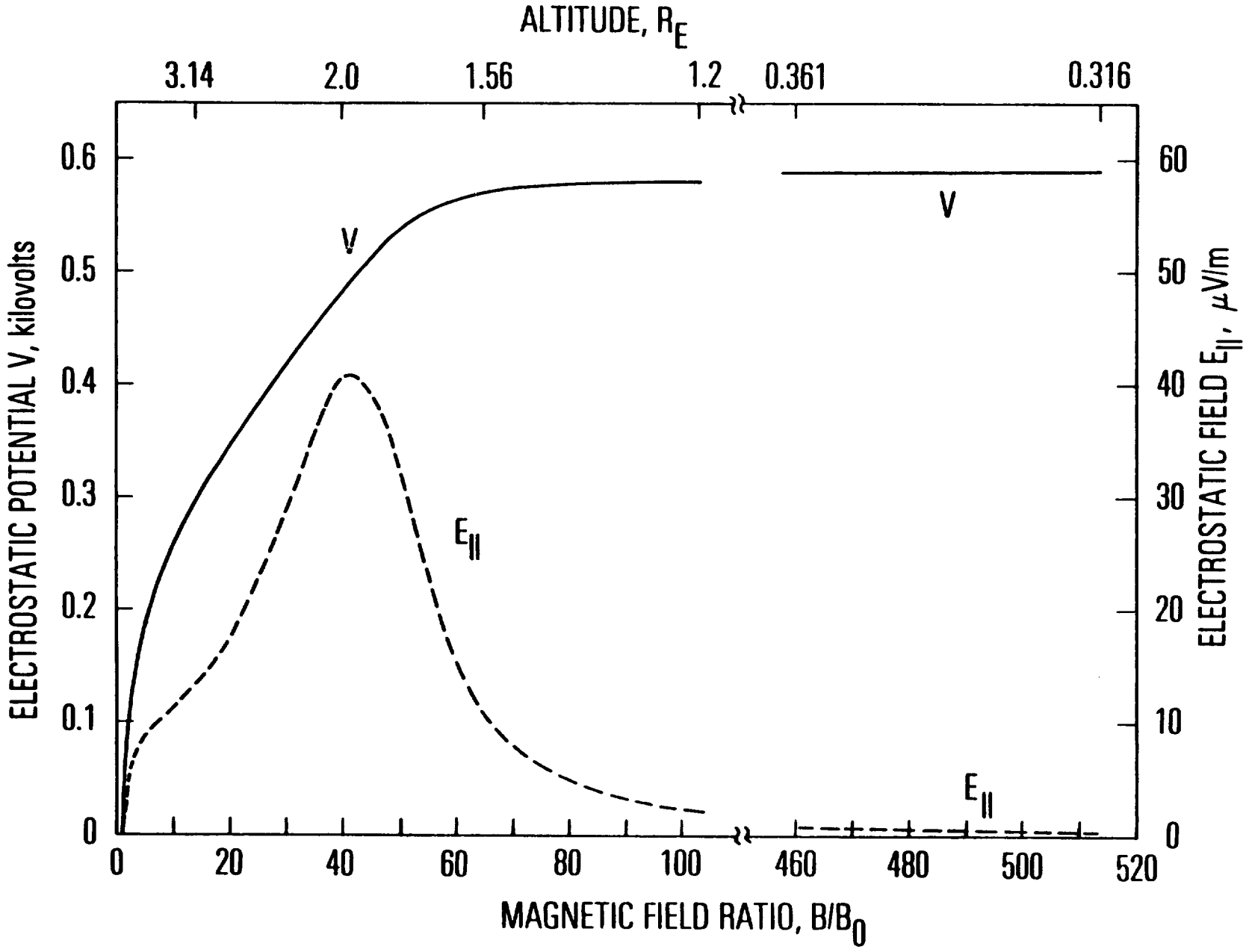
ALTITUDE, R_E
3.14
2.0
1.56
1.2
0.361
0.316
ELECTROSTATIC POTENTIAL V, kilovolts
ELECTROSTATIC FIELD $E_{||}$, μV/m
V
V
$E_{||}$
$E_{||}$
0
0.1
0.2
0.3
0.4
0.5
0.6
0
10
20
30
40
50
60
0
20
40
60
80
100
460
480
500
520
MAGNETIC FIELD RATIO, B/B_0

Fig. 4

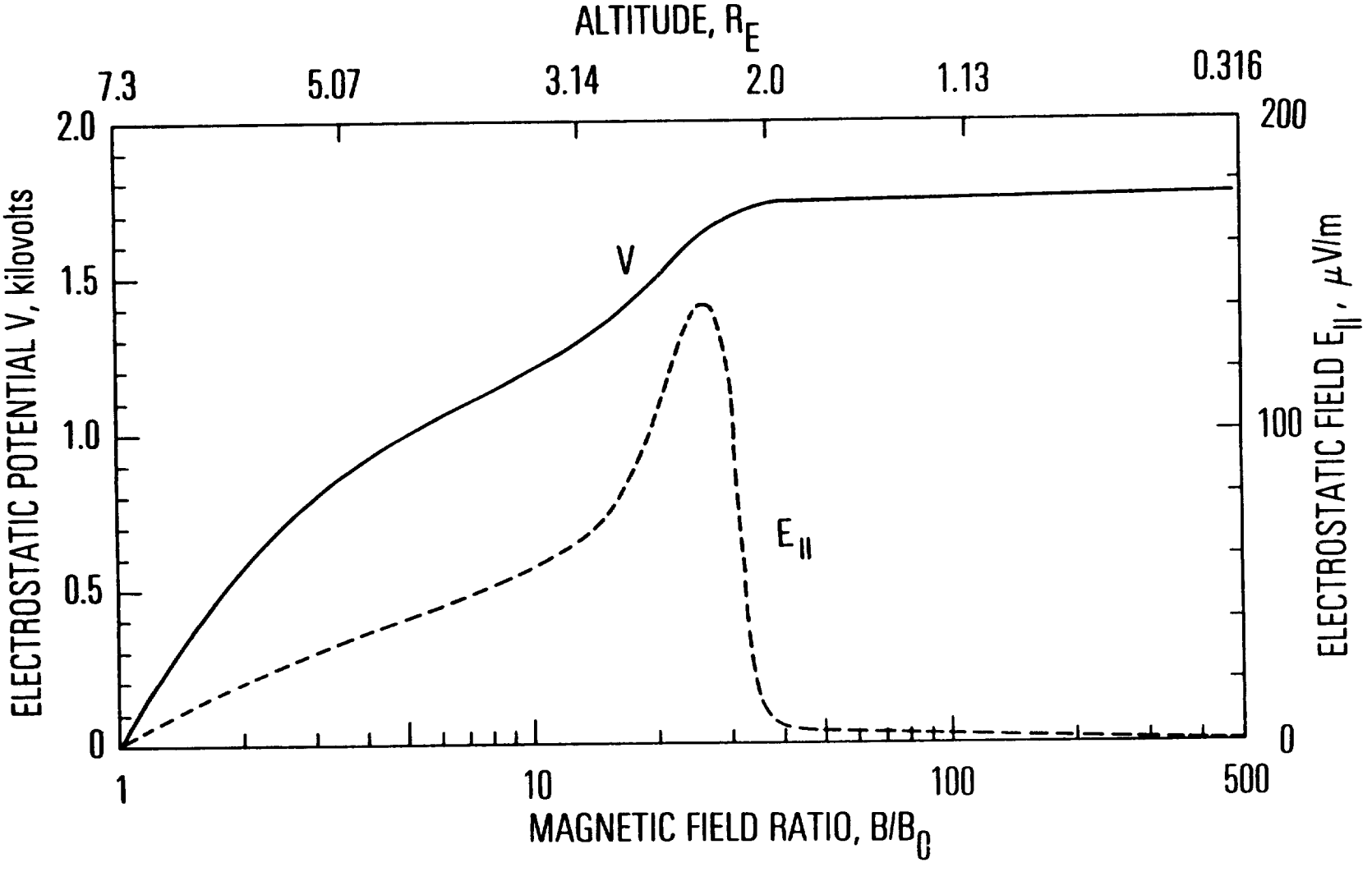
ALTITUDE, R_E
7.3
5.07
3.14
2.0
1.13
0.316
2.0
1.5
1.0
0.5
0
200
100
0
V
$E_{||}$
ELECTROSTATIC POTENTIAL V, kilovolts
ELECTROSTATIC FIELD $E_{||}$, μV/m
1
10
100
500
MAGNETIC FIELD RATIO, B/B_0

Fig. 5

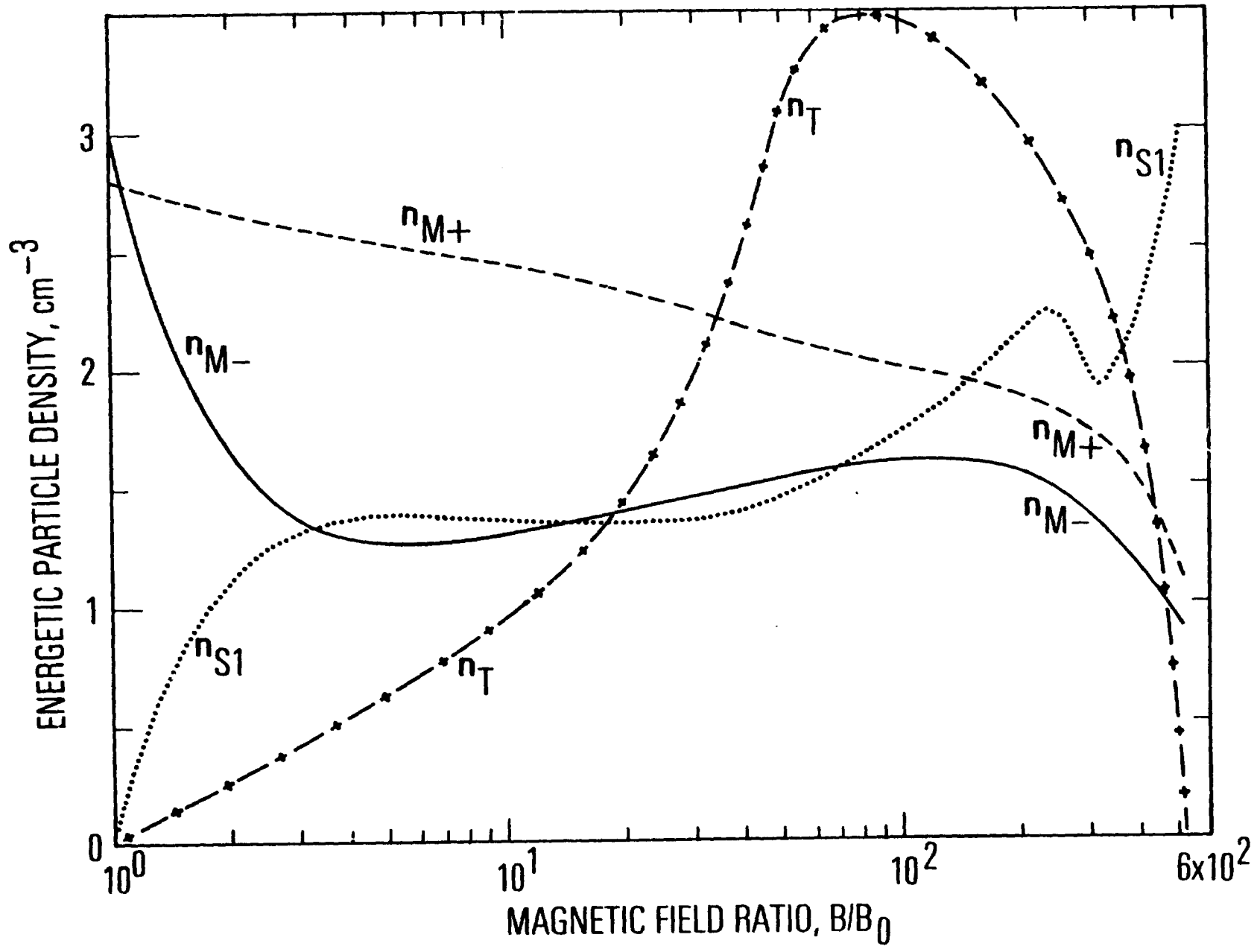
ENERGETIC PARTICLE DENSITY, cm^{-3}
MAGNETIC FIELD RATIO, B/B$_0$
0
1
2
3
10^0
10^1
10^2
$6x10^2$
n_{M+}
n_{M-}
n_{S1}
n_T
n_T
n_{S1}
n_{M+}
n_{M-}

Fig. 6

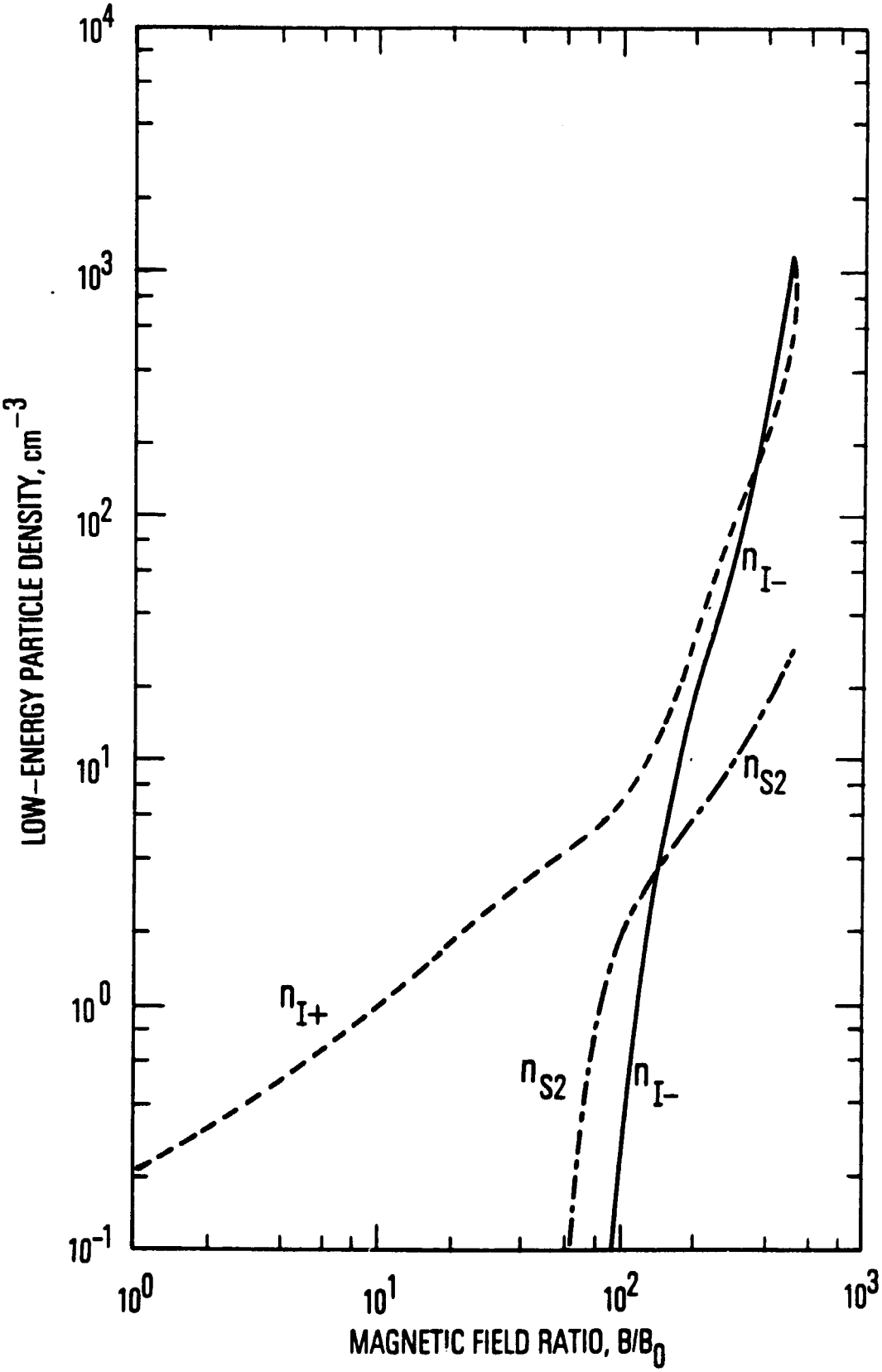
LOW-ENERGY PARTICLE DENSITY, cm^{-3}
10^4
10^3
10^2
10^1
10^0
10^{-1}
n_{I-}
n_{S2}
n_{I+}
n_{S2}
n_{I-}
10^0
10^1
10^2
10^3
MAGNETIC FIELD RATIO, B/B_0

Fig. 7

AURORAL MAGNETOSPHERE-IONOSPHERE COUPLING: A BRIEF TOPICAL REVIEW

Y. T. Chiu, J. M. Cornwall*, and Michael Schulz
Space Sciences Laboratory
The Aerospace Corporation
P. O. Box 92957
Los Angeles, CA 90009

*Permanent address: Department of Physics
University of California, Los Angeles, CA 90024

Auroral arcs result from the acceleration and precipitation of magnetospheric plasma in narrow regions characterized by strong electric fields both perpendicular and parallel to the earth's magnetic field. The various mechanisms that have been proposed for the origin of such strong electric fields are not mutually exclusive. Indeed, they are often complementary. Such mechanisms include: 1) electrostatic double layers; 2) double reverse shocks; 3) anomalous resistivity; 4) magnetic mirroring of hot plasma; and 5) mapping of the magnetospheric-convection electric field through an auroral discontinuity. Observations have not yet identified from among these mechanisms the one that is primarily responsible for the formation of auroral arcs.

I. INTRODUCTION

The latter half of the nineteen seventies has witnessed a spectacular increase in the understanding of the detailed dynamics of the auroral arc. This happy circumstance is supported on the one hand by the advent of high-resolution observations by auroral satellites at altitudes $\sim 1\ R_E$, such as those obtained by instruments on board the S3-3 satellite, and on the other by earlier rocket and radar backscatter observations at ionospheric altitudes. Since auroral processes are a major element in the coupling between the magnetosphere and the ionosphere, we undertake in this paper to review briefly what the new satellite observations imply and do not imply in the theoretical understanding of auroral dynamics in general and the coupling between the ionosphere and the magnetosphere in particular.

Because of the self-imposed restriction of brevity, the scope of this topical review is limited to those dynamical aspects of the aurora directly

related to the detailed processes of ionosphere-magnetosphere coupling. The very important optical observations of the aurora fall in a different category and are not included here. Global-scale morphology of ionospheric currents generated by auroral precipitation of energetic particles and the mapping of auroral electrostatic fields down to ionospheric heights are important consequences of the aurora; however, these effects are consequential rather than fundamental to the coupling between the ionosphere and the magnetosphere so we shall allude to them only briefly. In short, we limit our consideration to recent advances in the understanding of particle and field dynamics as they affect ionosphere-magnetosphere coupling in the aurora.

Further, since brevity is emphasized, works and authors referenced here are meant to be representative rather than exhaustive. We attempt to reference the latest work (circa 1978) representative of a particular area so that readers can find a more complete reference therein; therefore, works referenced in this paper do not necessarily carry with them any implication of special significance. Perhaps undue emphasis is placed on the implications of the S3-3 observations, which to some extent merely confirm what had been suspected from earlier rocket and satellite measurements; however, this is partially due to the timing of this review, falling at the point when the scope and coherence of the S3-3 observations have become clear to those of us who are interested in the theoretical aspects of ionosphere-magnetosphere coupling and possible predictions.

II. OBSERVATIONS

Before the advent of high-resolution observations by auroral satellites, data on ionospheric and magnetospheric coupling depended on balloon, rocket, and radar observations which were necessarily episodic; nevertheless, the basic physical properties of auroral ionospheric currents and electric fields (e.g., Cloutier, 1971; Mozer and Manka, 1971; Vondrak et al., 1971), together with their relationship to high-latitude convection electric fields (e.g., Cauffman and Gurnett, 1972; Heppner, 1972) measured by satellites, have been established. Generally, these measurements have indicated that the substorm convection electric field in the magnetosphere drives perpendicular ionospheric currents consistent with ionospheric perpendicular electric fields (meridional and zonal) of the order of tens of millivolts/meter. In addition, Birkeland currents parallel to auroral magnetic field lines seem to have been observed (e.g., Armstrong and Zmuda, 1973). These low-altitude observations are primarily concerned with the morphology and large-scale processes of auroral substorms and are instrumental in emphasizing the importance of the electric field in auroral processes. They, however, have relatively little to say about the microscopic processes taking place in the auroral region.

Even as the large-scale auroral processes were being unravelled, certain microscopic features of auroral low-energy particle precipitations were being discovered. Frank and Ackerson (1971) noted that occasionally

observations of low-energy (tens of keV) electron precipitation would show an "inverted-V" structure on an energy-time spectrum plot, i.e., the precipitating electron energy spectrum hardens and then softens as the Injun 5 satellite moves through the structure. Evans (1974; 1975) convincingly demonstrated that rocket measurements of auroral low-energy electrons indicated downward moving electron beams at keV energies, comparable to those of "inverted-V" structures. Further, by a careful study of electron backscatter from the atmosphere, Evans demonstrated that these auroral electron beams are indications of electric potential drops, along the magnetic field, existing between the equator and the ionosphere. At about the same time, observations of singly ionized energetic O^+ ions in the magnetosphere (Shelley et al., 1972; Sharp et al., 1974) also gave indication that microscopic processes in the aurora couple the ionosphere with the magnetosphere.

These observations of "inverted-V" structures, of electron beams, and of O^+ ions of probable ionospheric origin in the magnetosphere presage very interesting microscopic processes to be discovered in the auroral process in which the ionosphere plays an active rather than passive role. However, because of the episodic nature of rocket observations and because of the low resolution and low data rate of the early satellite observations, the scope of and inter-relationship between these phenomena were not understood until the launch of the polar-orbiting auroral satellite S3-3, which intercepts auroral field lines at altitudes up to ~8000 km, precisely in the region where ionospheric and magnetospheric plasmas are expected to interact. Included in the S3-3 payload are instruments to measure electric fields (Mozer et al., 1977), low energy electrons (Mizera et al., 1976), energetic ions (Shelley et al., 1976), and plasma waves (Kintner et al., 1978). While a co-ordinated data-analysis program among the various auroral measurements is presently being pursued, the separately reduced data have already yielded a coherent picture of the microscopic auroral processes in which magnetosphere-ionosphere coupling plays a central role.

The S3-3 observations not only confirmed Evans' observations of downward-moving field-aligned electron beam at keV energies but also revealed the existence of upward-moving ion beams aligned with the magnetic field in "inverted-V" structures. This certainly indicates that the three phenomena are intimately related, but more importantly the S3-3 particle observations leave little doubt that an electric potential drop of several to tens of kilovolts, aligned with the magnetic field, exists between the ionosphere and the magnetospheric equator. Electrostatic field measurements also indicate paired regions of oppositely directed perpendicular electric fields, with latitudinal scale lengths of some 50 km, reflecting a negative space-charge region presumably associated with downward-streaming electrons. Figure 1, which is a composite of particle and electric field data illustrates the above points. For further emphasis, Figure 2 shows an enlarged view of the perpendicular electric field data for the time period marked by the brace in the middle of Figure 1. A crucial, but seldom emphasized, feature which is brought out by the high sensitivity and high resolution of the S3-3 measurements is that the above correlated features are observed at the auroral zone pass after pass at all

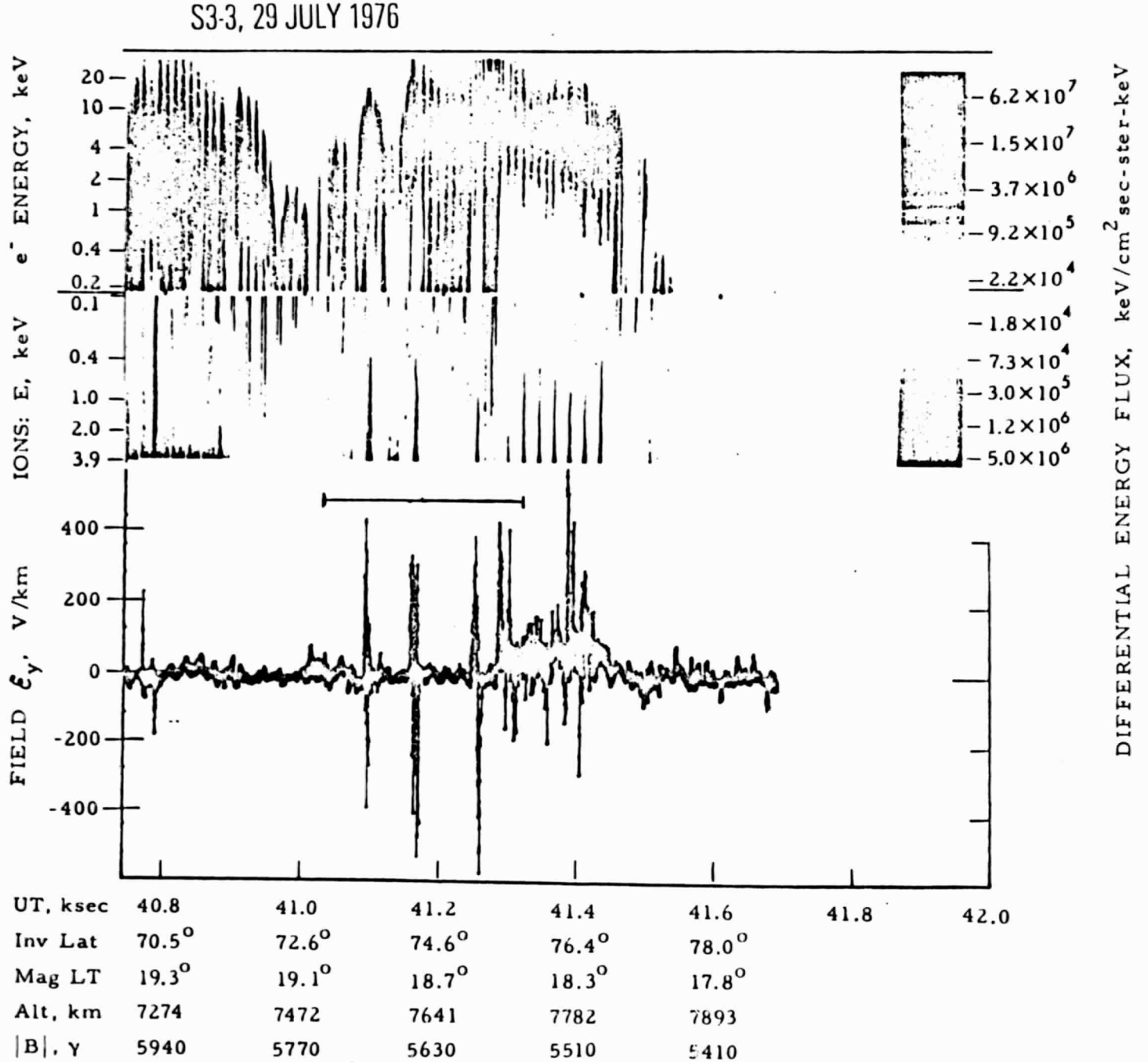
S3-3, 29 JULY 1976
e⁻ ENERGY, keV
20
10
4
2
1
0.4
0.2
IONS: E, keV
0.1
0.4
1.0
2.0
3.9
FIELD $\mathcal{E}_y$, V/km
400
200
0
-200
-400
DIFFERENTIAL ENERGY FLUX, keV/cm² sec-ster-keV
6.2×10⁷
1.5×10⁷
3.7×10⁶
9.2×10⁵
2.2×10⁴
1.8×10⁴
7.3×10⁴
3.0×10⁵
1.2×10⁶
5.0×10⁶
UT, ksec 40.8 41.0 41.2 41.4 41.6 41.8 42.0
Inv Lat 70.5° 72.6° 74.6° 76.4° 78.0°
Mag LT 19.3° 19.1° 18.7° 18.3° 17.8°
Alt, km 7274 7472 7641 7782 7893
|B|, γ 5940 5770 5630 5510 5410

Figure 1

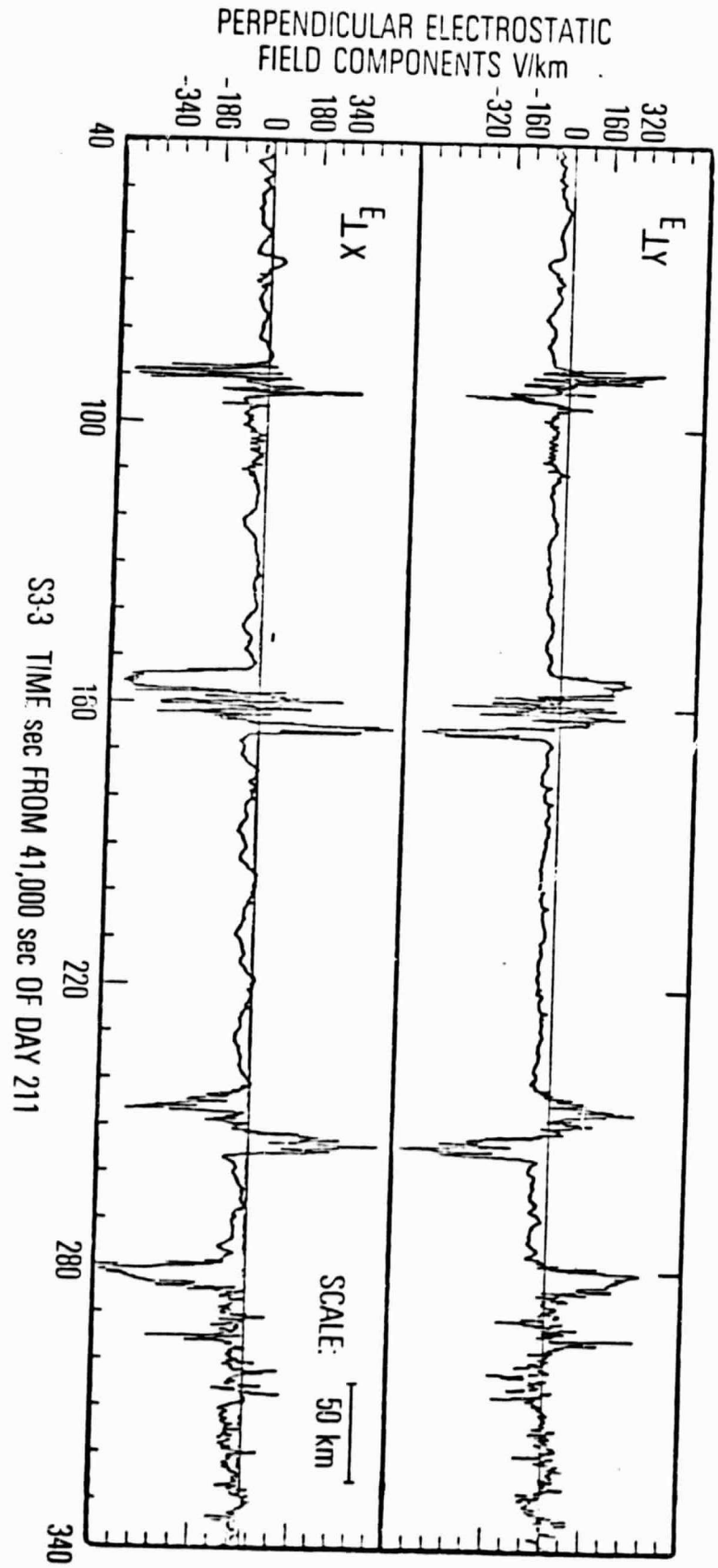
PERPENDICULAR ELECTROSTATIC
FIELD COMPONENTS V/km
320
160
0
-160
-320
340
180
0
-180
-340
$E_{\perp Y}$
$E_{\perp X}$
SCALE: 50 km
40
100
160
220
280
340
S3-3 TIME sec FROM 41,000 sec OF DAY 211

Figure 2

satellite altitudes. In other words, these are fundamental features of the aurora rather than episodic curiosities. Further, plasma waves are observed to be associated with particle beams.

Aside from measurements which give, for the first time, support to a simple electrostatic picture of auroral microscopic processes, the S3-3 observations also reveal a whole class of new phenomena. The most outstanding among these are: 1) observations of "conical" beams, i.e., intense ion fluxes with pitch-angles concentrated on a cone about the direction of the magnetic field, with relatively little ion flux along the magnetic field; 2) upward-going field-aligned electron beams, and 3) downward field-aligned ion beams which are more diffuse than the upward field-aligned ion beams. The signature of conical beams is a bifurcated trace on the ion spectrograms; one can see several examples in Figure 1. Such beams probably result from wave-particle interactions with the basic auroral particle beams, while the downgoing ions and upgoing electrons, observed at lower altitudes, are a signature of the return current driven by electrostatic processes in the ionosphere. The S3-3 auroral observations have opened new vistas in the theoretical study of auroral processes.

III. THEORETICAL INTERPRETATIONS

The key theoretical issue concerning the interpretation of the S3-3 observations really involves the electrodynamics of the auroral arc itself. A key fact which must be recognized is that a magnetic-field-aligned electrostatic potential difference of kilovolt magnitude exists between the ionosphere and the equator. In many respects, this feature has been anticipated in a number of theoretical considerations based on earlier observations. With regard to ionosphere-magnetosphere coupling, however, the crucial question is whether the mechanism for the buildup of such a field-aligned potential drop involves the ionosphere, for there is no doubt that the energy source of the aurora is derived from hot magnetospheric plasmas which are injected by substorm processes onto the auroral field lines. Some aspects of these theories of auroral field-aligned potential drop have been reviewed (Shawhan et al., 1978; Hudson and Mozer, 1978), but our discussions will be primarily concerned with the ionosphere-magnetosphere coupling aspects of these theories.

Theories of auroral processes involving magnetic field-aligned electrostatic potential differences can be roughly classified into five categories, although they are not mutually exclusive. These are: 1) double layer, 2) oblique electrostatic shock, 3) anomalous resistivity, 4) magnetic mirroring effects of differential pitch-angle anisotropy between ions and electrons, and 5) downward mapping of convection electric field discontinuities. These categories invoke theoretical arguments of varying degrees of sophistication and believability to show that kilovolt electrostatic potential drops may be produced in various assumed plasma distributions. The double-layer model is sharply differentiated from the others by its prediction of the scale length with which the total field-

aligned potential difference is distributed, i.e., the magnitude of the parallel electric field.

For the most part, these mechanisms have been considered in isolation of each other and of the ionosphere, not because physicists believe that it should be so, but because it is difficult to treat the couplings. In fact, a correct theoretical treatment of auroral phenomena will without doubt merge several of these mechanisms with each other and with ionospheric physics. It is unfortunate that much of the recent literature on auroral mechanisms pays so little attention to coupling with the ionosphere; some exceptions (with two of which the authors are connected) exist, though. As a general rule, the ionosphere couples neighboring field lines and allows for predictions of latitudinal structure and scale lengths. There is no such coupling in the individual mechanisms mentioned above (except that oblique shocks have an arbitrary structure which crosses field lines), so none can explain arc structure without going beyond the given mechanism. Our discussion begins with the traditional view of these mechanisms in isolation, then proceeds to a brief discussion of coupling schemes.

The double layer (Block, 1975; Shawhan et al., 1978) is a boundary layer between unmagnetized cold plasma on one side and hot plasma on the other. The potential drop across the layer is alleged to be $\geq kT_e/|e|$ and the layer thickness is of the order of several Debye lengths ($\sim$10 km); thus, the parallel electric field in double layers must be $\sim$(0.1 - 1) V/m. A current-driven instability is usually invoked as the formation mechanism of double layers, which requires a field-aligned current greater than a certain threshold value. If potential drops inferred by electron beam observations at S3-3 altitudes as high as $\sim$8000 km are all due to double layers above the satellite, then evidently the ionosphere does not seem to be a factor in double layer formation either. Frequently, based on observations of both electron and ion beams on S3-3, one may infer that potential drops exist both above and below the satellite (Mizera and Fennell, 1977; Croley et al., 1978). Since it is highly improbable that the satellite just happened to pass through within the double layer thickness, such frequent occurrences seem to require more than one double layer to be formed on the same field line. Theories of double layer formation are mathematically difficult, even for very simple plasma distributions (Montgomery and Joyce, 1969), and a quantitative theory has yet to be developed for auroral plasmas. Even supposing that the theory is finally developed, and that difficulties of interpreting satellite data in terms of double layers can be overcome, there is one fundamental problem with double-layer models. They do not account for the influence of the earth's magnetic field, which — except for the unrealistic case of a double layer exactly perpendicular to a magnetic field line — is unwarranted, as we point out below. With regard to our main subject of magnetosphere-ionosphere coupling, double layers are so thin that they are almost completely decoupled from the ionosphere themselves. Furthermore, they tend to decouple the ionosphere from the magnetosphere above the double layer by effectively short-circuiting the magnetospheric electrical structure well above the ionosphere as indicated on Figure 3. In such a model, the ionosphere interacts little with the magnetosphere.

Oblique electrostatic shocks (Swift, 1975; 1976; Kan, 1975) are similar to double layers except that they recognize the influence of the

DOUBLE LAYER

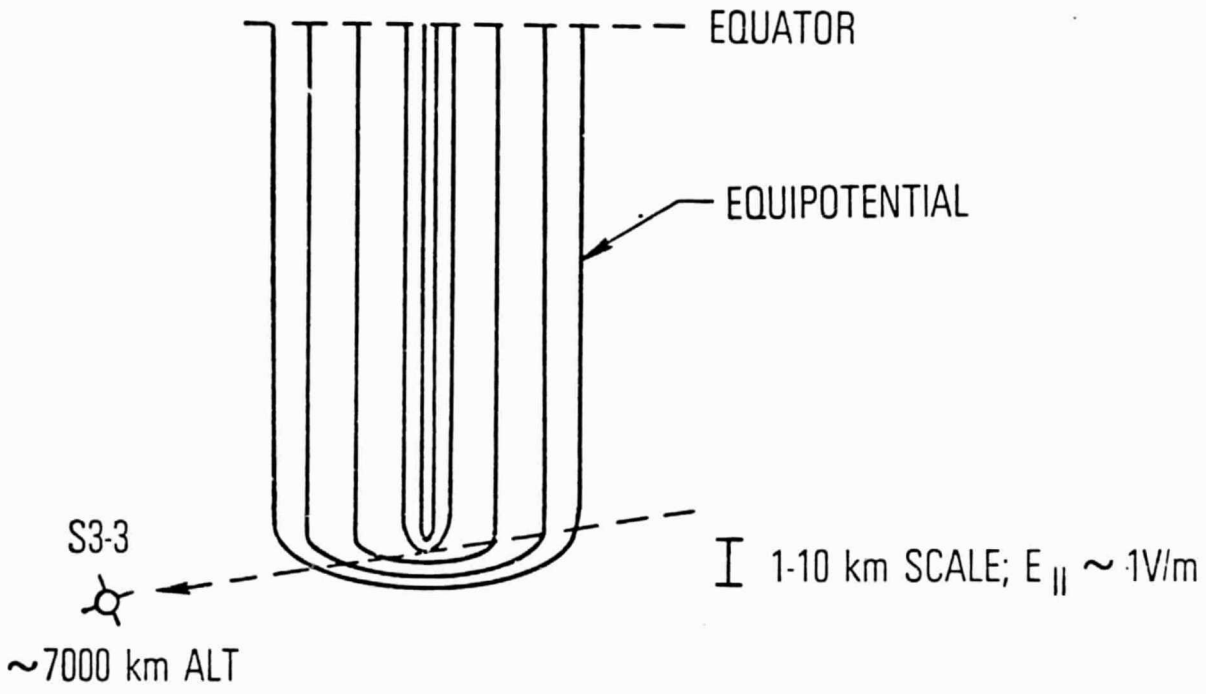

MAGNETOSPHERIC ELECTROSTATIC
FIELD SHORT-CIRCUITED

IONOSPHERE ~100 km ALT

Figure 3

magnetic field and consider that the shock normal is at an arbitrary angle α to the magnetic field direction. For $\alpha \neq 0$ the shock thickness ℓ is measured in units of the ion gyroradius of a few km, a typical cross-field scale being some 15-20 gyroradii (~100 km). The field-aligned scale length is $\ell/\cos\alpha$ which can be quite extensive if the shock normal angle α approaches $\pi/2$. Swift has shown that self-consistent oblique shock solutions can be obtained with simple plasma distributions not unlike auroral conditions. A schematic illustration of Swift's double reverse electrostatic shock is shown in Figure 4. In addition to the fact that solutions of Poisson's equation have been obtained for semi-realistic plasma distributions in a homogeneous magnetic field, the oblique shock geometry has certain advantages over the current-driven double layer in regard to the interpretation of S3-3 data, even though the theory was conceived prior to S3-3. This is because the field-aligned scale length $\ell/\cos\alpha$ can be chosen to be of the order of 1-2 R_e so that only one shock (or a pair of double reverse shocks) need be invoked to explain the existence of potential drops above and below the satellite. It is, of course, a disadvantage that the theory as developed by Swift does not predict α, or equivalently the cross-field scale length. As we discuss later, this scale length can be estimated by incorporating ionospheric physics. An oblique shock with parallel scale length of ≥ 1 R_e is almost certainly strongly coupled to the ionosphere, which at the very least supplies important boundary conditions for the shock. The ionosphere and the magnetosphere tend to be strongly coupled as well, if only because the shock is so extended along the magnetic field.

A third mechanism by which a magnetic field-aligned electric potential drop can allegedly be generated is anomalous resistivity in the field-aligned direction (Hudson et al., 1978). Such anomalous resistivity may be due to a large number of possible modes of AC electric-field turbulence in the auroral plasma (e.g., Kindel and Kennel, 1971; Papadopoulos and Coffey, 1975). Hudson et al. (1978) estimated that turbulent electric fields in the electrostatic ion cyclotron mode with amplitudes ~50 mV/m may yield sufficient anomalous resistivity to generate parallel electrostatic (DC) fields of ~1 mV/m. However, it is not clear how the largely perpendicular AC fields can affect parallel electron currents (and their resistivity). One feature common to oblique-shock models and anomalous-resistivity models is that the potential smoothly varies over a scale of ~1 R_e extension in order to accommodate potential drops of ~(1-10) kilovolts. This is schematically illustrated in Figure 5. It must be noted that the question of how such an extensive region of turbulence can be maintained at a high level (~ 50 mV/m AC), in the presence of non-linear stabilizing effects such as ion heating, must be addressed. A second feature of anomalous resistivity is that, unlike oblique shock models, there is little apparent relationship between the parallel and perpendicular electrostatic fields. In regard to ionosphere-magnetosphere coupling, the ionosphere plays a major role in at least one consideration of current-driven instabilities (Kindel and Kennel, 1971) since the effects of very weak ion-neutral and electron-neutral collisions, $\sim 2 \times 10^{-2}$ of the cyclotron frequency, are stabilizing, as are the effects of ion heating. It must be said, however, that hydrogen ion-cyclotron waves are measured (Kintner et al., 1978) and there is little doubt that these waves will turn out to play some role in the dynamics of the auroral beams.

DOUBLE REVERSE SHOCK

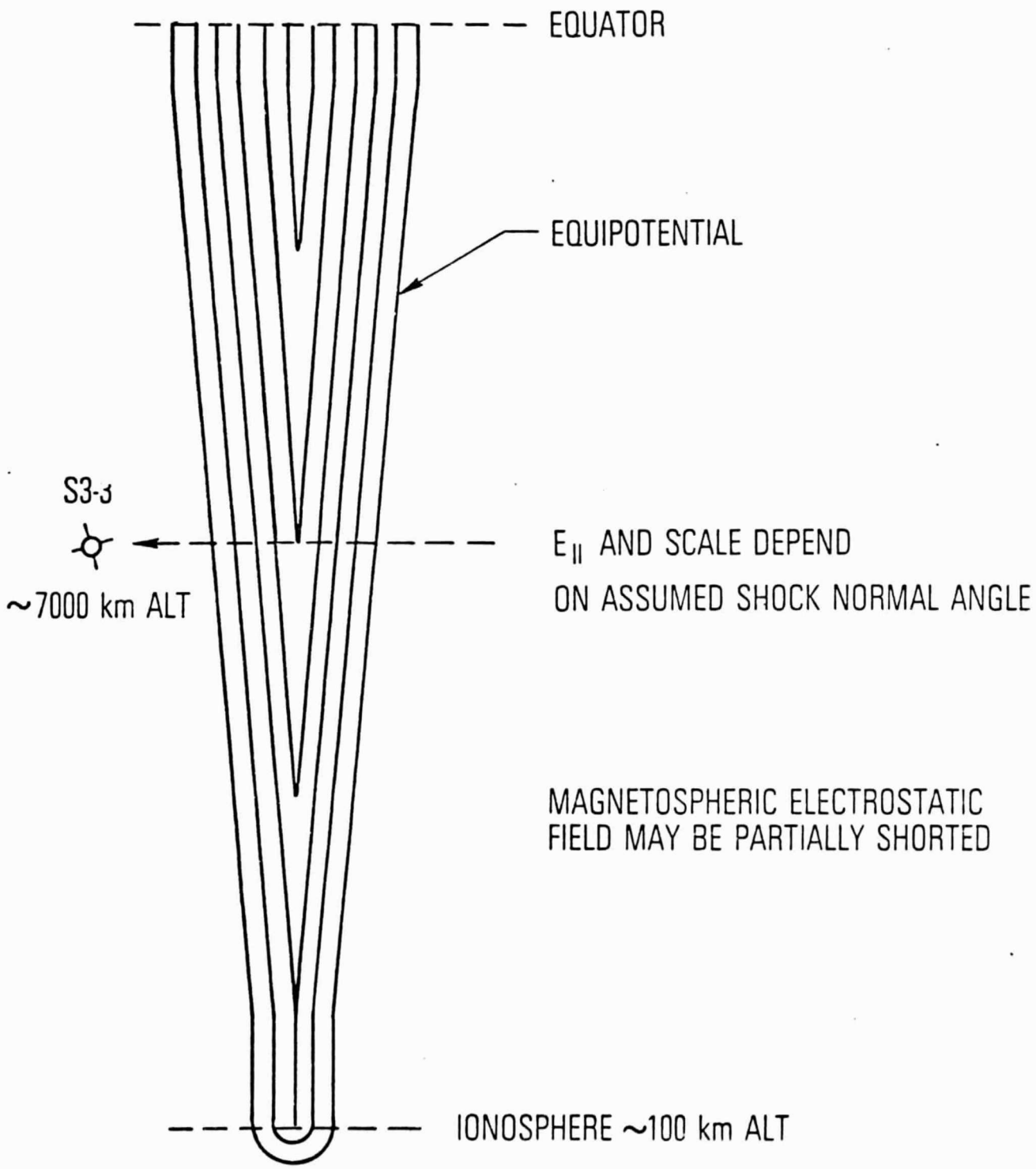

Figure 4

ANOMALOUS RESISTIVITY

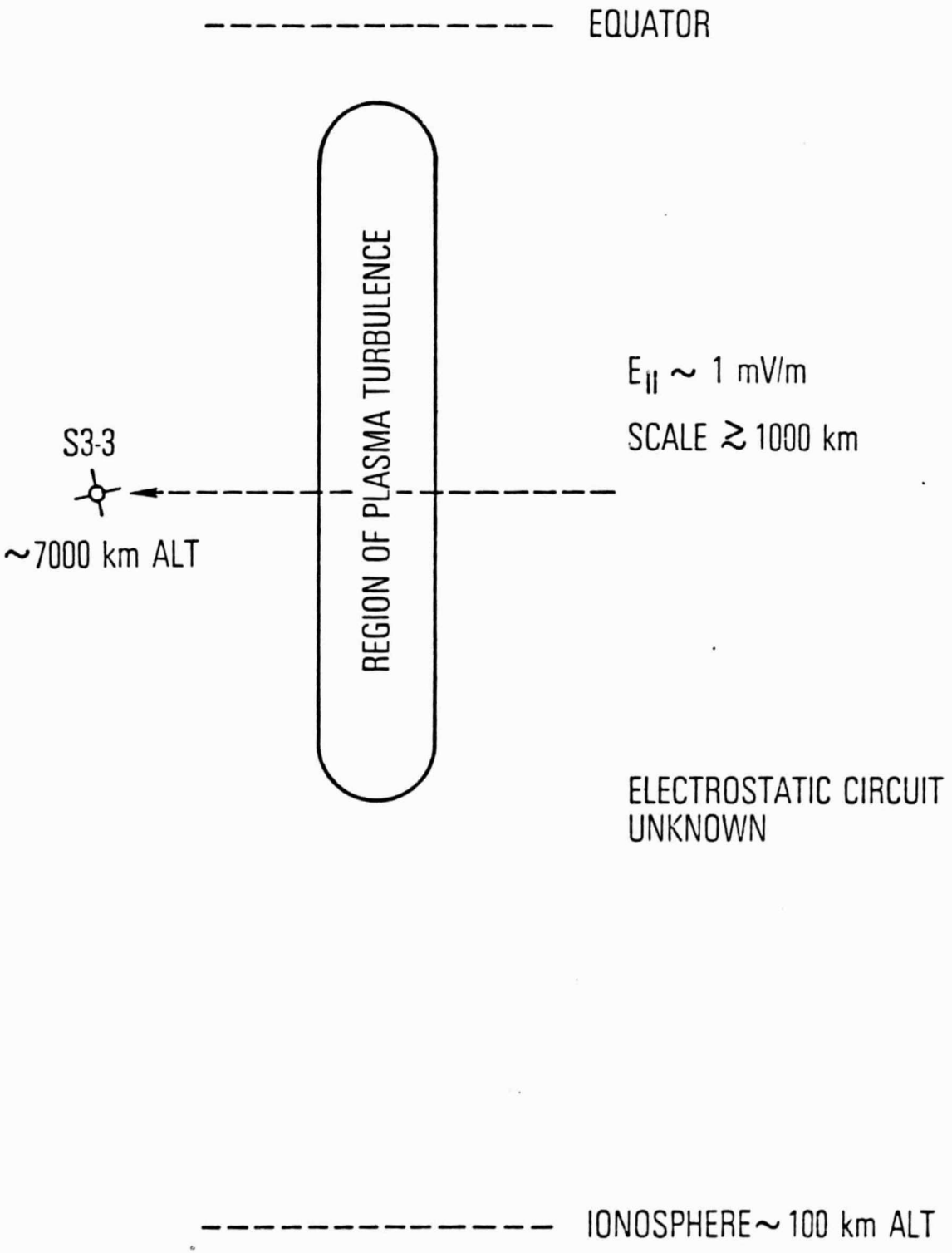

Figure 5

The fourth viable mechanism for maintaining a magnetic field-aligned electric potential drop is that due to the magnetic mirroring effects of differential pitch-angle anisotropy between ions and electrons (Alfvén and Fälthammar, 1963). Unlike the other mechanisms considered above, this mechanism depends on the magnetic field structure being suitable for mirroring of the energetic plasma injected into the auroral region, for if the equatorial pitch-angle distributions of such ions and electrons are different their "average" mirroring locations will be different, thus setting up a charge separation electrostatic field. A number of authors have considered such a mechanism for the case of auroral plasma (e.g., Lemaire and Scherer, 1974; Whipple, 1977; Lennartsson, 1977; Chiu and Schulz, 1978), assuming strict charge neutrality. This is one model where a careful consideration of the contribution of cold ionospheric electrons is absolutely essential. One-dimensional quasi-neutral calculations (Chiu and Schulz, 1978) indicated that ionospheric plasma is crucial in the magnetic mirroring mechanism not only in giving a proper account of electron distributions, as in the phenomenological model of Evans (1974), but also in partially short-circuiting the very large potential drops expected from consideration of magnetospheric plasma alone (Alfvén and Fälthammar, 1963). In any case, the parallel scale length of this mechanism is essentially the field line distance between the ionosphere and the magnetospheric equator, i.e., the region in which the plasma mirrors, yielding parallel electric fields well below 1 mV/m (see Figure 6).

There is yet another possible source of auroral electric fields that accelerate ions and electrons in opposite directions along the earth's magnetic field. This last possible source is the magnetospheric convection electric field. The convection electric field is perpendicular to the magnetic field at high altitudes, but its meridional (r, θ) component has a theoretical discontinuity at or near the boundary between closed and open magnetic field lines (see Figure 7, which shows the amplitudes of the diurnal variation of E at ionospheric altitudes). Ionospheric resistivity would partially connect electrostatic equipotentials across the discontinuity, but at too low an altitude to account properly for the observed component of E parallel to B. However, the "kinematical resistivity" associated with magnetic-mirror forces on a hot plasma may increase the altitude at which the parallel (to B) component of E would appear. The details of this latter effect, which (if it occurs) would produce the desired distribution of $E \cdot B$ with altitude, remain to be worked out. However, the effect would be such as to produce an upward electric field in the PM sector (maximal at dusk) and a downward electric field in the AM sector (maximal at dawn) of the auroral oval. This expectation is in good agreement with the diurnal distribution of upgoing ion beams observed by Ghielmetti et al. (1978).

It is evident that these physical mechanisms do not exist entirely independently of one another. For example, if the restrictive assumption of strict charge neutrality is removed in the magnetic-mirror model, one has an oblique electrostatic shock in a mirroring field. To the extent that no dissipative mechanisms such as wave-particle turbulence are included in such a "shock", the resulting electric-field structure is better described as a solution of Poisson's equation. From another point of view the oblique shock can be described as some sort of zero-frequency electrostatic ion-

MAGNETIC MIRRORING

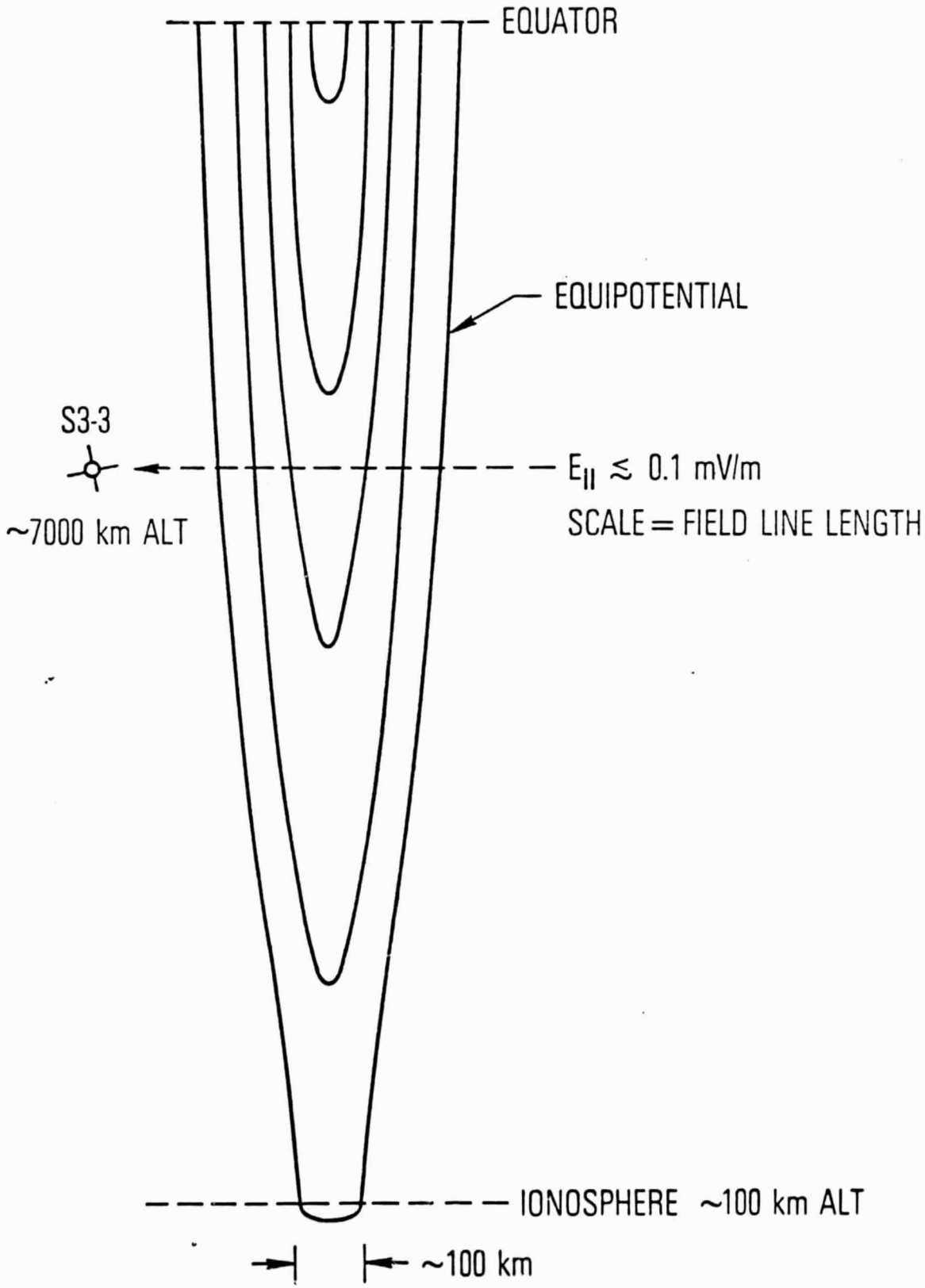

Figure 6

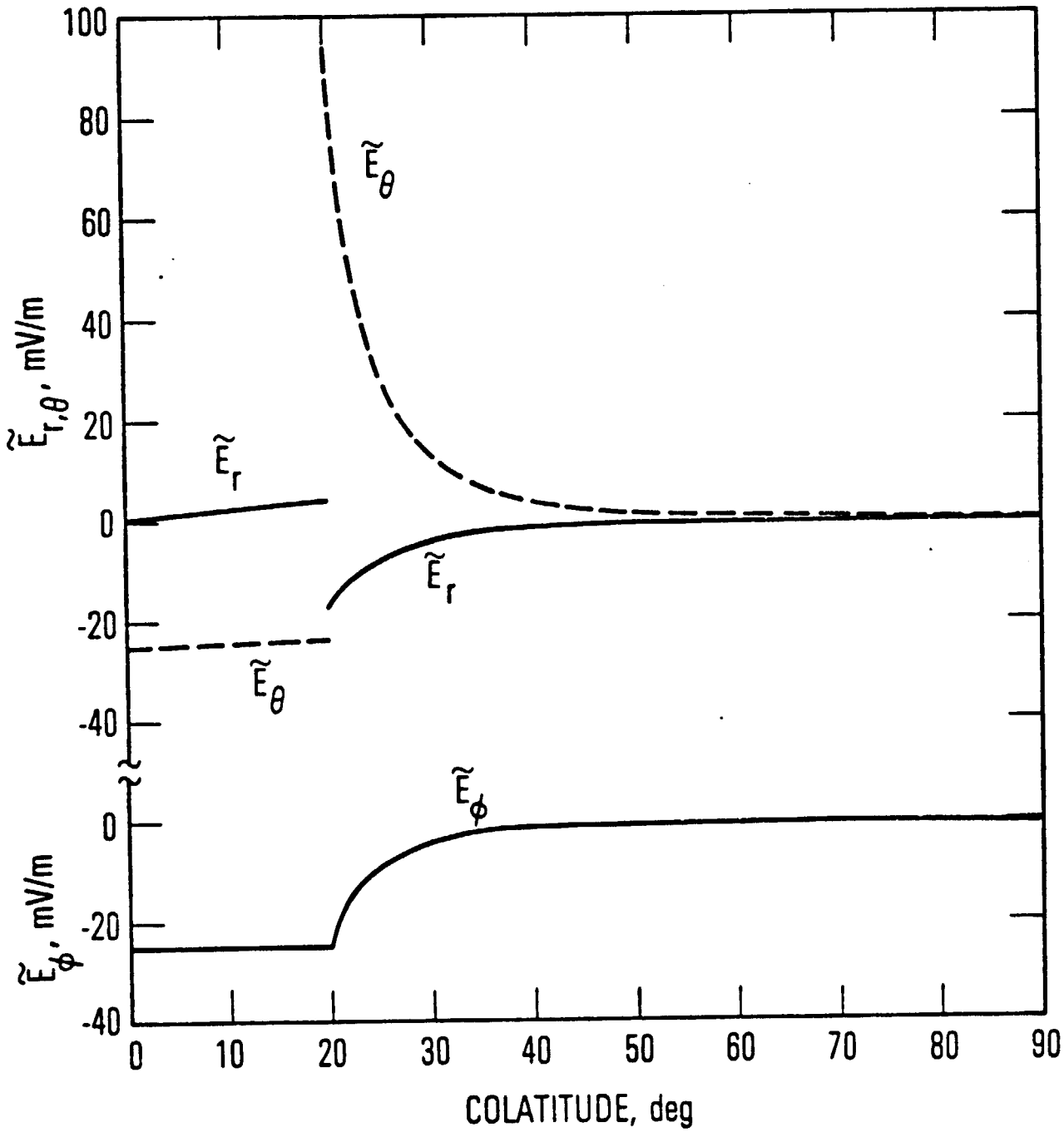
100
80
60
40
20
0
-20
-40
$\tilde{E}_{r,\theta}$, mV/m
$\tilde{E}_\theta$
$\tilde{E}_r$
$\tilde{E}_r$
$\tilde{E}_\theta$
$\tilde{E}_\phi$
0
-20
-40
$\tilde{E}_\phi$, mV/m
0
10
20
30
40
50
60
70
80
90
COLATITUDE, deg

Figure 7

cyclotron (EIC) mode. There surely is a great deal of EIC turbulence connected with auroras, and the physical distinction between the oblique shocks of Swift and this turbulence is at best imprecise. Yet the merging of wave turbulence and shocks can lead to substantial parallel electric potential drops in the complete absence of anomalous resistivity. (The reader need not be reminded that turbulence is not synonymous with anomalous resistivity; in fact, it is quite difficult to make anomalous resistivity out of even the most turbulent waves.)

In a recent work, Chiu and Cornwall (1978) have considered Poisson's equation in dipolar magnetic geometry, coupled with ionospheric physics. In such a model the parallel potential drop is intimately coupled to the perpendicular electrostatic field structure as indicated in Figure 1. Further, the scale length of the perpendicular electrostatic field structure is related not only to the field-aligned current to the ionosphere but also to the ionospheric Pedersen conductivity. Thus, ionosphere-magnetosphere coupling is a crucial ingredient determining the geometric structure as well as the energetics of the quiet auroral arc in such a model. At present, no satisfactory solution of such a model has yet been obtained in the return-current region, although an approximate solution in the central electron beam region has been obtained. A schematic illustration of this model is given in Figure 6.

Because the various mechanisms are not necessarily mutually exclusive, it is difficult to rule out any particular mechanism by observations; however, the parallel scale length, or equivalently, the peak magnitude of the parallel electric field, may be used to distinguish some models from others. Since the current-driven double layer is distinguished by a very short parallel scale length, one may ask if the parallel (to B) electrostatic-field observations of S3-3 would be able to distinguish the double layer from other mechanisms. Mozer et al. (1977) reported very large parallel electrostatic fields ($\geq$100 mV/m) in the presence of $>$ 100 mV/m perpendicular electrostatic fields. These have been identified as $\sim$ 800 mV/m parallel electrostatic fields of double layers (Shawhan et al., 1978). Hudson and Mozer (1978) were cautious in making such an identification because "the angular resolution of the instrument may alias the parallel electric field measurement in the presence of strong perpendicular electric fields greater than 100 mV/m." Particle measurements on S3-3 cannot resolve the question of parallel scale length either, although they do put constraints on double-layer models such as the necessity of multiple formation pointed out earlier. Thus, for the time being, no mechanism discussed above can be ruled out, but it must be said that double layers are unlikely both theoretically and experimentally. Clearly, further theoretical development of these models is needed to help the process of experimental elimination of unsuitable candidates. Identification of the auroral mechanism is especially important for ionospheric-magnetospheric coupling studies because the ionosphere plays roles of varying importance in various mechanisms. It would be very hard to believe that the ionosphere plays no active role at all in the dynamics of the aurora. In such an eventuality, ionospheric currents would be entirely decoupled from the magnetospheric currents, and our growing understanding of the relationship between auroral dissipation of currents and energy input into the magnetosphere would be lost. On the contrary, it seems that there is a genuinely strong

coupling between magnetospheric, auroral, and ionospheric phenomena.

IV. PROSPECTS

As we have seen in previous sections, the S3-3 measurements not only confirm the suspected existence of kilovolt electrostatic potential drops along auroral field lines but also clarify the relationship between inverted-V structures, electron and ion beams, and electrostatic fields in the aurora. However, because of aliasing problems, the parallel electric field measurements on board are unable to determine the parallel scale length of the electrostatic potential drops with confidence. We would have to depend on future experiments to settle this crucial question. If parallel electrostatic fields are as large as 800 mV/m, as one experiment suggests, then there is no question that some sort of double layer or electrostatic shock with small obliquity is involved. If on the other hand, the parallel electrostatic field turns out to be ≤ 1 mV/m, as many experiments suggest, then anomalous resistivity, oblique shocks, and magnetic mirroring are all candidates. Undoubtedly these three mechanisms go hand in hand, so it is not a question of choosing only one of them.

Theorists are not yet ready to pronounce judgment in favor of one or another model, thus leaving open one vital question: Do parallel electric fields isolate the magnetosphere from the ionosphere? We (in agreement with traditional views) think not, but we know of no definitive experimental evidence which shows how magnetospheric and ionospheric current paths are closed. It may be that radar and other ground-based studies combined with satellites such as S3-3 can provide this evidence.

Another important issue is the mapping of perpendicular electric fields along field lines from the magnetosphere to the ionosphere. For most models other than the double layer, the mapping modifications induced by parallel electric fields may not be terribly significant, but there may be almost complete decoupling in double-layer models, so the mapping question will have to be completely reexamined. Presently, calculations of ionospheric currents, and their concomitant heating of the thermosphere (Straus and Schulz, 1976), depend on a variety of electrostatic models which depend on direct mapping of convection electric fields (e.g., Volland, 1975). If double layers exist over regions as extensive as inverted-V structures (to explain the electron beams), then the question of how convection electric fields map through a double layer must be addressed. Indeed, the role of the observed paired perpendicular auroral electrostatic fields (Figure 1) has not been considered in double layer theory.

Proponents of active ionospheric coupling with the magnetosphere will surely note that the observation of oxygen ion beams on S3-3 is evidence that the ionosphere may be a major source of charged particles for the auroral magnetosphere. Very recent isotopic-ratio observations of ring-current ions in the magnetosphere indicate that the ionosphere (via the aurora) may be a major source for the ring current as well (e.g., Young et al., 1977). We suggest that the next major advance in ionosphere-

magnetosphere coupling may be the understanding, both observational and theoretical, of the ultimate fate of these ion beams. Since downward moving ion beams are not observed at high altitudes, and since conical beams are primarily an ionic phenomena, the question of what happens to ion beams before they reach the equator appears to be interesting indeed.

ACKNOWLEDGMENT

This work is partially supported by NASA under Grant NASW-3120 and partially by The Aerospace Corporation Sponsored Research Program.

REFERENCES

Alfvén, H., and C.-G. Fälthammar (1963): Cosmical Electrodynamics, pp. 163-167, Clarendon Press, Oxford.

Armstrong, J. C., and A. J. Zmuda (1973): Triaxial magnetic measurements of field-aligned currents at 800 km in the auroral region: Initial results, J. Geophys. Res., 78, 6802.

Block, L. P. (1975): Double layers, in Physics of the Hot Plasma in the Magnetosphere, pp. 229-249, edited by B. Hultqvist and L. Stenflo, Plenum Press, N. Y.

Cauffman, D. P., and D. A. Gurnett (1972): Satellite measurements of high latitude convection electric fields, Space Sci. Rev., 13, 369.

Chiu, Y. T., and J. M. Cornwall (1978): Electrostatic model of a quiet auroral arc, submitted to J. Geophys. Res.

Chiu, Y. T., and M. Schulz (1978): Self-consistent particle and parallel electrostatic field distributions in the magnetospheric-ionospheric auroral region, J. Geophys. Res., 83, 629.

Cloutier, P. A. (1971): Ionospheric effects of Birkeland currents, Rev. Geophys. Space Phys., 9, 987.

Croley, D. R., Jr., P. F. Mizera, and J. F. Fennell (1978): Signature of a parallel electric field in ion and electron distributions in velocity space, J. Geophys. Res., 83, 2701.

Evans, D. S. (1974): Precipitating electron fluxes formed by a magnetic field-aligned potential difference, J. Geophys. Res., 79, 2853.

Evans, D. S. (1975): Evidence for the low altitude acceleration of auroral particles, in Physics of the Hot Plasma in the Magnetosphere, pp. 319-340, edited by B. Hultqvist and L. Stenflo, Plenum Press, N. Y.

Frank, L. A., and K. L. Ackerson (1971): Observation of charged particle precipitation into the auroral zone, J. Geophys. Res., 76, 3612.

Ghielmetti, A. G., R. G. Johnson, and E. G. Shelley (1978): The latitudinal, diurnal and altitudinal distributions of upward flowing energetic ions of ionospheric origin, Geophys. Res. Letters, 5, 59.

Heppner, J. P. (1972): Electric field variations during substorms: Ogo 6 measurements, Planet. Space Sci., 20, 1475.

Hudson, M. K., and F. S. Mozer (1978): Electrostatic shocks, double layers, and anomalous resistivity in the magnetosphere, Geophys. Res. Letters, 5, 131.

Hudson, M. K., R. L. Lysak, and F. S. Mozer (1978): Magnetic field-aligned potential drops due to electrostatic ion cyclotron turbulence,

Geophys. Res. Letters, 5, 143.

Kan, J. R. (1975): Energization of auroral electrons by electrostatic shock waves, J. Geophys. Res., 80, 2089.

Kindel, J. M., and C. F. Kennel (1971): Topside current instabilities, J. Geophys. Res., 76, 3055.

Kintner, P. M., M. C. Kelley, and F. S. Mozer (1978): Electrostatic hydrogen cyclotron waves near one earth radius altitude in the polar magnetosphere, Geophys. Res. Letters, 5, 139.

Lemaire, J., and M. Scherer (1974): Ionosphere-plasmasheet field-aligned currents and parallel electric fields, Planet. Space Sci., 22, 1485.

Lennartsson, W. (1977): On high-latitude convection field inhomogeneities, parallel electric fields and inverted-V precipitation events, Planet. Space Sci., 25, 89.

Mizera, P. F., and J. F. Fennell (1977): Signatures of electric fields from high and low altitude particle distributions, Geophys. Res. Letters, 4, 311.

Mizera, P. F., D. R. Croley, Jr., and J. F. Fennell (1976): Electron pitch-angle distributions in an inverted-'V' structure, Geophys. Res. Letters, 3, 149.

Montgomery, D. C., and G. Joyce (1969): Shock-like solutions of the electrostatic Vlasov equation, Plasma Phys., 3, 1.

Mozer, F. S., and R. H. Manka (1971): Magnetospheric electric field properties deduced from simultaneous balloon flights, J. Geophys. Res., 76, 1697.

Mozer, F. S., C. W. Carlson, M. K. Hudson, R. B. Torbert, B. Paraday, J. Yatteau, and M. C. Kelley (1977): Observations of paired electrostatic shocks in the polar magnetosphere, Phys. Rev. Letters, 38, 292.

Papadopoulos, K. (1977): A review of anomalous resistivity for the ionosphere, Rev. Geophys. Space Phys., 15, 113.

Sharp, R. D., R. G. Johnson, E. G. Shelley, and K. K. Harris (1974): Energetic O^+ ions in the magnetosphere, J. Geophys. Res., 79, 1844.

Shawhan, S. D., C. G. Fälthammar, and L. P. Block (1978): On the nature of large auroral zone electric fields at 1-R_E altitude, J. Geophys. Res., 83, 1049.

Shelley, E. G., R. D. Sharp, and R. G. Johnson (1976): Satellite observations of an ionospheric acceleration mechanism, Geophys. Res. Letters, 6, 54.

Shelley, E. G., R. G. Johnson, and R. D. Sharp (1972): Satellite observation of energetic heavy ions during a geomagnetic storm, J. Geophys. Res., 77, 6104.

Straus, J. M., and M. Schulz (1976): Magnetosphere convection and upper atmospheric dynamics, J. Geophys. Res., 81, 5822.

Swift, D. W. (1975): On the formation of auroral arcs and acceleration of auroral electrons, J. Geophys. Res., 80, 2096.

Swift, D. W. (1976): An equipotential model for auroral arcs, 2, numerical solutions, J. Geophys. Res., 81, 3935.

Volland, H. (1975): Models of global electric fields within the magnetosphere, Ann. Geophys., 31, 154.

Vondrak, R. R., H. R. Anderson, and R. J. Spiger (1971): Rocket-based measurements of particle fluxes and currents in an auroral arc, J. Geophys. Res., 76, 7701.

Whipple, E. C., Jr. (1977): The signature of parallel electric fields in a collisionless plasma, J. Geophys. Res., 82, 1525.

Young, D. T., J. Geiss, H. Balsinger, P. Eberhardt, A. Chielmetti, and H. Rosenbauer (1977): Discovery of He_2^+ and O_2^+ ions of terrestrial origin in the outer magnetosphere, Geophys. Res. Letters, 4, 561.

Space Sciences Laboratory
Report No. SSL-79(9553)-4

A CORRELATION OF THERMOSPHERIC GRAVITY WAVES WITH TROPOSPHERIC LIGHTNING

by

Y. T. Chiu, B. C. Edgar, C. J. Rice and L. R. Sharp

Space Sciences Laboratory
THE AEROSPACE CORPORATION
Los Angeles, California 90009

JANUARY 1979

Submitted for Publication:
Geophysical Research Letters

This work is supported partially by NASA Grant NASW-3120 and partially by Aerospace Corporation-Sponsored Research Program.

ABSTRACT

It is demonstrated that a remarkable geographic correlation exists between occurrence frequencies of wave-like structures in the thermosphere and tropospheric lightning at dawn, which is an indicator of deep convective activity.

I. INTRODUCTION

Considerable scientific interest has recently been focused upon the possible coupling of dynamical processes between the troposphere and the upper atmosphere. However, because of numerous limitations in the collection and interpretation of data, there is little, if any, evidence that upper and lower atmospheric processes are coupled in a physically discernible manner (e.g. Pittock, 1978). While the major attention to date has been directed toward upper atmospheric influences on tropospheric processes, we would like to point out that the reverse, tropospheric influences upon upper atmospheric phenomena, should also be examined, not just because they may provide clues to understanding atmospheric coupling but also because they might be misinterpreted as a sun-weather signal. Indeed, considering the relative energetics of upper and lower atmospheric processes, it is rather surprising that tropospheric "signals" are not prominent in the thermosphere, although, to be sure, such "signals" cannot be easily identified unless one has globally distributed data sets with extensive statistical coverage.

In this letter, we report on some correlative features of two sets of space-based atmospheric measurements, which are globally distributed with good statistical coverage. One set of data, pertaining to tropospheric processes, is lightning occurrence frequency derived from measurements of a lightning detector onboard a Defense Meteorological Satellite Program (DMSP) satellite in a dawn-dusk polar orbit sampling lightning activity worldwide (cf. Turman and Edgar, 1978; Edgar, 1978). The second set of data, pertaining to thermospheric phenomena, is the occurrence frequency of wave-like structures in neutral atmospheric density profiles derived from measurements of several cold cathode ion gauges onboard Atmospheric Explorer spacecrafts AE-C and AE-D (cf. Rice and Sharp, 1977), and onboard the Air Force spacecraft S3-1. We found a significant correlation between the occurrence patterns of dawn lightning, indicative of

massive long-lived tropospheric convective activity, and the occurrence patterns of wave-like structures in the thermosphere.

In contrast to statistical correlations for which no plausible physical mechanisms are apparent (cf. Wilcox, 1975), our search for a correlative connection between the occurrence patterns of thermospheric wave-like structures and lightning distribution at dawn is in fact suggested by the qualitatively-understood mechanism of gravity wave generation by deep convective activity and by wind shears in the upper troposphere (e.g. Mastrantonio et al., 1976; Paul, 1977). Ground-based observation of large amplitude gravity waves near the troposphere have from time to time been reported for specific occurrence episodes (e.g. Gedzelman and Rilling, 1973). Indeed, it has been claimed on such a basis that atmospheric gravity waves inferred from disturbances measured by an ionospheric Doppler sounder array may be associated with severe local thunderstorms, tornadoes and hurricanes (Hung et al., 1978). Such studies, while intriguing, do not necessarily bear upon questions of sources and distributions of thermospheric gravity waves on a global scale. Rice and Sharp (1977) made a study of wave-like structures in the AE-C cold cathode ion gauge data and noted that their occurrence patterns are spatially correlated with the locations of strong tropospheric wind shears associated with subtropical jet streams. In this paper, we pursue the question of the source and distribution of wave-like structures in the thermosphere with AE-C, AE-D, and S3-1 data, which provide better global coverage than AE-C data alone. Because of the significant clues suggested by the above-cited studies, we attempt to locate specific tropospheric phenomena which may be a source of these wave-like structures of the thermosphere. Indices of tropospheric convective activity or wind shear, which are derived with high statistical sampling (i.e. excluding computer constructions based on data gathered from only a few stations), do not exist on a global scale. However, in 1978 data have become available from a unique lightning detector flown on a DMSP satellite.

The data are available on an essentially continuous basis with sampling frequency of some 14 dawn-dusk orbits per day. Since lightning is associated with tropospheric convective and frontal activities, the satellite-based lightning distribution data represent an unbiased, un-reconstructed index of such tropospheric activities. Indeed, the geographic distributions of lightning at dawn and dusk reflect the tremendous rise of small-scaled convective activity over land masses in the summer hemisphere (Turman and Edgar, 1978; and Edgar, 1978). Therefore, we attempt a correlative study of the distributions of lightning activity and of thermospheric wave-like structures not because the two are directly connected but because lightning is a good indicator of tropospheric activities which are thought to be physical generators of gravity waves.

II. DATA AND CORRELATION

Data on thermospheric wave-like structures were obtained onboard AE-D and S3-1 with cold cathode ion gauges similar to Pressure Sensor A on AE-C described in Rice et al., (1973). Figure 1 depicts a relatively disturbed neutral density profile as a function of altitude; similar wave-like structures observed by other instruments onboard AE-C have been interpreted as gravity waves (Reber et al., 1975). For this study we confine the data to 5 km intervals in the altitude range 135-200 km where identification of wave-like structure is most certain. In Figure 1, four classes of wave-like structure are illustrated; the four wave classifications are identified with an index value running from 1 to 4 (Rice and Sharp, 1977). The classifications are: I = 1, indicating a smoothly varying profile; I = 2, indicating minor activity with up to 5% density amplitude; I = 3, indicating waves of 5-15% density amplitude peak to peak; and I = 4, indicating waves of density amplitude greater than 15%. For some phases of this study, wave classifications 3 and 4 have been combined as an indication of the unambiguous presence of a gravity wave. Data from all three satellites are used in order to assure adequate global and statistical coverage over the small seasonal interval, November through January, over which lightning data were available. In this same seasonal interval, a total of 1212 density profiles similar to Figure 1 have been examined, which resulted in 10,505 measurements of the presence or absence of gravity waves. The gravity wave data cover the years 1973-1976, though not with uniform coverage throughout.

Data on lightning occurrence were obtained with a lightning detector onboard a DMSP satellite in a dawn-dusk polar orbit (Turman and Edgar, 1978; and Edgar, 1978), which would detect and record optical pulse profiles from lightning flashes occurring below the spacecraft within a circle of 780 km radius. Details of the instrument, the statistical properties of the lightning wave-form and the characteristics of instrumental

thresholds and the logic to eliminate triggers by high energy particles and by glints has been discussed in Edgar (1978). With a very high sampling rate of about 14 orbits per day at fixed local time (dawn or dusk), approximately 1600 events were accumulated over the seasonal intervals November 6-17 and November 21 - December 3, 1977 and January 10-18, 1978 for the construction of geographical distributions of lightning occurrence frequency over the latitudinal interval (70^{o} S - 70^{o} N). It should be noted that, although the seasonal intervals of both data sets are similar, the lightning data were observed in 1977-1978 whereas the thermospheric wave data were obtained in 1973-1976; therefore, the element of possible inter-annual variations in the data sets cannot be eliminated.

To correlate the two data sets on an equivalent basis, we divide the globe into 648 bins, each covering an area 10^{o} of latitude and longitude on a side. Observations of wave-like structure and lightning in the seasonal intervals specified above are converted to occurrence frequencies in each bin by normalizing to the satellite coverage (AE-C, AE-D, S3-1 and DMSP) of the same bin. Obviously, division into square latitude-longitude bins is not appropriate for the high-latitude regions; however, we have excluded these regions ($> 70^{o}$ S and $> 70^{o}$ N) from consideration because gravity waves in these regions are likely to be of auroral origin. Indeed, such characteristics are reflected in the AE-D data at high-latitudes, the details of which will be discussed elsewhere. Thus, in the latitudinal interval (70^{o} S - 70^{o} N) the use of square latitude-longitude bins is appropriate.

Figure 2(a) shows the percentage frequency of occurrence of thermospheric wave-like structures with peak-to-peak density amplitude exceeding 5% of the background density. Figure 2(b) shows the geographic distribution of lightning occurrence rate at dawn. Comparison of Figures 2(a) and 2(b) shows a significant correspondence between the occurrence distributions. Two features are probably notable in the correlation.

First, both Figures 2(a) and 2(b) show latitudinal bands of high occurrence frequency at the southern high and middle latitudes ($\sim 40^{\circ}$ S to $\sim 70^{\circ}$ S). Second, there is a suggestion of correlated longitudinal structure showing a tendency for decreased occurrence frequency over low latitude ($\sim 30^{\circ}$ S to $\sim 20^{\circ}$ N) ocean basins such as the Indian, the South Pacific and the South Atlantic oceans. There is even a suggestion of longitudinal clustering of high occurrence frequency values at the South African, Australian and South American sectors, although we do not attach too much significance to this correlation of longitudinal structure. In the Northern Hemisphere, occurrence frequencies of both lightning and gravity waves are considerably reduced, as has been pointed out above as the latitudinal affect. Correlated higher occurrence frequencies may perhaps be discerned in Europe - Western Asia, in the North Pacific and in the North Atlantic. It is interesting to point out also that there seems to be a singular lack of correlation in equatorial Southeast Asia, in the Caribbean basin and in equatorial South America. The dawn lightning in these humid and warm areas may perhaps not be associated with deep convective activity in the troposphere, but rather with remnants of afternoon squalls which may persist through the night without being suppressed by nighttime cooling.

In addition to constructing the maps, we have made a calculation of the average lightning occurrence frequency in events per minute for each wave classification index. The results are presented in Table 1.

TABLE 1

Wave Index	1	2	3	4
Lightning Occurrence Rate	.087	.093	.124	.141
Number of Points	1217	6856	1963	469

These results confirm the findings of the map study and demonstrate that the amplitude of the wave structure may also be correlated with the lightning occurrence rate.

It is rather unfortunate that we cannot quantify the above-mentioned correlations much further than the present stage of pattern recognition, and the results of Table 1. Obviously, major obstacles such as inter-annual variability can only be surmounted with simultaneous data accumulation over long durations. Instrumental resolution also imposes stringent limits on quantification of these correlations even though we have good statistical coverage. The field-of-view of the lightning detected is approximately a circle of 1500 km diameter. Gravity wave train occurrences can also be of similar extension. Since each event, lightning or gravity wave, is assumed to be located at the sub-satellite point, there is a natural uncertainty associated with spatial data location. Further, since gravity waves may propagate predominantly horizontally from the source regions, there is also a natural uncertainty associated with the extent of wave dispersal about its source. Such elements are natural disadvantages of satellite observations and must be considered as trade-offs for good spatial and statistical coverage which cannot be obtained from ground-based observations unless data from a dense network of observations, including ocean areas, were available.

III. CONCLUSIONS

We note in this letter that the global occurrence frequency and geographic distribution of thermospheric wave-like density perturbations measured by cold cathode ion gauges on board three satellites correspond remarkably well with the occurrence frequency and geographic distribution of tropospheric lightning at dawn measured by a lightning detector on board a DMSP satellite. The correlative study with extensive statistical coverage is restricted to winter months during which both types of data were available. We shall pursue this correlative study for other seasonal intervals as further lightning data become available.

REFERENCES

Edgar, B. C., Global lightning distribution at dawn and dusk for August - December 1977 as observed by the DMSP lightning detector, URSI XIX General Assembly, Helsinki, Finland, August 1978.

Hung, R. J., T. Phan and R. E. Smith, Observation of gravity waves during the extreme tornado outbreak of 3 April 1974, J. Atmos. Terr. Phys., 40, 831, 1978.

Gedzelman, S. D., and R. A. Rilling, Short-period atmospheric gravity waves: A study of their dynamic and synoptic fractures, Mon. Wea. Rev., 106, 196, 1978.

Mastrantonio, G., F. Einaudi, D. Fua and D. P. Lalas, Generation of gravity waves by jet streams in the atmosphere, J. Atmos. Sci., 33, 1730, 1976.

Paul, D. P., Nonlinear gravity wave-wind interactions and jet stream gravity wave generation, Ph. D. dissertation, MIT, 112 pp, 1977.

Pittock, A. B., A critical look at long-term sun-weather relationships, Rev. Geophys. Space Phys., 16, 400, 1978.

Reber, C. A., A. E. Hedin, D. T. Pelz, W. E. Potter, and L. H. Brace, Phase and amplitude relationships of wave structure observed in the lower thermosphere, J. Geophys. Res., 80, 4576, 1975.

Rice, C. J. and L. R. Sharp, Neutral atmospheric waves in the thermosphere and tropospheric weather systems, Geophy. Res. Letters, 4, 315, 1977.

Rice, C. J., V. L. Carter, S. R. LaValle, W. T. Chater, D. A. Jones, C. G. King, and D. F. Nelson, Atmosphere explorer pressure measurements: Ion gauge and capacitance manometer, Radio Sci., 8, 305, 1973.

Turman, B. N. and B. C. Edgar, Global lightning distribution at dawn and dusk for August-September 1977, 1978 Spring Meeting AGU, Miami, Florida, April 1978.

Wilcox, J. M., Solar activity and the weather, J. Atmos. Terr. Phys., 37, 237, 1975.

Figure Captions

1. Atmospheric neutral density (g/cm^2) vs. altitude (km) profile from the PSA instrument illustrating the 4 classes of wave-like Structure.

2(a) Global map showing the percentage frequency of occurrence of wave classifications 3 and 4 as a function of latitude (10^o bins) and longitude (10^o bins).

2(b) Global map showing the distribution of dawn lightning occurrence rate (events/min) as a function of latitude (10^o bins) and longitude (10^o bins).

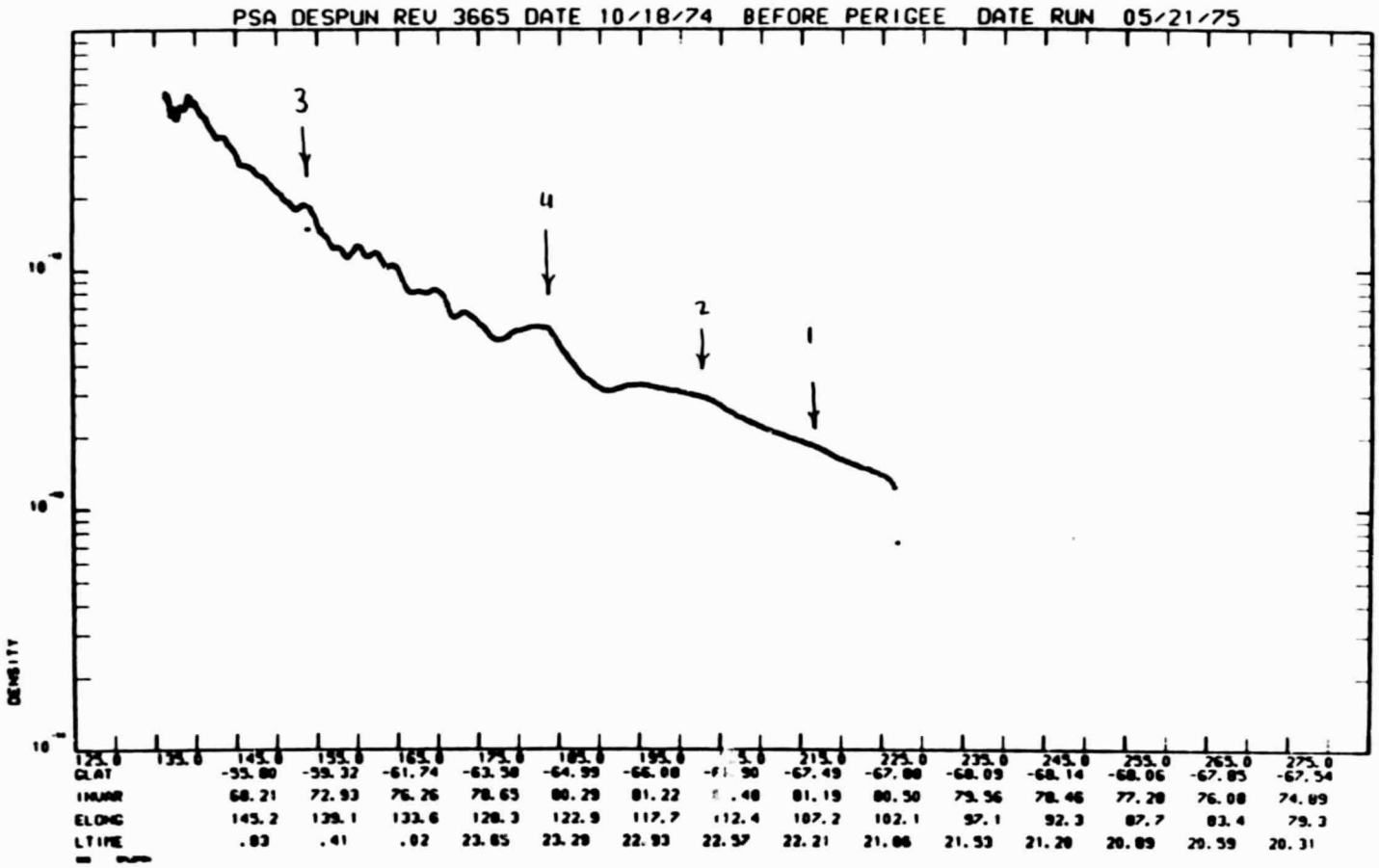
PSA DESPUN REV 3665 DATE 10/18/74 BEFORE PERIGEE DATE RUN 05/21/75
3
4
2
1
DENSITY
CLAT -55.80 -59.32 -61.74 -63.58 -64.99 -66.08 -67.49 -67.88 -68.09 -68.14 -68.06 -67.85 -67.54
INVAR 68.21 72.93 76.26 78.65 80.29 81.22 81.19 80.50 79.56 78.46 77.28 76.08 74.89
ELONG 145.2 139.1 133.6 128.3 122.9 117.7 112.4 107.2 102.1 97.1 92.3 87.7 83.4 79.3
LTIME .83 .41 .02 23.85 23.29 22.93 22.57 22.21 21.86 21.53 21.20 20.89 20.59 20.31

Figure 1

Wave Occurrence Frequency

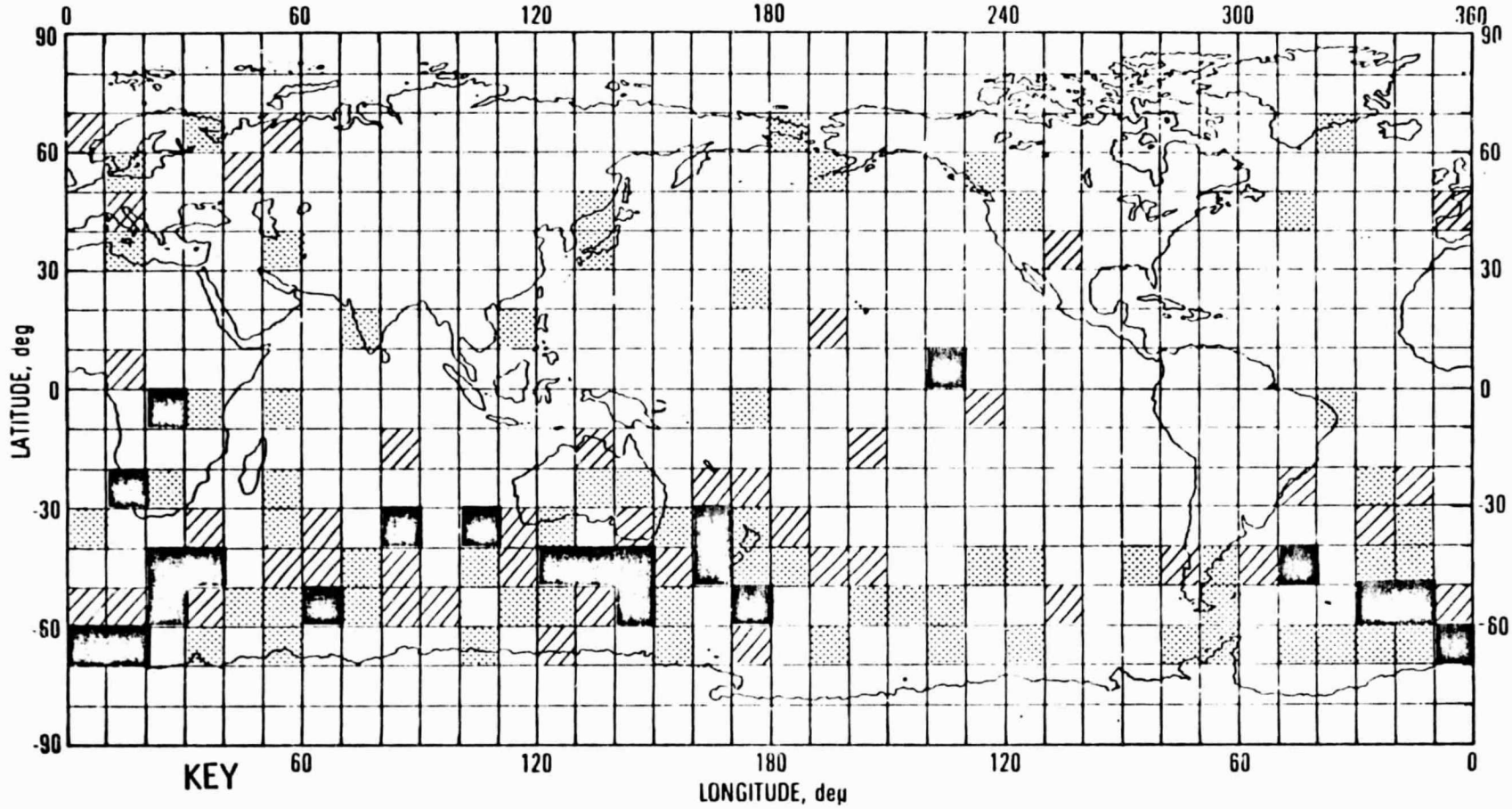

Figure 2a

Dawn Lightning Occurrence

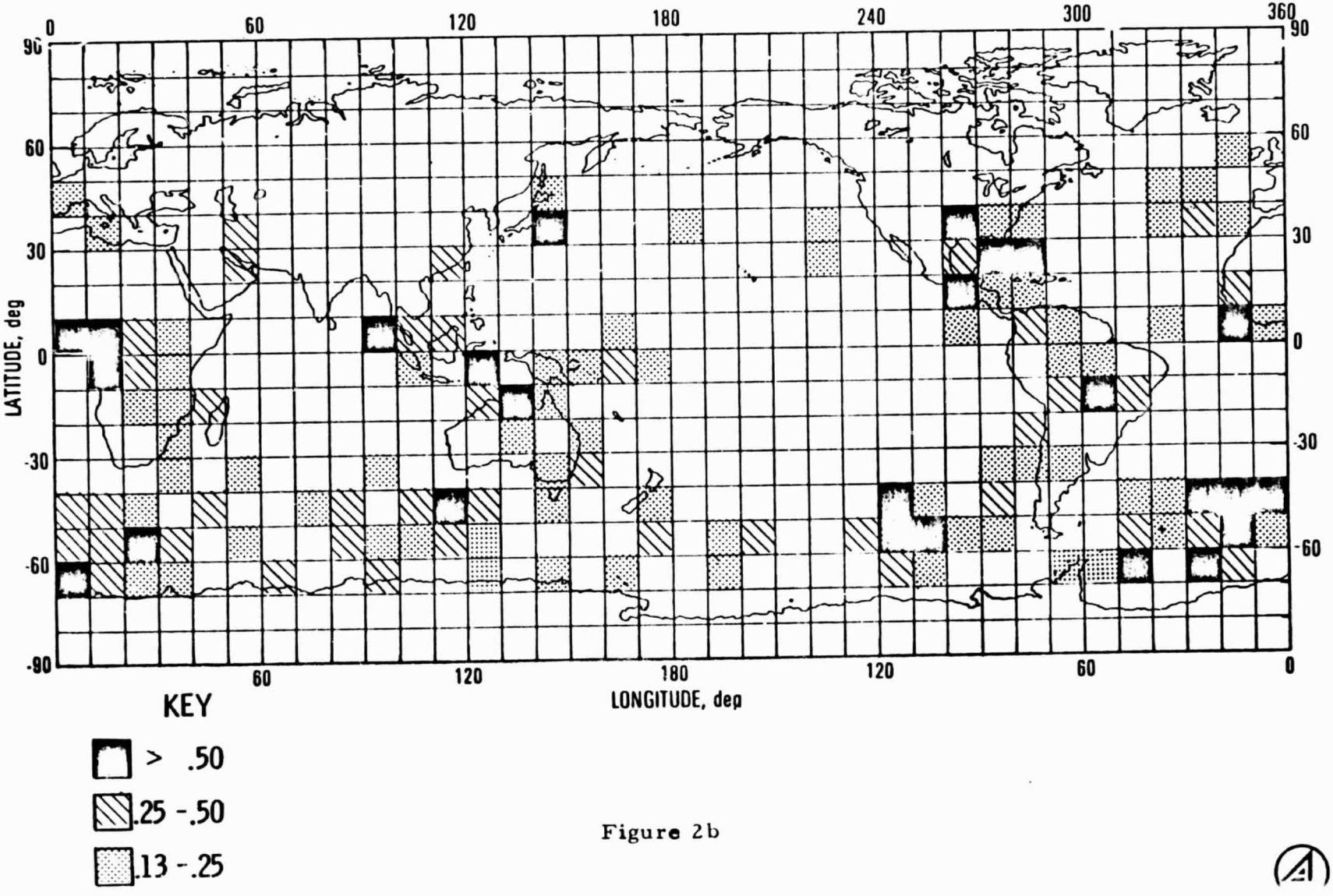

Figure 2b

Space Sciences Laboratory
Report No. SSL-78(3960-06)-1

THE RESPONSE OF ATMOSPHERIC AND LOWER IONOSPHERIC LAYER STRUCTURES TO GRAVITY WAVES

Y. T. Chiu and B. K. Ching
Space Sciences Laboratory

The Ivan A. Getting Laboratories
THE AEROSPACE CORPORATION
Los Angeles, California 90009

DECEMBER 1977

Published in:
Geophysical Research Letters

ABSTRACT

We solve the linear and quasi-linear problems of the density response of a neutral or ionospheric layer structure of arbitrary density profile to gravity wave perturbations in the background atmosphere. It is shown that the density response of the bottomside of the structure is of larger amplitude than the topside, whereas the general magnitude of the density response depends on the relative sharpness of the layer density gradient in comparison to the gradient of background atmosphere stratification. The sharper the layer gradient, the larger the layer density response. Interpretation and application of our results to the ozone and atomic oxygen layers, the sporadic-E layer and to the D and E regions of the ionosphere are discussed.

I. INTRODUCTION

It is well-known that lower ionospheric layers such as the D-layer and the stratospheric ozone layer exhibit large variations of density (see Fig. 1), which are reminiscent of gravity wave structures. Further, in some thin layer structures, such as noctilucent clouds (Fogle and Haurwitz, 1966) and the sporadic-E layer (Miller and Smith, 1975; 1976), the existence of wave-like structure has become a singularly dominant feature. Since the presence of gravity waves of low frequency and short vertical wave-length is expected in the atmosphere, the exhibition of wave structure in atmospheric and lower ionospheric layers is not at all surprising. What is surprising, however, is that the wave-like density variations of the layer structures are generally of large amplitude whereas the density variations in the background atmosphere are usually observed in the middle and upper atmosphere to be less than or of the order of 10-15% (see Fig. 2a, b). For example, the wave-like partial pressure variations of the ozone layer shown in Fig. 1 are of order of 50 μmb out of the layer background partial pressure of some 100 μmb. Density variations associated with such wave-like structures in the middle atmosphere have been observed (Faire et al., 1974). Bounds on the stratospheric wave-like density variations can also be estimated from observed wave-like horizontal wind components in the stratosphere (Webb, 1966) by means of perturbation theory (Hines, 1960). The result is that wave-like density variations in the stratosphere are less than 10% of the background stratospheric density, in agreement with direct density observations. Indeed, one may contrast wave-like density variations of the D and E regions of the ionosphere with that of the neutral atmosphere in the same altitude region and find a similar relationship.

While numerous authors have from time to time qualitatively espoused the view that wave-like density variations observed in the atmospheric and lower ionospheric constituent layers are somehow due to layer response to gravity waves in the background atmosphere rather than due to some chemical or mechanical instability in the layer itself, the very large amplitudes observed in the density fluctuations of the layer structures remain a major obstacle to a quantitative resolution of such a view. Recently, the unifying feature of the gravity wave response mechanism was further strengthened by a consideration of Dudis and Reber (1976) who showed that density variations in the minor constituents of the neutral thermosphere obey relationships consistent with gravity wave perturbation of the background atmosphere, although the thermospheric collisional frequency may not be large enough to support the approximation that the constituents are strongly coupled to the wave motion by collisions (Del Genio et al., 1977).

In this paper we give a calculation of the linear and quasi-linear response of a constituent layer of general density profile to a gravity wave perturbation of the background atmosphere. It is assumed that the motion of the layer is collisionally coupled to the wave motion of the background neutral atmosphere; therefore, our results are applicable to layers below 200 km altitude only. Above 200 km altitude, the layer motion depends on gradient and diffusive drifts; however, since there are no interesting layer structures, except for the F-layer of the ionosphere, above 200 km, our assumption is quite adequate for the purpose of considering layer responses. We shall show that the amplitude of the density response of the layer is a strong function of

the gradient of the layer density profile relative to the scale height of the background neutral atmosphere. For sharply defined layers such as the ozone layer and the D and E regions of the ionosphere, the density response of the layer is of considerably larger amplitude than the wave density variation in the background neutral atmosphere. For cases where the layer response can no longer be regarded as a small perturbation, the exact quasi-linear solution shows singular behaviour at sufficiently sharp layer density gradients, thus signifying the onset of turbulence forced by gravity waves.

II. RESPONSE TO PERTURBATIONS.

Consider a constituent layer of density n(z) embedded in the neutral atmosphere of background density $N_0(z)$ which is stratified with scale height H_0. A linear gravity wave perturbation of density N, horizontal wind component V_x and vertical wind component V_z is assumed to exist in the background atmosphere. According to linear gravity wave theory, V_x and V_z are related to N/N_0 by

$$V_x = (ikg/\omega) (N/N_0) [\omega^2 \gamma H_0 - g (\gamma - 1)] / [i\omega^2 + g (\gamma - 1) K_z] \qquad (1)$$

$$V_z = (N/N_0) [- g\omega (1 - i\gamma H_0 K_z)] / [i\omega^2 + g (\gamma - 1) K_z] \qquad (2)$$

where g is the gravitational acceleration and $\gamma \equiv c_p/c_v$, the ratio of heat capacities. The wave density perturbation N/N_0 is given in terms of amplitude A and phase ϕ by

$$N/N_0 \equiv A \exp\phi \equiv A \exp (i\omega t - ikx - iK_z z) \qquad (3)$$

where $K_z = k_z + i/2H_0$. Equation (3) defines the wave frequency ω, horizontal wave number k and vertical wave number k_z. The gravity wave perturbation forces a response in the constituent layer density n and the constituent velocity $\vec{v}$. For a neutral constituent layer, the constituent momentum equation relates the time rate of wave velocity variation to wave

gradient drifts and to collisional coupling to the background wave velocity $\vec{V}$. Since the neutral atmospheric collisional frequency below 200 km is orders of magnitude larger than the wave variations, the constituent momentum equation reduces to

$$\vec{v} = \vec{V} \ , \tag{4}$$

which is the usual assumption that the layer moves with the background medium. For an ionospheric layer in the E and F1 regions, the collisional coupling at frequency ν_{in} between ions and neutrals and the gyration about the magnetic field with frequency $\Omega_i = eB/m_i c$ are both much larger than the gravity wave frequency and drifts; therefore the constituent momentum equation is approximately

$$\Omega_i \vec{v} \times \hat{b} - \nu_{in} (\vec{v} - \vec{V}) = 0 \ , \tag{5}$$

for low frequency gravity wave perturbations in the lower ionosphere. Inclusion of gradient drift terms in (4) and (5) can be easily accommodated; however, these terms will detract from the simplicity of our analysis without adding any significant content.

For constituent layers whose chemical and/or ionization equilibrium lifetimes are long compared to the gravity wave period, such as the ozone layer and the sporadic-E layer, the response of layer density n is governed by the continuity equation

$$\frac{\partial n}{\partial t} + \nabla \cdot (\vec{v}\, n) = 0 \quad , \tag{6}$$

where $\vec{v}$ is related to the gravity wave forcing velocity $\vec{V}$ by either (4) or (5). For ordinary ionospheric layers in the D and E regions at night, the recombination lifetimes are comparable to gravity wave periods; therefore, the effects of recombination must be taken into account in (6). The realization of the importance of recombination, when taken together with the results of the present analysis, is crucial in the consideration of nighttime E-region turbulence; however, for the sake of simplicity these effects will be dealt with elsewhere. Hence, our considerations here as applied to layers whose recombination lifetimes are shorter than or comparable to gravity wave periods will be regarded as indicative rather than quantitative results. For the remainder of the analysis, results based on (5) will be given without proof, since the derivation is entirely analogous to the one presented in terms of (4).

Without making a small perturbation assumption for layer response, the constituent layer density n can be written as the sum of a layer density profile in the absence of a gravity wave in the background atmosphere $n_0(z)$ and a gravity wave density response $\tilde{n}(x, z, t)$, i.e.

$$n = n_0(z) + \tilde{n}(x, z, t) \tag{7}$$

In our calculation, $n_0(z)$ is regarded as a general layer density profile generated by some production mechanism. Substitution of (4) and (7) into (6) yields the partial differential equation

$$\left(\frac{\partial}{\partial t} + \vec{V}\cdot\nabla\right)\left(\tilde{n}/n_0\right) + \left(\frac{1}{n_0}\frac{dn_0}{dz} - iK_z\right)\left(1+\tilde{n}/n_0\right)V_z - ik\left(1+\tilde{n}/n_0\right)V_x = 0\,, \qquad (8)$$

which relates the layer density response $(\tilde{n}/n_0)$ to the background gravity wave perturbation (N/N_0) via (1) and (2). The layer density profile n_0 manifests itself in (8) in terms of a gradient length function $L(z)$, defined as

$$L(z) = \left[\frac{1}{n_0}\frac{dn_0}{dz}\right]^{-1}\,. \qquad (9)$$

The boundary condition defined for (8) is that $(\tilde{n}/n_0)$ should vanish for vanishing gravity wave amplitude A in $(N/N_0) = Ae^{\phi}$. The general solution to (8) is very difficult to obtain not only because (8) depends on "second order" terms of the form $(\tilde{n}/n_0)(N/N_0)$ but also because L is an arbitrary function of z. Thus, the exact vertical structure of the response requires specification of a model of n_0. However, for purposes of interpretation it is much more advantageous to consider the local approximation for which $L(z)$ is a slowly varying function since the background wave is almost never a steady wave train. In this limit, it is a simple matter to solve the linear response version of (8). A more exact solution of (8) can be sought in the quasi-linear limit that the response $(\tilde{n}/n_0)$, similar to (N/N_0), depends on (x,z,t) through the phase function $\phi = i\omega t - ikx - iK_z z$. Inspection of (8) shows that indeed $(\tilde{n}/n_0)$ is purely a function of ϕ if the gradient length $L(z)$ is large compared to $(\partial\phi/\partial z)$, i.e. $k_z >> 1/L(z)$. Strictly speaking the quasi-linear limit is invalid at the layer peak where dn_0/dz vanishes; however, separate investigation in the neighborhood of the layer peak shows that the quasi-linear solution given below approaches the proper small perturbation response even when $L(z)$ approaches infinity, i.e. when dn_0/dz vanishes. In the quasi-linear limit, (8) can be transformed into a non-linear ordinary differential equation in ϕ, whose solution is given by

$$\left(\tilde{n}/n_0\right) = \left(\alpha/\delta\right)\ln\left[1 + \left(\delta/\beta\right)\left(N/N_0\right)\right] \qquad (10)$$

where

$$\alpha = -\omega^2 + (g/H_0)(1 + H_0/L) - igK_z(1 + \gamma H_0/L)$$

$$\beta = -\omega^2 + ig(\gamma - 1)K_z$$

$$\delta = -(g/L)(1 - i\gamma H_0 K_z) + 2\omega^2 + 2ig(\gamma - 1)K_z$$

For low frequency gravity waves, i.e. $\omega^2 << g(\gamma - 1)/(\gamma H_0)$, $k_z >> 1/H_0$ and $\omega^2 k_z^2 \simeq k^2 g(\gamma - 1)/(\gamma H_0)$, we obtain

$$(\tilde{n}/n_0) \simeq -\frac{1}{\gamma - 1} \cdot \frac{[1 + \gamma H_0/L]}{[2 + \gamma H_0/(\gamma - 1)L]} \cdot \ln\left\{1 + (N/N_0)[2 + \gamma H_0/(\gamma - 1)L]\right\} \qquad (11)$$

In the small perturbation limit, (N/N_0) is infinitesimal and (11) approaches the limit

$$(\tilde{n}/n_0) \simeq -\frac{1}{\gamma - 1}(1 + \gamma H_0/L)(N/N_0) \quad , \qquad (12)$$

which is exactly the result obtained from (8) under the linear approximation. Further, for $L = -H_c$, the constituent scale height of a stratified atmospheric constituent, (12) is exactly the result of Dudis and Reber (1976).

For the ionospheric case (5), the situation becomes more complex since the orientation of the magnetic field is involved. If we consider equatorial E and F1 regions in the case for which the magnetic field is assumed to be perpendicular to the x - z plane, an analogous quasi-linear solution to (6) can

again be found, although the validity of quasi-linearity depends also on $k_z >> (d \Omega_i/dz)/ \Omega_i$ and $k_z >> (d \nu_{in}/dz)/ \nu_{in}$. The exact quasi-linear solution for this case is too complicated to be exhibited here; instead, the linear limit analogous to (12) will be given as a basis for interpretation in the next section.

$$(\tilde{n}_i/n_0) \simeq - \frac{1}{\gamma - 1} \left\{ 1 + i \tilde{\nu} \gamma H_0 k_z + (\gamma H_0/L)[1 - \tilde{\nu}(1 + \Omega_i k/\nu_{in} k_z)] \right\} (N/N_0) \qquad (13)$$

where

$$\tilde{\nu} = (k_z/k) [\nu_{in} \Omega_i / (\nu_{in}^2 + \Omega_i^2)] \quad . \qquad (14)$$

In the derivation of (13) and (14), the low frequency gravity wave approximation has been assumed. Note that in the D-region $\nu_{in} >> \Omega_i$ and $\tilde{\nu} << 1$, thus the response behaves exactly as that of a neutral layer. In the F-region $\nu_{in} << \Omega_i$ and (13) approaches the limit $(\tilde{n}_i/n_0) \simeq - (N/N_0) / (\gamma - 1)$, which does not depend on the layer structure.

III. INTERPRETATION

In this paper we shall limit our interpretation of the results of the previous section in terms of their application of layer structures in the atmosphere and lower ionosphere. The interpretation of the linear results for the particular case of density relations between stratified neutral thermospheric constituents of different masses has been undertaken by Dudis and Reber (1976).

For a general layer structure such as the ozone layer shown in Fig. 1, the inverse gradient length $1/L(z)$ is positive in the bottomside, vanishes at the layer peak and is negative in the topside. According to (12), which is more transparent for interpretation purposes then (10) or (11), one immediately obtains the result that the bottomside response is necessarily of larger amplitude than the topside response, whereas at the layer peak the response is given by $(\tilde{n}/n_0) \simeq - (N/N_0) / (\gamma - 1)$. Such a relationship is generally borne out in an examination of ozonesonde observations (Komhyr and Sticksel, 1967; Komhyr and Grass, 1968). The magnitude of response $(\tilde{n}/ n_0)$ relative to the background wave (N/N_0) depends on the magnitude of the layer profile gradient $L(z)$ relative to the atmospheric scale height H_0. For a sharp layer density profile, $| \gamma H_0/L | > 1$, the layer density response $\tilde{n}/n_0$ can be considerbly larger than the background gravity wave density variation N/N_0. For example, on the bottomside of the ozone layer shown in Fig. 1 the "amplification" factor $| (1 + \gamma H_0/L)/(\gamma - 1) |$ is approximately 5, whereas on the topside this factor is approximately 2. Further, it is of interest to note that if $| \gamma H_0/L | > 1$ then the phase of the

response ($\tilde{n}/n_0$) is 180° out of phase with (N/N_0) at the bottomside and near the layer peak, but the phase difference takes a 180° jump just above the layer peak such that ($\tilde{n}/n_0$) becomes in phase with (N/N_0) at the topside. The apparent 180° phase jump of ozone density variations just above the layer peak, shown in Fig. 1, may perhaps be interpreted in terms of this relationship. In the bottomside D and E regions of the ionosphere, very large wave-like density variations have been observed (e.g. Pfister and Ulwick, 1958; Knight, 1972). Again, these observations are qualitatively consistent with the relationship between the "amplification" factor of (12) or (13) and the variation of the layer density gradient L(z), although our results must be modified by inclusion of recombination effects.

The sporadic-E layer of metallic ions is of particular interest since the layer is sharply defined and the recombination lifetime is long compared to gravity wave periods. Recently, incoherent backscatter experiments have shown that the layer is strongly turbulent and exhibits large variations of density (Miller and Smith, 1975; 1976). Indeed, at times definite gravity wave effects can be identified (Miller and Smith, 1976). We wish to point out here that the "amplification" factor for the sporadic-E layer can be quite large. At the vicinity of 100 km altitude where sporadic-E occurs $\nu_{in}/\Omega_i \sim 30$; therefore the ionospheric layer relation (13) collapses to that of the neutral layer relations (11) and (12). Since L for the sporadic-E layer is of order of 1 km and H_0 is of order of 8 km, $\gamma H_0/L$ is sufficiently large that the linear relation (12) becomes invalid and our interpretation must rely on the quasi-linear relation (11). For a background gravity wave with $|N/N_0| \sim 10\%$,

we obtain the sporadic-E layer response amplitude $| \tilde{n} / n_0 | \sim 1.4$, which certainly signifies the formation of very dense knots of sporadic-E layer density observed by Miller and Smith (1976). Indeed, for gravity waves with $k_z \sim 1/L(z)$, even the quasi-linear solution becomes invalid and the response $(\tilde{n} / n_0)$ is dominated by a resonance between the layer structure and the wave structure which would result in turbulence. Although the exact non-linear solution for such a case is too difficult to obtain, that the layer response presages turbulence in such a case can be argued from a consideration of the relative phase between $(\tilde{n} / n_0)$ and (N/N_0) in (11). When $| \gamma H_0/L | >> 1$ in (11), the complex agrument of the logarithm in (11) may approach its negative real axis branch cut; as a result, the phase of $(\tilde{n} / n_0)$ may take on an infinite number of branch values separated by multiples of π. The major characterization of turbulence is that the phases of its density variations are not well correlated. Based on these considerations, we would like to suggest that gravity wave forcing is the major mechanism in the generation of density irregularities in sharply defined constituent layers of the atmosphere and ionosphere. Further, sharp layer gradients are necessarily "turbulent".

The generation of turbulence is of great interest in the nighttime equatorial ionosphere in the 200 km region. It has been suggested that the nighttime equatorial F-region is susceptible to Rayleigh-Taylor instability (e.g. Woodman and LaHoz, 1976; Hudson and Kennel, 1975); however, the Rayleigh-Taylor growth rate in the 200 km region, $g/(2 \nu_{in} L) \approx 10^{-4}$ sec^{-1}, is sufficiently small that gravity wave response effects at wave

period short compared to Rayleigh-Taylor growth time may be more important. We wish to point out here that the gravity wave response at the bottomside of the layer is subject to Rayleigh-Taylor instability also. An analysis of the gravity wave response of an ionospheric layer structure in the limit $\nu_{in} << \Omega_i$ shows that internal wave modes are also susceptible to Rayleigh-Taylor growth. Since internal wave modes, unlike the surface waves of the pure Rayleigh-Taylor instability, can propagate throughout the layer structure, we would expect that gravity wave response at the steepened bottomside of the nighttime equatorial ionospheric layer structure will play a major role in the "bottomside turbulence" phenomenon. Detailed analysis of such a situation will be given elsewhere.

As a final example, we wish to consider the atomic oxygen layer which maximizes slightly above the mesopause at altitudes between 90 and 100 km. Although very few direct measurements of the atomic oxygen distribution in this region of the atmosphere are available, some examples of wave structure may be seen in the rocket-borne mass spectrometer data presented by Philbrick et al. (1973, 1974). In these cases the wave amplitudes were relatively modest (~10 - 15%) and no wave features were apparent in the simultaneously measured background gas profile. This behavior is consistent with our theory since the amplification factor is predicted by (12) to be about 2.5 at the layer peak and larger below the peak. Further evidence of irregular structure in the atomic oxygen distribution near the layer peak, which would appear as wave-like oscillations in a vertical profile, may be found in latitude-altitude contours derived by Wasser and Donahue (1978) from 5577-Å airglow measurements. In these remotely-sensed data under-dense "patches" are seen particularly, though not exclusively, on the bottomside of the layer. The latitudinal extent of the patches is a few degrees, i.e. of the order of a few hundred kilometers. It would be interesting to determine in the future whether wave perturbations of the stratospheric ozone layer may similarly be "patchy" in their horizontal extent.

IV. CONCLUSION

By comparing observations with the solution of the linear and quasi-linear problems of the density reponse of a neutral or ionospheric layer structure of gravity wave perturbations in the background atmosphere below 200 km altitude, we conclude that large wave-like and turbulent density variations in the ozone layer and the sporadic-E can be interpreted as layer density response to gravity waves. Limited observations of wave structure in the atomic oxygen profile near its maximum also support this interpretation. The layer density response is generally of larger amplitude at the bottomside than at the topside, although the amplitude of both depends on the relative sharpness of layer density gradient in comparison to the gradient of background atmosphere stratification. It is suggested that gravity wave response plays a major role in the generation of turbulence in the nighttime equatorial ionosphere at the 200 km region.

ACKNOWLEDGEMENTS

We are indebted to Dr. K. L. Miller for a discussion of sporadic-E effects, to Dr. B. Wasser and Dr. T. M. Donahue for a preprint of their paper, and to Drs. A. C. Faire and W. D. Komhyr for permission to use their data. This work is supported by U. S. Air Force SAMSO contract No. F04701-76-C-0077 and by The Aerospace Corporation Company Financed Research Program.

REFERENCES

Del Genio, A. D., J. M. Straus, and G. Schubert, Effects of Wave-Induced Diffusion on Thermospheric Acoustic-Gravity Waves, Submitted to Geophys. Res. Letters 1977.

Dudis, J.J., and C. A. Reber, Composition Effects in Thermospheric Gravity Waves, Geophys. Res. Letters, 3, 727, 1976.

Faire, A. C., E. A. Murphy, and R. O. Olson, Atmospheric Density, Temperature and Winds Measured During Aladdin II, Space Research XIV, p. 97, Akademie-Verlag, Berlin, 1974.

Fogle, G. and B. Haurwitz, Noctilucent Clouds, Space Sci. Rev., 6, 279, 1966.

Hines, C.O., Internal Atmospheric Gravity Waves at Ionospheric Heights, Can. J. Phys., 38, 1441, 1960.

Hudson, M.K., C.F. Kennel, Linear Theory of Equatorial Spread-F, J. Geophys. Res., 80, 4581, 1975.

Knight, P., A Classification of Night-Time Electron Density Profiles, J. Atm. Terr. Phys., 34, 401, 1972.

Komhyr, W.D., and R.D. Grass, Ozonesonde Observations 1962-1966, ESSA Technical Report ERL 80-APCL3, Vol. II, 1968.

Komhyr, W.D., and P.R. Sticksel, Ozonesonde Observations 1962-1966, ESSA Technical Report IER 51-IAS 1, Vol. I, 1967.

Miller, K. L., and L. G. Smith, Horizontal Structure of Midlatitude Sporadic-E Layers Observed by Incoherent Scatter Radar, Radio Science, 10, 271, 1975.

Miller, K. L., and L. G. Smith, Midlatitude Sporadic-E Layer, Thesis by K. L. Miller, Aeronomy Laboratory, University of Illinois, Urbana, Ill., Library of Congress ISSN0568-0581, 1976.

Pfister, W., and J. C. Ulwick, The Analysis of Rocket Experiments in Terms of Electron Density Distributions, J. Geophys. Res., 63, 315, 1958.

Philbrick, C. R., G. A. Faucher, and E. Trazcinski, Rocket Measurements of Mesospheric and Lower Thermospheric Composition, Space Research XIII, p. 255, Akademie-Verlag, Berlin, 1973.

Philbrick, C. R., D. Golomb, S. P. Zimmerman, T. J. Keneshea, M. A. MacLeod, R. E. Good, B. S. Dandkar, and B. W. Reinisch, The Aladdin II Experiment: Part II, Composition, Space Research XIV, p. 89, Akademie-Verlag, Berlin, 1974.

Wasser, B., and T. M. Donahue, Atomic Oxygen Between 80 and 120 km: Evidence for a Rapid Spatial Variation in Vertical Transport near the Mesopause, to be published in J. Geophys. Res., 1978.

Webb, W. L., Structure of the Stratosphere and Mesosphere, p. 146, Academic Press, New York, 1966.

Woodman, R. F., and C. LaHoz, Radar Observations of F Region Equatorial Irregularities, J. Geophys. Res., 81, 5447, 1976.

FIGURE CAPTIONS

1. Stratospheric ozone layer showing wave structure. (Komhyr and Gross, 1968).

2a. Wave structure in the stratospheric total density. (Faire et al., 1974).

2b. Wave structure in the lower thermospheric density measured by a satellite-borne accelerometer (Ching, unpublished data).

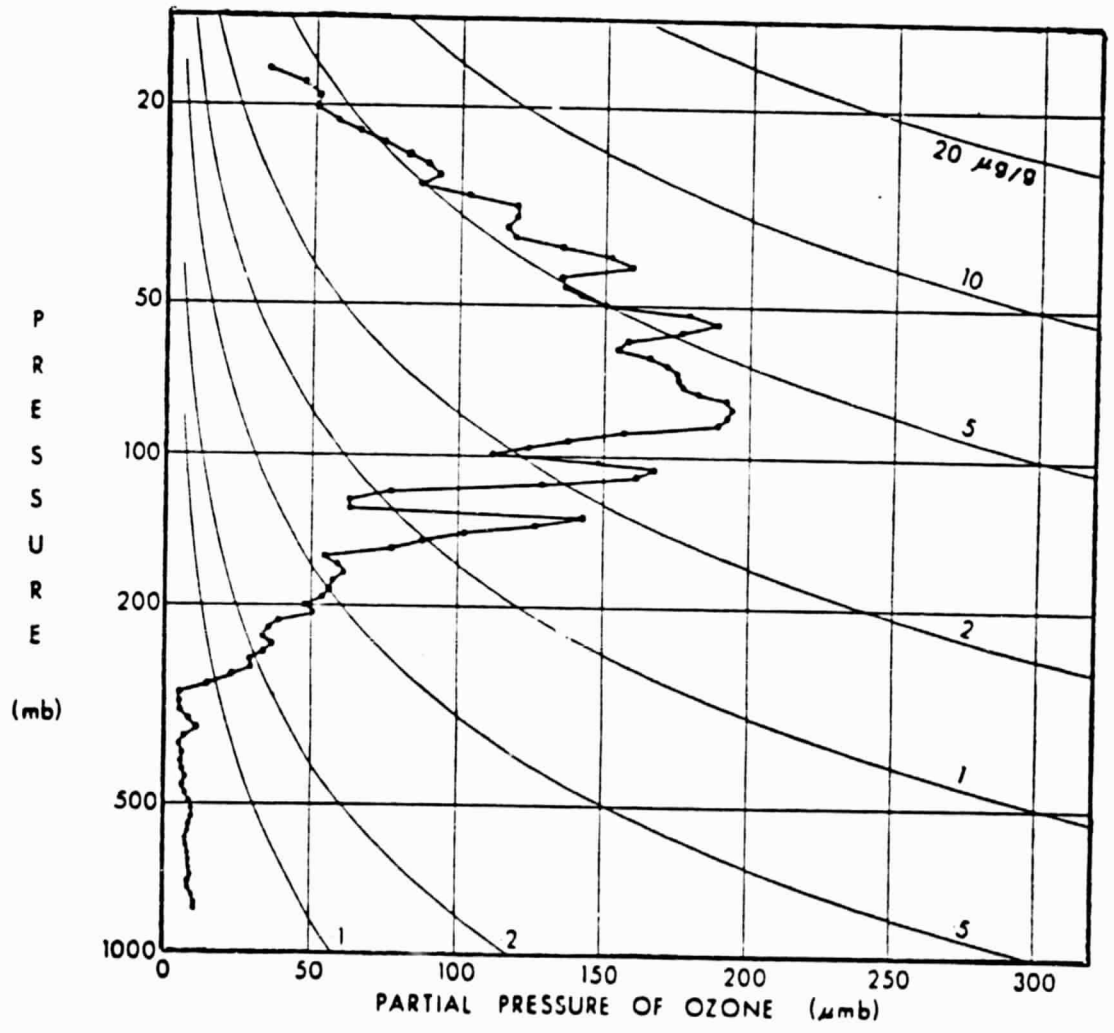
20
50
100
200
500
1000
PRESSURE (mb)
0
50
100
150
200
250
300
PARTIAL PRESSURE OF OZONE (μmb)
20 μg/g
10
5
2
1
5
1
2

Fig. 1

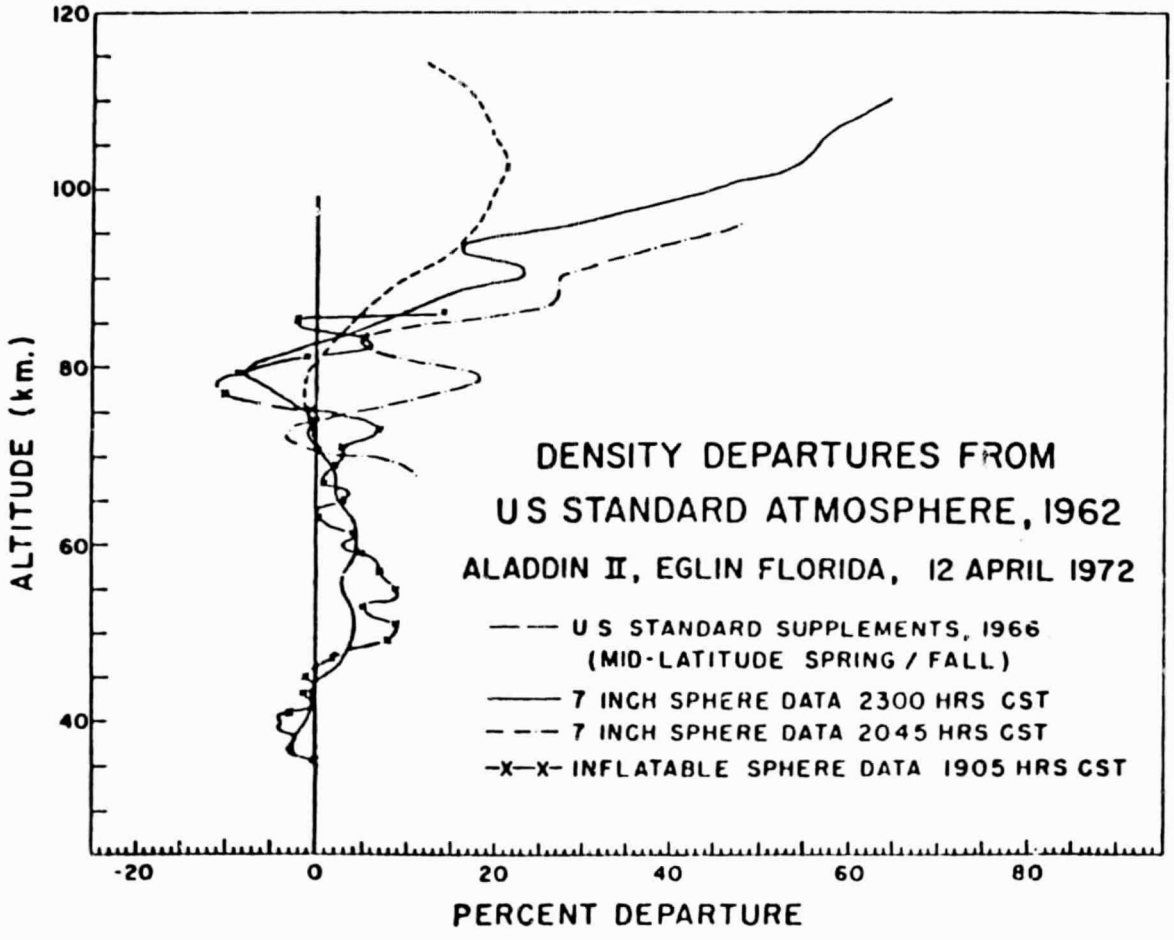
DENSITY DEPARTURES FROM
US STANDARD ATMOSPHERE, 1962
ALADDIN II, EGLIN FLORIDA, 12 APRIL 1972
U S STANDARD SUPPLEMENTS, 1966
(MID-LATITUDE SPRING / FALL)
7 INCH SPHERE DATA 2300 HRS CST
7 INCH SPHERE DATA 2045 HRS CST
INFLATABLE SPHERE DATA 1905 HRS CST
ALTITUDE (km.)
120
100
80
60
40
-20
0
20
40
60
80
PERCENT DEPARTURE

Fig. 2a

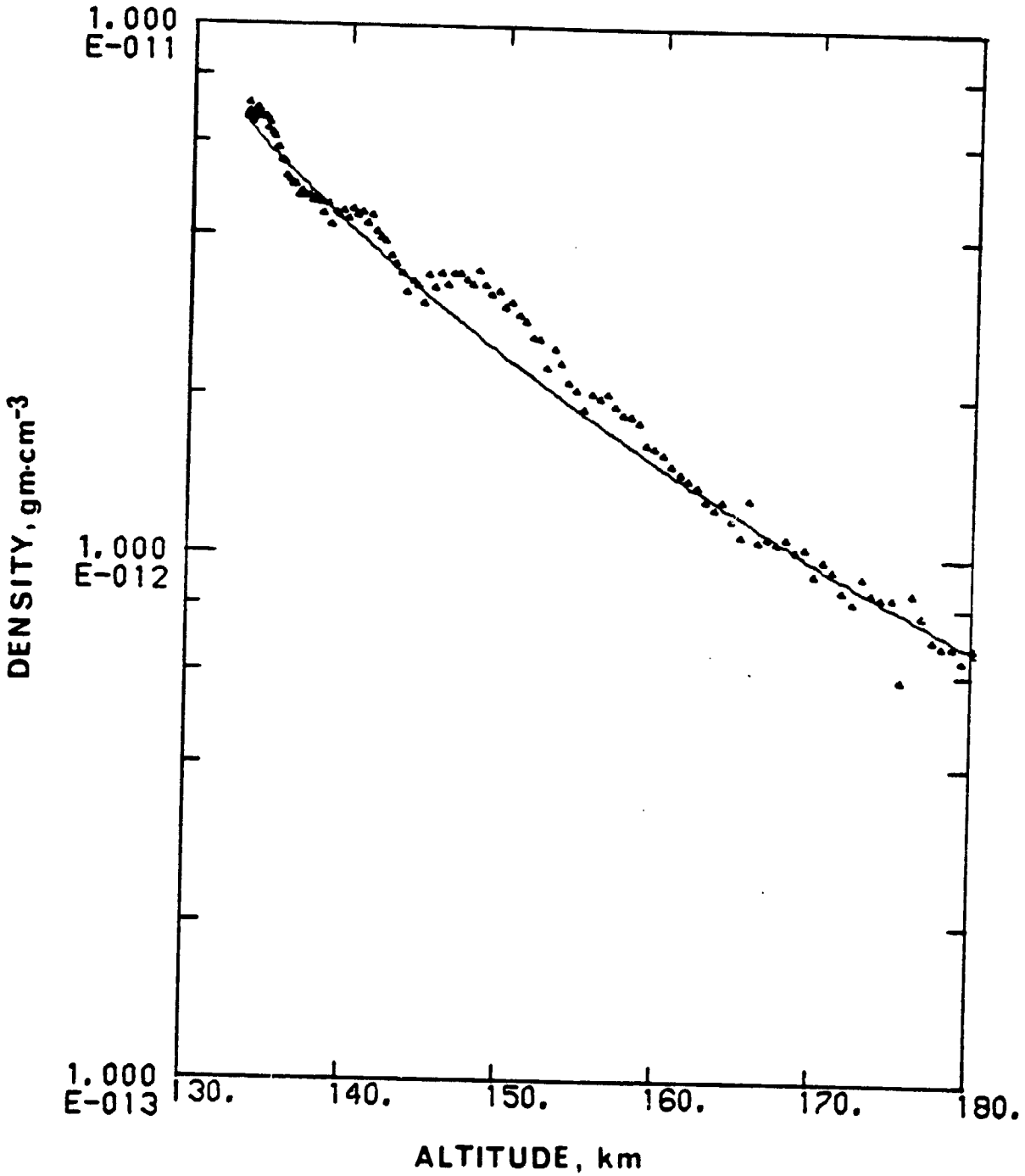
1.000
E-011
1.000
E-012
1.000
E-013
DENSITY, gm·cm⁻³
130.
140.
150.
160.
170.
180.
ALTITUDE, km

Fig. 2b

Space Sciences Laboratory
Report No. SSL-78(7738)-1
Revised July 1978

RAYLEIGH-TAYLOR AND WIND-DRIVEN INSTABILITIES OF THE NIGHTTIME EQUATORIAL IONOSPHERE

by

Y. T. Chiu and J. M. Straus
Space Sciences Laboratory

The Ivan A. Getting Laboratory
THE AEROSPACE CORPORATION
P. O. Box 92957
Los Angeles, California 90009

MAY 1978

Accepted for Publication in:
Journal of Geophysical Research

This research was supported by NASA under NASW - 3120
and by the Aerospace Corporation Programs for Research and Investigation.

ABSTRACT

We have made a thorough re-examination of the Rayleigh-Taylor instability in the nighttime equatorial ionosphere from ~ 100 km to the bottomside F-region. We have taken into account explicitly the following effects which have been ignored by other workers in various combinations: (1) The eastward drift of the ionosphere caused by the nighttime polarization electric field, (2) the eastward nighttime neutral wind, and (3) recombination in the F and E-regions. We found that, well below the bottomside F-region, the Rayleigh-Taylor mode can be unstable and is driven by an eastward neutral wind rather than by gravitational drift. Formation of ionospheric bubbles below the bottomside F-region is consistent with the observation of lower ionospheric ions in F-region ionospheric holes; furthermore, seasonal and shorter term variations in spread-F occurrence may be associated with variations in the neutral wind and polarization electric field.

I. INTRODUCTION

As the result of ionospheric observations with ground-based and satellite-borne instruments, major advances in the understanding of the nighttime equatorial spread-F phenomenon have been achieved in recent years. Observations of spread-F irregularities with ground-based radar (Woodman and La Hoz, 1976), as well as in situ measurements of ionospheric density with rockets (Kelley et al., 1976; Morse et al., 1977) and satellites (McClure et al., 1977; Brinton et al.,1975), have yielded a coherent picture in which nighttime equatorial spread-F irregularities are associated with regions of sharp ion density depletion (holes or bubbles). Such a coherent interpretation of data has in turn promulgated a revival (Balsley et al., 1972; Hudson and Kennel, 1975b) of the Rayleigh-Taylor instability theory of equatorial spread-F (Dungey, 1956). According to such a theoretical interpretation of the spread-F phenomenon, the primary spread-F bubbles develop at the bottomside F-region as Rayleigh-Taylor mode perturbations whose growth is intensified as the nighttime bottomside density gradient rises to the 300 km altitude region (Hudson and Kennel, 1975a and b). Subsequently, the bubble rises through the denser F-region (Scannapieco and Ossakow, 1976; Ott, 1978) creating steep density gradients at its edges, where small scale density irregularities are likely to be generated as drift waves and other higher frequency waves usually associated with steep plasma density gradients (Haerendal, unpublished manuscript, 1974; Hudson et al., 1973). Whether these secondary instabilities can account for the observed spectral characteristics of equatorial spread-F (Dyson et al., 1974; Woodman and Basu, 1978) is still an open question and is currently undergoing active investigation.

Although the general outline for the development of the primary Rayleigh-Taylor perturbation seems to be consistent with the dynamical aspects of the observations, there are still a number of puzzling chemical and occurrence aspects of the observations which are seemingly in conflict with this theory of Rayleigh-Taylor instability at the bottomside F-layer. These are:

1. The ion composition found inside the F-region bubbles (McClure et al., 1977; Brinton et al., 1975) suggests that the ion density depletion inside the bubble is mainly due to the depletion of the F-region ion O^+. Indeed, study of ion chemistry inside the bubble (Szuszczewicz, 1978) suggests that the ion composition is characteristic of the lower ionosphere, where NO^+ and O_2^+ are dominant. Thus, if the bubbles originate at the bottomside F-layer ($\gtrsim$ 250 km), some anomalous transport mechanism must be invoked to explain the predominance of lower ionospheric ($\lesssim$ 150 km) ions inside the bubbles.

2. Heavy ions, identified as Fe^+, have been found to be strongly but not exclusively associated with spread-F (Hanson and Sanatani, 1971; Hanson et al., 1972). Again, a lower ionospheric ion is found to be associated with an F-region phenomenon.

3. The basic criterion of Rayleigh-Taylor instability (Hudson and Kennel, 1975a and b; Scannapieco and Ossakow, 1976) is satisfied by nighttime bottomside conditions of the equatorial F-layer virtually all the time, yet the occurrence of spread-F is extremely variable not only on the time scale of days but also shows strong seasonal-longitudinal effects.

C 3

It may be argued that the chemical and occurrence characteristics do not have any direct impact upon the conditions for instability of purely dynamical origin, such as the Rayleigh-Taylor instability. This is true in a plasma for which the conditions of the neutral component play a minor role. In the ionosphere, however, the chemical and dynamical structures are largely determined by interaction with neutrals; therefore, the chemical composition and occurrence statistics of ionospheric bubbles are crucial clues to the location and processes of their formation. Consequently, we have made a thorough re-examination of the Rayleigh-Taylor instability for the equatorial nighttime ionosphere throughout the region from ~ 100 km to the bottomside F-region taking care to consider the importance of various effects governed by the electron and ion fluid equations. Among the effects taken into account explicitly are: (1) the eastward drift of the ionosphere due to the nighttime polarization electric field (Rishbeth, 1971), (2) interaction with the neutral wind, and (3) recombination by various chemical processes. We have found that the Rayleigh-Taylor mode can be driven unstable in the region well below the bottomside F-region (referred to hereafter as the "F1-region" although the F1-region does not exist at night) by an eastward neutral wind, rather than by the gravitational drift. We suggest that ionospheric bubbles originate considerably below the bottomside F-layer, and appear as deep density "bite-outs" when they propagate into the F-region.

In Section II, the details of the perturbation analysis of the Rayleigh-Taylor mode and the physical features of various important terms of the fluid equations will be discussed. Sections III and IV will be devoted to solutions of the dispersion relations indicating F-region and "F1-region" instabilities respectively. Physical implications of the suggested wind-driven "F1-region" instability will be given in Section IV.

II. PERTURBATION ANALYSIS

We consider the equatorial ionosphere in slab geometry with the magnetic field $\vec{B}$ directed along z (northward), gravitational acceleration $\vec{g}$ directed along -x (downward) and a neutral wind $\vec{v}_n$ directed along + y (eastward) or -y (westward). The co-ordinate system defined is similar to that of Hudson and Kennel (1975a). The fluid equations governing the motion of ionospheric component j(= i, or e) are those of mass, momentum and current conservation. This set of nine component equations governs the development of the set of nine dynamical variables: density (n_i , n_e), velocity ($\vec{v}_i$, $\vec{v}_e$) and electrostatic potential φ .

a. The ion and electron continuity equations are

$$\frac{\partial n_j}{\partial t} + \nabla \cdot (n_j \vec{v}_j) = q (x) N_n - \beta (x, N_n, n_j) ; j = i, e, \qquad (1)$$

where $q (x)$ is the rate of ionization production from the neutral gas of density N_n, and β is the rate of ionization loss due to recombination. In the F-region, we assume

$$\beta = \gamma N_n n_e, \qquad (2a)$$

where γ is a rate constant for the loss of O^+ by atom-ion interchange. At lower altitudes, we assume

$$\beta = \bar{\gamma} n_e n_i \qquad (2b)$$

where $\bar{\gamma}$ is a rate constant for the loss of molecular ions by dissociative recombination.

b. In the momentum equations, we assume that the ion and electron fluids move linearly (dropping advective derivative terms) under the influences of an electrostatic field $\vec{E} = -\nabla\varphi$, neutral wind $\vec{v}_n$ and gravity $\vec{g}$. We shall use the form of the momentum equations given by Alfvén and Fälthammar (1963, p. 176) which are commonly used in ionospheric physics.

$$\frac{\partial \vec{v}_j}{\partial t} = \frac{|e|}{m_j}(\delta_{je} - \delta_{ji})\left(\nabla\varphi + \frac{\vec{B}}{c} \times \vec{v}_j\right) - \frac{1}{m_j n_j} \nabla p_j - \nu_{jn}(\vec{v}_j - \vec{v}_n)$$

$$- \delta_{je}\,\nu_{ei}(\vec{v}_e - \vec{v}_i) + \vec{g}\,;\; j = i,\ e, \qquad (3)$$

where δ_{ab} is the Kronecker delta and ν_{ab} is the collision frequency between species a and b, assumed to be of the form (Chapman, 1956)

$$\nu_{ab} = K_{ab} N_b \,. \qquad (4)$$

K_{ab} is a constant and N_b is the basic state density of species b. The partial pressure p_j for component j must be treated with some care. We write

$$p_j = n_j T_j \,, \qquad (5)$$

where T_j is the thermal energy of species j. (Note: we have suppressed the Boltzmann constant in (5) so that the "temperature" T_j is equivalent to the thermal energy.) Since we shall not consider thermal exchange in the

perturbation analysis, we shall assume that T_j in (5) is strictly a function of x and is not perturbed at all. (We have also considered cases for which the thermal structure is perturbed adiabatically; however, the additional complication detracts from the simplicity of the analysis without introducing any significant changes in our conclusions.)

c. Current conservation is assumed to take the form

$$\nabla \cdot \vec{J} = \nabla \cdot \left[|e| \left(n_i \vec{v}_i - n_e \vec{v}_e \right) \right] = 0 , \tag{6}$$

where $\vec{J}$ is the total current. It should be noted that (6) is equivalent to quasi-neutrality, and so quasi-neutrality need not be redundantly invoked. To see this, we can combine Poisson's equation

$$\nabla \cdot \vec{D} = 4\pi e \left(n_i - n_e \right) \tag{7}$$

with Ampere's law

$$\nabla \times \vec{B} = \frac{4\pi e}{c} \left(n_i \vec{v}_i - n_e \vec{v}_e \right) + \frac{1}{c} \frac{\partial \vec{D}}{\partial t} \tag{8}$$

for any general displacement electric field $\vec{D}$ and magnetic field $\vec{B}$ to obtain

$$\frac{\partial}{\partial t} \left(n_i - n_e \right) + \nabla \cdot \left(n_i \vec{v}_i - n_e \vec{v}_e \right) = 0 , \tag{9}$$

which is the rigorous form of current conservation. The equivalence of (6) to quasi-neutrality is immediately obvious if one substitutes (6) into (9).

Furthermore, in our formulation, (9) is obeyed by our continuity equations, as the reader can easily demonstrate by subtracting the $j = e$ component of (1) from the $j = i$ component of (1).

As in all perturbation analysis, a properly prepared basic state is very important. This is especially true for the nighttime equatorial ionosphere because the basic state is known to have pressure gradients and associated drifts, as well as externally imposed drifts associated with the nighttime polarization electric field (Rishbeth, 1971) and neutral winds. Since some of these drifts may counteract the gravitational drift which drives the Rayleigh-Taylor instability, a careful accounting is required to give a proper assessment of the instability criterion for the nighttime equatorial ionosphere.

We assume the undisturbed basic state, characterized by the set of capitalized variables ($N = N_i = N_e$, $\vec{V}_i$, $\vec{V}_e$, Φ), to be time-independent and quasi-neutral. Strictly speaking, our basic state analysis should proceed with the solution for the above variables from (1), (3) and (6). However, since the basic physics of ion sources for the nighttime ionosphere is as yet not completely understood, we shall rely upon density observations to give $N(x)$ and upon the observed ionospheric drifts of the nighttime ionosphere to give Φ. A downward nighttime polarization field drives an eastward $\vec{E} \times \vec{B}$ drift (~ 100 m/sec), as well as a small downward electric drift, for the F-region (Rishbeth, 1975). In the E-region, an eastward electrojet field drives the observed eastward drift (~ 500 m/sec) of the E-region at night. Curiously, the E-region east-west drifts are correlated with the F-region vertical polarization drifts (Balsley and Woodman, 1969), implying the extension of the F-region polarization field down to the E-region. These effects can be roughly simulated by

$$\phi = E_0 x - \bar{E}_0 y \delta_{\alpha E} ; \alpha = E, F \quad . \tag{10}$$

Assuming a neutral wind $\vec{v}_n = v_n \hat{y}$, we obtain the basic state ion drifts from (3) with $\partial / \partial t = \partial / \partial z = 0$,

$$\vec{V}_i = \{ [\nu_{in} (- |e| E_0/m_i - T_i/m_i L - g + \Omega_i v_n) + \Omega_i (- |e| \bar{E}_0 \delta_{\alpha E}/m_i)] \hat{x}$$

$$+ [\Omega_i (|e| E_0/m_i + T_i/m_i L + g + \nu_{in}^2 v_n/\Omega_i) + \nu_{in} (- |e| \bar{E}_0 \delta_{\alpha E}/m_i)] \hat{y} \}$$

$$/ (\Omega_i^2 + \nu_{in}^2) \tag{11}$$

where $\Omega_j \equiv |e| B/m_j c$ is the gyrofrequency of the species j. The local density gradient length L is given by $L = 1/[d (\ell n N) /dx]$, where L is positive at the bottomside and negative at the topside. For the F-region, the limit $\nu_{in} << \Omega_i$ is appropriate and (11) is identical to that given by Hudson and Kennel (1975a, eq. 7a) except for the inclusion in (11) of the neutral wind induced drift. It should be noted that although the neutral wind induced horizontal drift is of order $(\nu_{in}/\Omega_i)^2$, the quantity $\nu_{in}^2 v_n$ with $| v_n | \sim 100$ m/sec may be comparable to the gravitational drift $g \Omega_i$ at or below about 200 km. Chaturvedi and Ossakow (1977, eq. 6) ignored all drifts except the gravitational drift; since the growth rate of the Rayleigh-Taylor instability will be shown to be related to the relative basic state drifts, these truncations, while realistic for the F-region, are not suitable for consideration of the lower regions.

The electron basic state drifts are obtained from (3) in terms of $\vec{V}_i$. We obtain to lowest order in $(\nu_{en}/\Omega_e) << 1$ and $(\nu_{ei}/\Omega_e) << 1$,

$$\vec{V}_e \simeq (- |e| \bar{E}_0 \delta_{aE}/m_i\Omega_i) \hat{x} + (|e| E_0/m_i\Omega_i - T_e/m_i\Omega_i L) \hat{y} \quad . \qquad (12)$$

Note that (12) is not to be applied to the electrojet region (~ 90 km) where the above approximations do not apply and $\bar{E}_0$ dominates $\vec{V}_e$. Hudson and Kennel (1975a, eq. 7b) ignored the electron gradient drift but retained the polarization field drift in the F-region. Chaturvedi and Ossakow (1977) ignored the electron basic state drift altogether. Examination of (11) and (12) shows that the polarization drift (~ 100 m/sec) is dominant and is the same for both ions and electrons, thus accounting for the general eastward drift of the ionosphere. The gradient, gravity and neutral wind induced drifts, though small, force the ions and electrons to move differentially and are largely responsible for the or damping of perturbations.

The first order perturbation equations for the system can be straightforwardly derived from (1), (3) and (6). We will consider the special case for which the perturbation variables ($\vec{v}_i'$, $\vec{v}_e'$, n_e'/N, n_i'/N) represent horizontal propagation only, while the basic state variables ($\vec{V}_i$, $\vec{V}_e$, ϕ , N) are functions of x only. Thus, defining the dimensionless perturbation density $\tilde{n}_j \equiv n'_j/N$

$$(\vec{v}_i, \vec{v}_e, \varphi, n_e, n_i) \equiv (\vec{V}_i, \vec{V}_e, \phi, N, N)_x + (\vec{v}_i', \vec{v}_e', \varphi', \tilde{n}_e, \tilde{n}_i)_{y,\,t} \, . \qquad (13)$$

To obtain the perturbation equations, we use the strict procedure of substituting (13) into (1), (3) and (6) and subtracting the basic state equations.

We obtain from (3) and (5),

$$\frac{\partial \vec{v}_j'}{\partial t} = \frac{|e|}{m_j} (\delta_{je} - \delta_{ji}) (\nabla\varphi' + \frac{\vec{B}}{c} \times \vec{v}_j') - \frac{T_j}{m_j N} \nabla \tilde{n}_j$$

$$- \nu_{jn} \vec{v}_j' - \delta_{je} \nu_{ei} (\vec{v}'_e - \vec{v}_i') , \quad j = i, e. \tag{14}$$

We note several features of (14) which appear to be different from the treatment of various authors. First, the gravity term $\vec{g}$ does not appear in (14) because the gravitational force is already taken into account in (10) and (12). Hudson and Kennel (1975a; eq. 8b) include a term $- g n_i'/\Omega_i N$ in the expression for v_{iy}' , which does not seem to be consistent with their equation (7a) where $\vec{V}_i$ already includes the gravitational drift. Second, the pressure gradient terms for the electronic version of (14) are of the same order of magnitude as the pressure gradient terms for ions. This is easily seen if one considers the solution of (14) for $\vec{v}'_e$; then the pressure gradient drifts are proportional to the factor $T_e/m_e\Omega_e$ which can be rewritten as $T_e/m_i\Omega_i$. Therefore, the pressure gradient perturbation terms cannot be ignored in the electron drifts even though $\Omega_e >> \nu_{ei}$, $\Omega_e >> \nu_{en}$ and $\Omega_e >> \omega$, the wave frequency, as is done in Hudson and Kennel (1975a; eqn. 10a and b). However, as we shall see in the next section, the effect of ignoring the electron pressure gradient perturbation terms results only in a small increase of the minimum unstable wavelength.

To proceed with our perturbation analysis, we will only consider the special case for which the perturbation variables are proportional to exp ($- i\omega t + iky$), independent of x and z. This is done, for example, by Hudson and Kennel (1975a) and is included in the discussion of Ossakow et al. (1978). We obtain for the continuity equation (1),

$$-i\omega\tilde{n}_j + v'_{jx}/L + ikv'_{jy} + ikV_{jy}\tilde{n}_j = -\delta_{\alpha F}\gamma N_n\tilde{n}_e - \delta_{\alpha E}\bar{\gamma}N(\tilde{n}_e+\tilde{n}_i), \quad (15)$$

where the subscript j (= i, e) denotes species and the subscript α (= E, F) denotes the appropriate regions of the ionosphere in the generic sense. The current conservation equation (6) yields

$$ik(v'_{iy} - v'_{ey}) + (v'_{ix} - v'_{ex})/L + ik(V_{iy}\tilde{n}_i - V_{ey}\tilde{n}_e) = 0, \quad (16)$$

which, together with (15), emphasizes the importance of keeping proper account of the differential drifts V_{iy} and V_{ey}.

The perturbation drifts $\vec{v}'_i$ and $\vec{v}'_e$ are obtained from (3), yielding

$$\vec{v}'_i = \{[(-i\omega + \nu_{in})(ik|e|\varphi'/m_i - ikT_i\tilde{n}_i/m_i)]\hat{y}$$

$$+ [\Omega_i(ik|e|\varphi'/m_i - ikT_i\tilde{n}_i/m_i)]\hat{x}\} / [\Omega_i^2 + (-i\omega + \nu_{in})^2]. \quad (17)$$

This experssion is valid for $kL >> \nu_{in}/\Omega_i$. The full expression for $\vec{v}'_e$ is quite complicated, but under the same approximation as (12), we obtain

$$\vec{v}'_e = \{(ik|e|\varphi' + ikT_e\tilde{n}_e)\hat{x}\} / \Omega_i m_i. \quad (18)$$

Substitution of $\vec{v}'_i$ and $\vec{v}'_e$, (17) and (18), into (15) and (16) gives three linear equations for $\tilde{n}_e$, $\tilde{n}_i$ and φ'. Setting the determinant of the coefficient matrix of these three equations to zero yields the dispersion relation for the Rayleigh-Taylor mode, which is a cubic equation in ω. However, we note

that for applications in either the F or the E-regions, the denominator $\left[\Omega_i^2 + (- i\omega + \nu_{in})^2 \right]$ in (17) is well approximated by $(\Omega_i^2 + \nu_{in}^2)$ because at least one of the inequalities $\Omega_i >> \omega$ and $\nu_{in} >> \omega$ is satisfied in these regions. Under such an approximation, one of the cubic solutions becomes $\omega = 0$ and we obtain a quadratic dispersion relation

$$\left[\omega - kV_{ey} - k (T_i + T_e) / m_i \Omega_i L + 2i\bar{\gamma} N \delta_{\alpha E} + i\gamma N_n \delta_{\alpha F} \right] \frac{\Omega_i}{D} \quad .$$

$$\left[kL (\omega + i\nu_{in}) - \nu_{in}^2 / \Omega_i \right] - k (T_i + T_e) \nu_{in}^2 / m_i \Omega_i LD$$

$$+ k \left[V_{iy} - V_{ey} - \Omega_i (T_i + T_e) / m_i DL \right] = 0 \quad , \qquad (19)$$

where $D = \Omega_i^2 + \nu_{in}^2$.

In the next two sections, specific cases of the dispersion relation (19) suitable for application to the F-region and to the "F1-region" will be discussed in detail. In particular, calculations of the rates of growth and damping will be given. These calculations are performed with numerical parameters summarized in the Appendix.

III. F-REGION

In the region above 200 km altitude, we have $\nu_{in} \leq 4$ sec^{-1} whereas $\Omega_i \simeq 125$ sec^{-1} in the equatorial ionosphere; therefore, the dispersion relation (24) simplifies to

$$\left[\omega - kV_{ey} - k (T_e + T_i) / m_i \Omega_i L + i \gamma N_n \right] \frac{kL}{\Omega_i} (\omega + i \nu_{in})$$

$$+ k \left[V_{iy} - V_{ey} - (T_i + T_e) / \Omega_i m_i L \right] = 0 , \qquad (20)$$

where

$$V_{iy} - V_{ey} \simeq g/\Omega_i + (T_i + T_e) / \Omega_i m_i L + \nu_n (\nu_{in} / \Omega_i)^2 . \qquad (21)$$

Hudson and Kennel (1975a; eq. 19b with $k_z = 0$) have derived a dispersion relation of similar structure but for $\gamma = \nu_n = 0$ and $V_{ey} = - T_e / \Omega_i m_i L$. The differences between (20) and their dispersion relation (19b) are traceable to approximations (and/or misprints) in their equations (8b), (8c), (10a), (10b), which correspond to our (17) and (18). The dispersion relation of Chaturvedi and Ossakow (1977) corresponds to setting $T_i = T_e = \nu_n = 0$. Equation (20) yields growth rates similar to those given by Hudson and Kennel (1975a) and Chaturvedi and Ossakow (1977).

In the low frequency limit $\omega << \nu_{in}$ (20) is linear in ω. The solution for the imaginary part of ω is

$$\text{Im } \omega \simeq - \gamma N_n + \frac{\Omega_i}{\nu_{in} L} \left[\frac{g}{\Omega_i} + \nu_n \left(\frac{\nu_{in}}{\Omega_i} \right)^2 \right] . \qquad (22)$$

Now, $g/\Omega_i \simeq 8$ cm/sec, and for reasonable neutral wind speeds ($v_n \lesssim 200$ m/sec), the neutral wind term may contribute to the instability below the 250 km region where $\nu_{in} \simeq 1\ sec^{-1}$. Nevertheless, the growth rate (22) does not depend on factors that are observed to be intermittent or geographically variable. Indeed, radar backscatter measurements indicate that unstable values of L are observed virtually all the time at night at equatorial sites.

Further, the observations of chemical composition in F-region density bite-outs, cited in the previous section, seem to have crucial impact upon the interpretation of the recombination rate in (22). In Fig. 1 we show the atom-ion interchange recombination rate (γN_n), which is responsible for O^+ recombination, and the dissociative recombination rate ($2\bar{\gamma}N_0$), which is responsible for O_2^+ and NO^+ recombination, assuming that the ionosphere is made up entirely of these molecular ions. The ion density profile N_0 used to compute $2\bar{\gamma}N_0$ is the average profile taken from Morse et al. (1977), where the bottomside F-region ledge is ≥ 270 km. It is seen that above ~ 200 km the dissociative recombination rate becomes orders of magnitude faster than atom-ion interchange rate. The natural consequence is that NO^+ and O_2^+ are absent above ~ 200 km; therefore, the use of γN_n in (22) is justified and the bottomside F-region ledge is unstable to the Rayleigh-Taylor mode. However, it is crucial to note that this result requires that the ion composition above ~ 200 km is mainly O^+; yet the observations found that O_2^+ and NO^+ are as abundant as, if not more abundant than, O^+ in the density bite-outs. If, on the other hand, there were some unknown mechanisms by which NO^+ and O_2^+ were brought to the region just below the ledge (~ 260 km) so that the general

composition at ~ 260 km is similar to what is found in density bite-outs then the proper recombination rate in (22) is not γN_n, but a combination of γN_n and $2\bar{\gamma} N_0$. Figure 2 shows an evaluation of the F-region collisional growth rate for various assumed concentrations of molecular ions. Thus, to explain the observations of chemical composition in F-region bite-outs, one requires some mechanism which would bring the molecular ions from below 200 km through the bottomside ledge, which consists mainly of O^+ ions, without recombination. We suggest that this is possible if occluded bubbles of molecular ions can be formed in the region below 150 km.

IV. "F1-REGION"

We now consider the stability criterion in the region below the F-layer bottomside ledge, usually at about 250-300 km altitude (Morse et al., 1977), and above ~ 100 km altitude where our drift considerations of Section II apply. For the lack of better terminology, we shall loosely call this region the "F1-region" although there is no F1-layer at night. The nighttime plasma density in this region is highly variable in time and irregular in profile (see for example Morse et al., 1977, Fig. 13); there is no steady density ledge as is seen in the bottomside F-region at night. However, it is suggested that the seasonal variation, intermittency and chemical composition of F-region bubbles may have their origin at the "F1-region".

To consider instability criteria in this region, we cannot use the approximation $\Omega_i >> \nu_{in}$; therefore, the dispersion relation (19) applies rather than the F-region approximation (20). On the other hand, since ν_{in} lies in the range $(10\text{-}10^3)$ $\sec^{-1}$ in this region, $\nu_{in} >> \omega$ clearly applies, and we obtain a linear "F1-region" dispersion relation from (19).

$$\left[\omega - kV_{ey} - k (T_i + T_e) / m_i \Omega_i L + 2i \bar{\gamma} N \right] \frac{\nu_{in}}{D} (ikL\Omega_i - \nu_{in})$$

$$- k (T_i + T_e) \nu_{in}^2 / m_i \Omega_i LD + k \left[V_{iy} - V_{ey} - \Omega_i (T_i + T_e) / m_i DL \right] = 0 , \qquad (23)$$

where

$$V_{iy}-V_{ey} \simeq \left\{ \nu_{in}^2 \left(v_n - |e| E_0/m_i\Omega_i \right) + \Omega_i \left(g + T_i/m_iL \right) \right\}/D + T_e/m_i\Omega_iL \ .$$

The imaginary part of ω gives the growth rate

$$\text{Im}\,\omega = -2\bar{\gamma}N + \left(k^2L\Omega_i/\nu_{in} \right) \left\{ \nu_{in}^2 \left[v_n - |e| E_0/m_i\Omega_i \right] + g\Omega_i \right\} / \left(\nu_{in}^2 + k^2L^2\Omega_i^2 \right) \ . \qquad (25)$$

From the analytic form of (25), a number of physically satisfying features concerning the possible growth of Rayleigh-Taylor instability in the "F1-region" may be noted.

a. In order for growth to take place, one requires $(\text{Im}\,\omega + 2\bar{\gamma}N) > 0$. Hence, an eastward neutral wind ($v_n > 0$) may drive the instability in this region. According to Hong and Lindzen (1976), the dominant neutral wind in this region is probably due to the solar semi-diurnal tide — the (2, 2) mode. The westerly (eastward) component of the (2, 2) mode maximizes in the range (50-100) m/sec during the period (1800-2100) hours in the altitude region (100-200) km. Since such tidal modes are expected to be affected by season, as well as local orographic and solar activity conditions, it is perhaps not a coincidence that equatorial spread-F also shows these dependences. This leads us to suggest that the bottomside F-region Rayleigh-Taylor instability may be triggered by bubbles formed from the wind-driven instability of the "F1-region".

b. The nighttime polarization electric field ($E_0 > 0$), which drives an eastward ionospheric drift, enters into the "F1-region" growth rate and is primarily stabilizing. Since the $\vec{E} \times \vec{B}$ drift is of the same order of magnitude as the neutral wind, the effect of the eastward $\vec{E} \times \vec{B}$ drift is to stabilize the wind-driven instability throughout most of the night. Conversely, this implies that instability is most likely to occur when the ionospheric drift changes from the daytime westward pattern to the nighttime eastward pattern, i.e. $E_0 \sim 0$. Systematic radar observations (Farley et al., 1970, Fig. 7) seem to be in agreement with this feature of our model. In particular, Balsley and Woodman (1969) reported a case in which spread-F occurs at 2000 hrs at precisely the time when the E-region drift switches from westward to eastward and when the F-region switches from upward to downward. In this section, all growth rates are calculated with $E_0 = 0$.

c. The growth rate is a function of the wave number $k \equiv 2\pi/\lambda$. This implies that there is a natural outer scale size for the primary ionospheric bubbles, as is illustrated in Figure 3. This is primarily due to the k-dependence of the denominator in (25).

Figure 3 shows the growth rate Im ω as function of ν_n and λ for an unstable density gradient situated at 140 km altitude where the plasma density is assumed to be 10^3 cm^{-3}. It should be noted that the growth times are about an hour and the outer scale sizes are approximatley equal to $\bar{L} \simeq 100$ km. Further, all wavelengths below the outer scale size have equal growth rates. Figure 4 shows the growth rate as function of the density gradient length L and plasma density N for bubbles of 1 km wavelength

driven by a 80 m/sec eastward neutral wind at 120 km altitude. It is seen that the "F1-region" instability can be driven for a large range of density gradient lengths provided the plasma density is sufficiently low. Figure 5 shows the growth (damping) rate of the combined Rayleigh-Taylor and neutral-wind-driven instabilities in the region (100-300) km for wavelength of 1 km and gradient length L = 10 km. The ionosphere above 190 km is assumed to be purely O^+ and that below 190 km is assumed to consist purely of NO^+ and O_2^+. Bubbles formed at an intermittent ledge below 150 km must move through a stable region before triggering the F-region instability.

V. PHYSICAL INTERPRETATION

Having shown the factors which may drive the Rayleigh-Taylor mode in the "F1-region", we now consider the consequences of a coherent theory of equatorial ionospheric bubbles initiated by the combined effects of neutral wind and polarization drifts in the "F1-region".

We suggest, with reference to Section IV, that plasma bubbles in the nighttime equatorial ionosphere originate as wind-driven waves at one of the highly variable density gradients below 200 km altitude, rather than at the seldom variable density gradient at the bottomside of the F-region. The growth of such bubbles requires an eastward neutral wind at the time when the east-west ionospheric drift, or equivalently, the upward-downward F-region drift (Balsley and Woodman, 1969) changes direction. The instability mechanism, discussed in Section IV, has a growth time of $\sim 10^2$ sec and has an outer scale size perpendicular to the magnetic field of ~ 100 km. Once an occluded bubble is formed, with internal densities typical of the "F1-region" (10^3-10^4 cm^{-3}) and consisting mainly of molecular ions NO^+, O_2^+ as well as possible high proportions of metallic Fe^+, it propagates non-linearly into the seldom-variable bottomside F-region and triggers the Rayleigh-Taylor mode there in much the same way suggested by Ossakow and Scannapieco (1976), Ott (1978) and Chaturvedi and Ossakow (1977). (The non-linear propagation of such bubbles into the F-region is beyond the scope of our consideration.) Our suggestion differs from theories of bottomside F-region instability

primarily on the location, chemical characterization and environmental condition of bubble formation. Thus, in our model, bubbles are noticed in the F-region because they show the most drastic contrast with the ambient F-region densities, not because they originate there.

In order to bring out more fully the physical interpretation of our model, we now consider observational aspects which may further clarify the physics of equatorial spread-F:

a. The observations of ion composition (McClure et al., 1977; Brinton et al., 1975; Hanson and Sanatani, 1971; Hanson et al., 1971) inside and outside the bubbles have been interpreted by us as indicators of the "F1-region" origin of ionospheric bubbles, especially since the bottomside F-region "instability" requires the bottomside F-region density gradient to be raised to higher altitudes. We are aware that, although ion composition measurments (McClure et al., 1977) probably favor a lower ionospheric origin of bubbles, the detailed consideration must include interaction with the ambient neutral atmosphere (Szuszczewicz, 1978). It is unfortunate that systematic observations of ion composition in the nighttime equatorial ionosphere in the region (100-300) km altitude are not yet available. We suggest that such measurements will be crucial in determining the physical origin of ionospheric spread-F bubbles.

b. Satellite observations of plasma density inside bubbles (McClure et al., 1977; Brinton et al., 1975) indicate values of $\sim (10^3\text{-}10^4)\ cm^{-3}$, whereas the single case of rocket observation (Costa and Kelley, 1978) gave a value of $\sim 10^5\ cm^{-3}$. These different values of density inside bubbles are

not necessarily inconsistent since the density inside is expected to evolve as the bubble propagates into the F-region. We interpret the extraordinarily low density values of satellite observations to be evidence that bubbles are occluded regions of plasma well below the bottomside F-region density gradient. Consequently, we suggest that a statistical study of bubble densities would throw some light upon their origin as well.

c. In our model of "F1-region" instability, the growth rate given in Fig. 2 shows a typical outer scale size of $\sim$ 100 km perpendicular to the magnetic field, since perturbations with wavelengths greater than $\sim$ 100 km are damped. This definite prediction of the theory can be tested if statistically significant in situ measurements such as those proposed for the EQUION satellite are available.

d. As has been pointed out in Section IV, the "F1-region" instability requires the eastward nighttime polarization drift to be minimized during the period ($\sim$ 1800 - 2000 LT) when the neutral wind is expected (Hong and Lindzen, 1976) to be maximum and eastward. Although this feature of our model seems to be consistent with observations of spread-F occurrence (Farley et al., 1970; Balsley and Woodman, 1969), we suggest that in situ measurement of the ionospheric electric field at the "F1-region" will be a crucial test of our theory.

e. Since the neutral wind is the primary factor in the condition for "F1-region" instability, the importance of correlating the magnitude and direction of the neutral wind in the equatorial lower thermosphere to occurrence probability of spread-F cannot be over-emphasized. In this regard, it is rather unfortunate that there is virtually no systematic observation of nighttime

neutral winds in the equatorial lower thermosphere; so much so that our model relies on the theoretical calculations of Hong and Lindzen (1976) to predict the diurnal occurrence behaviour of spread-F considered in the previous paragraphs. Further, if mesospheric neutral wind observations (Woodman, 1977) are indicators of lower thermospheric winds, then the intermittency of spread-F occurrence is readily understandable since mesospheric neutral winds are exceedingly variable.

If we accept the hypothesis that ionospheric bubbles are driven by lower thermospheric neutral winds, then the expected seasonal dependence of the neutral wind north and south of the meteorological equator will manifest itself as a seasonal-longitudinal dependence of equatorial spread-F. This could explain the difference between the seasonal occurrence patterns of spread-F at Jicamarca and at Guam-Kwajalein-India because these sites have substantially different geographic latitudes. Therefore, we suggest that a co-ordinated satellite and world-wide ground-based observation program would be a major step toward the basic understanding of the origins of spread-F.

VI. CONCLUSIONS

Based on a thorough re-examination of the Rayleigh-Taylor instability in the equatorial ionosphere, we show that the Rayleigh-Taylor mode can be driven unstable in the "F1-region" by neutral winds, thus introducing factors which are capable of accounting for the occurrence patterns of spread-F. We suggest that plasma bubbles, observed in the F-region because they show sharp contrast with the denser ambient ionosphere, are occluded patches of the "F1-region" with its characteristic chemical composition and density. We suggest a number of correlative studies which will not only test our model but also clarify the puzzling origin of the equatorial spread-F phenomenon.

APPENDIX

Numerical evaluations of the growthrate of the Rayleigh-Taylor instability were carried out using the following values of relevant parameters. The ion-neutral collision frequency $\nu_{in} = 2.6 \times 10^{-9} N_n/\sqrt{m}$, where N_n is the neutral number density, taken from the CIRA-1972 model for $T_\infty = 800\,K$, and m is the molecular weight of the gas in atomic mass units. The F-region recombination rate γ is due to ion-atom interchange; recombination of O^+ via N_2 and O_2 were considered, and thr rates for these two processes (at 600 K) were taken to be 5×10^{-13} cm^3/sec and 10^{-11} cm^3/sec, respectively (Banks and Kockarts, 1973, pp. 256-261). The "F1-region" recombination is due to dissociative recombination of molecular ions, for which we took $\bar{\gamma} = 5 \times 10^{-7}$ cm^3/sec (Banks and Kockarts, 1973, pp. 253-255).

ACKNOWLEDGMENTS

We appreciate communications and/or discussions with M. C. Kelley, F. A. Morse, C. J. Rice and M. Schulz. We appreciate the referee's help in catching a crucial error in the original manuscript. This work is conducted inpart under NASA contract NASW-3120 and in part under the Areospace Corporation Programs for Research and Investigation.

REFERENCES

Alfvén, H., and C.-G. Fälhammar, Cosmical Electrodynamics, p. 176. Clarendon, Oxford, 1963.

Balsley, B. B., and R. F. Woodman, On the Control of the F-region Drift Velocity by the E-region Electric Field: Experimental Evidence, J. Atm. Terr. Phys., 31, 865, 1969.

Balsley, B. B., G. Haerendel, and R. A. Greenwald, Equatorial Spread-F: Recent Observations and a New Interpretation, J. Geophys. Res., 77, 5625, 1972.

Banks, P. M., and G. Kockarts, Aeronomy (part B), Academic Press, N. Y., 1973.

Brinton, H. C., H. G. Mayr, and G. P. Newton, Ion Composition in the Nighttime Equatorial F-region: Implication for Chemistry and Dynamics, Trans. Am. Geophys. Union, 56, 1038, 1975.

Chapman, S., The Electrical Conductivity of the Ionosphere: A Review, Nuovo Cimento, 4, suppl. 4, 1385, 1956.

Chaturvedi, P. K., and S. L. Ossakow, Nonlinear Theory of the Collisional Rayleigh-Taylor Instability in Equatorial Spread-F, Geophys. Res. Letters, 4, 558, 1977.

Costa, E., and M. C. Kelley, On the Role of Steepened Structures and Drift Waves in Equatorial Spread-F, Geophys. Res. Letter, in press 1978.

Dungey, J. W., Convective Diffusion in the Equatorial F-region, J. Atm. Terr. Phys., 9, 304, 1956.

Dyson, P. L., J. P. McClure, and W. B. Hanson, In Situ Measurements of the Spectral Characteristics of F-region Ionospheric Irregularities, J. Geophys. Res., 79, 1497, 1974.

Farley, D. T., B. B. Balsley, R. F. Woodman and J. P. McClure, Equatorial Spread-F: Implications of VHF Radar Observations, J. Geophys. Res., 75, 7199, 1970.

Hanson, W. B., and S. Sanatani, Relationship Between Fe^+ ions and Equatorial Spread-F, J. Geophys. Res., 76, 7761, 1971.

Hanson, W. B., D. L. Sterling, and R. F. Woodman, Source and Identification of Heavy Ions in the Equatorial F-layer, J. Geophys. Res., 77, 5530, 1972.

Hong, S.-S., and R. S. Lindzen, Solar Semidiurnal Tide in the Thermosphere, J. Atm. Sci., 33, 135, 1976.

Hudson, M. K., and C. F. Kennel, The Electromagnetic Interchange Mode in a Partly-Ionized Collisional Plasma, J. Plasma Phys., 14, 121, 1975a.

Hudson, M. K., and C. F. Kennel, Linear Theory of Equatorial Spread-F, J. Geophys. Res., 30, 4581, 1975b.

Hudson, M. K., C. F. Kennel, and P. K. Kaw, A Two-Step Drift Mode Theory of Equatorial Spread-F, Trans. Am. Geophys. Union, 54, 1147, 1973.

Kelley, M. C., G. Haerendel, H. Kappler, A. Valenzuela, B. B. Balsley, D. A. Carter, W. L. Eaklund, C. W. Carlson, B. Hansler, and R. Torbert, Evidence for a Rayleigh-Taylor Type Instability and Upwelling of Depleted Density Regions During Equatorial Spread-F, Geophys. Res. Letters., 3, 448, 1976.

McClure, J. P., Diurnal Variation of Neutral and Charged Particle Temperatures in the Equatorial F-Region, J. Geophys. Res., 74, 279, 1969.

McClure, J. P., W. B. Hanson, and J. H. Hoffman, Plasma Bubbles and Irregularities in the Equatorial Ionosphere, J. Geophys. Res., 82, 2650, 1977.

Morse, F. A., B. C. Edgar, H. C. Koons, C. J. Rice, W. J. Heikkila, J. H. Hoffman, B. A. Tinsley, J. D. Winningham, A. B. Christensen, R. G. Woodman, J. Pomalaza, and N. R. Teixeira, Equion, an Equatorial Ionospheric Irregularity Experiment, J. Geophys. Res., 82, 578, 1977.

Ossakow, S. L., S. T. Zalesak, B. E. McDonald and P. K. Chaturvedi, Nonlinear Equatorial Spread-F: Dependence on Altitude of the F-peak and Bottomside Background Electron Density Gradient Scale Height, to appear in J. Geophys. Res., 1978.

Ott, E., Theory of Rayleigh-Taylor Bubbles in the Equatorial Ionosphere, J. Geophys. Res., 83, 2066, 1978.

Rishbeth, H., Polarization Fields Produced by Winds in the Equatorial F-Region, Planet. Space Sci., 19, 357, 1971.

Scannapieco, A. J., and S. L. Ossakow, Nonlinear Equatorial Spread-F, Geophys. Res. Letters, 3, 341, 1971.

Szuszczewicz, E. P., Ionospheric Holes and Equatorial Spread-F: Chemistry and Transport, J. Geophys. Res., in press, 1978.

Woodman, R. F., Mesospheric Winds at Equatorial Latitudes: A Review on Observational Aspects, J. Atm. Terr. Phys., 39, 941, 1977.

Woodman, R. F., and S. Basu, Comparison Between in situ Spectral Measurements of F-Region Irregularities and Backscatter Observations at 3 m, Geophys. Res. Letters, in press, 1978.

Woodman, R. F., and C. La Hoz, Radar Observations of F-Region Equatorial Irregularities, J. Geophys. Res., 81, 5447, 1976.

FIGURE CAPTIONS

Figure 1. The atom-ion interchange recombination rate for O^+ ions and the dissociative recombination rate for molecular ions are shown as functions of altitude. For purposes which are made clear in the text, the dissociative recombination rate shown assumes that the ionosphere consists entirely of molecular ions.

Figure 2. The collisional F-region growth rate as a function of L is shown for various assumed molecular ion concentrations N_m. Note that the F-region instability is quenched if $N_m \gtrsim 10^3/cm^3$.

Figure 3. Growth rate of the "F1-region" Rayleigh-Taylor instability at 140 km altitude with $E_0 = 0$. The background electron number density was taken to be $10^3/cm^3$. The growth rate, calculated using equation 30, is illustrated as a function of horizontal wavelength for several values of v_n and L. For $L \gtrsim 100$ km the validity of (30) must be taken with caution because $kL \sim \nu_{in}/\Omega_i$.

Figure 4. Growth rate of the "F1-region" Rayleigh-Taylor instability at 120 km altitude with $E_0 = 0$, $\lambda = 1$ km and $v_n = 80$ m/sec as a function of L for two values of the background electron density N.

Figure 5. The growth and damping rates of the combined Rayleigh-Taylor and wind-driven instabilities are shown as functions of altitude for wavelength of 1 km and for gradient length of 10 km. For this figure, the growth rates below 110 km are extrapolated values and must be taken with some caution because $kL \sim \nu_{in}/\Omega$ in this region.

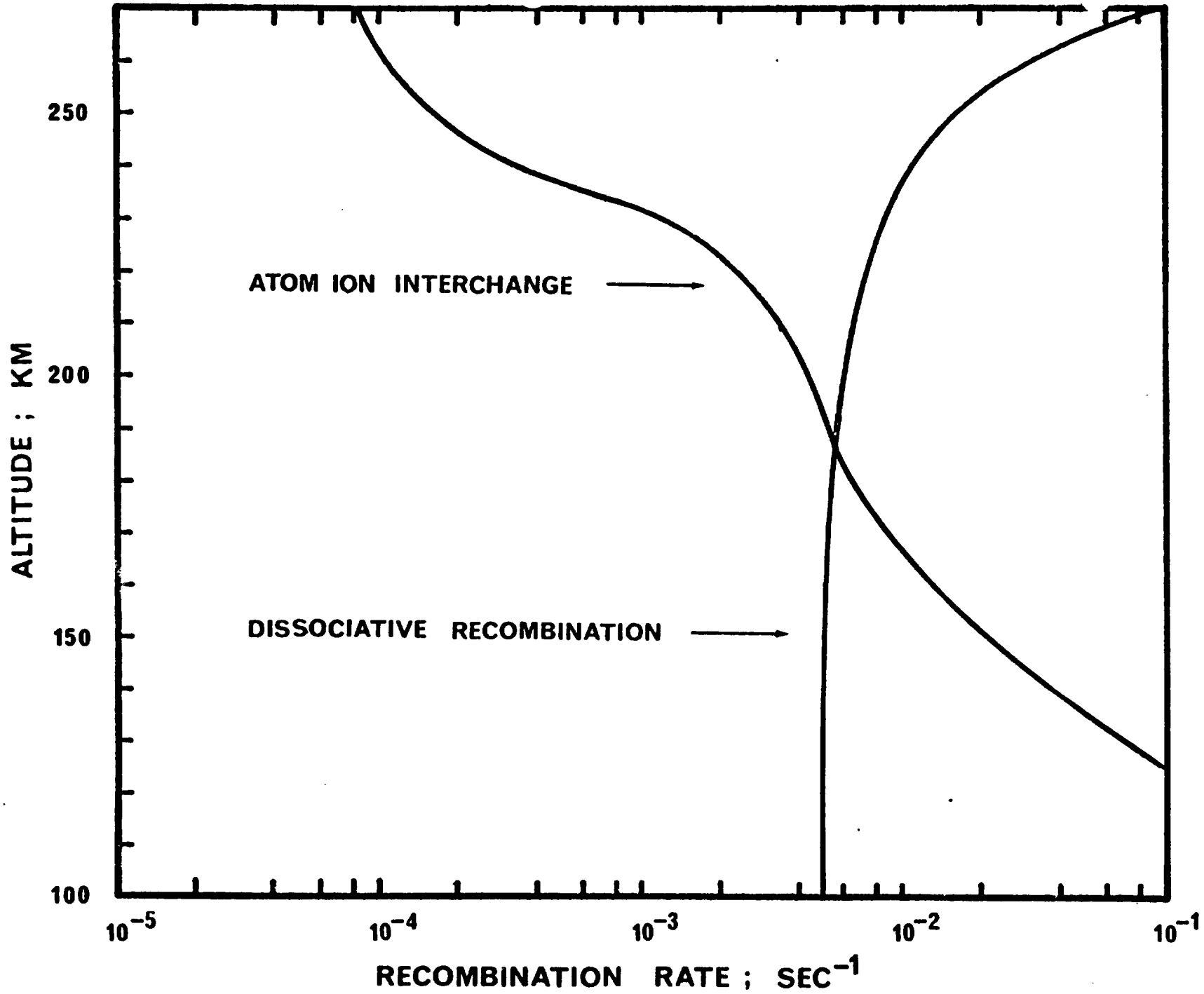
250
200
150
100
ALTITUDE ; KM
ATOM ION INTERCHANGE
DISSOCIATIVE RECOMBINATION
10^{-5}
10^{-4}
10^{-3}
10^{-2}
10^{-1}
RECOMBINATION RATE ; SEC^{-1}

F18
1

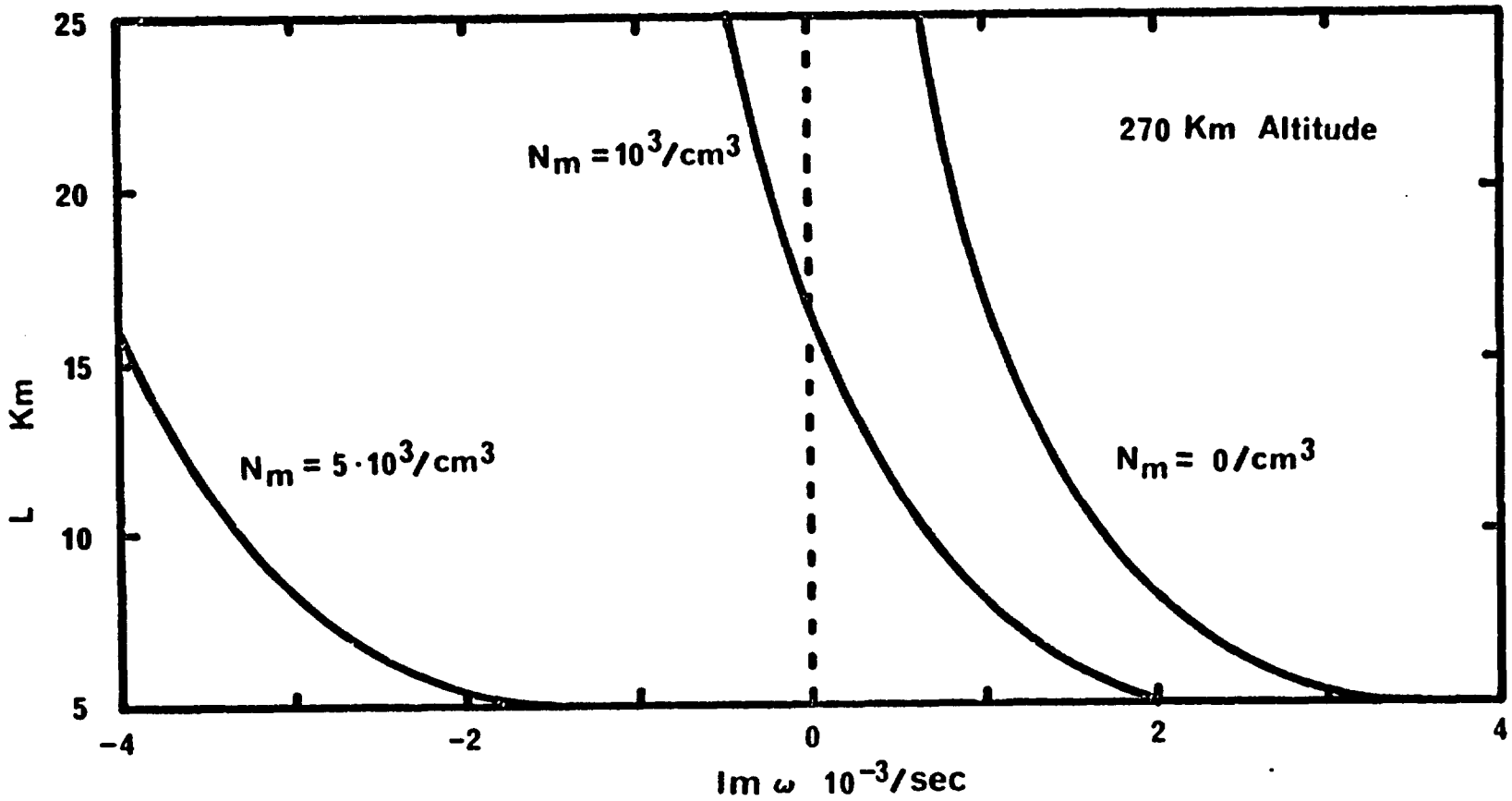
25
20
15
10
5
L Km
270 Km Altitude
$N_m = 10^3/cm^3$
$N_m = 5 \cdot 10^3/cm^3$
$N_m = 0/cm^3$
-4
-2
0
2
4
Im ω 10^{-3}/sec

Fig 2

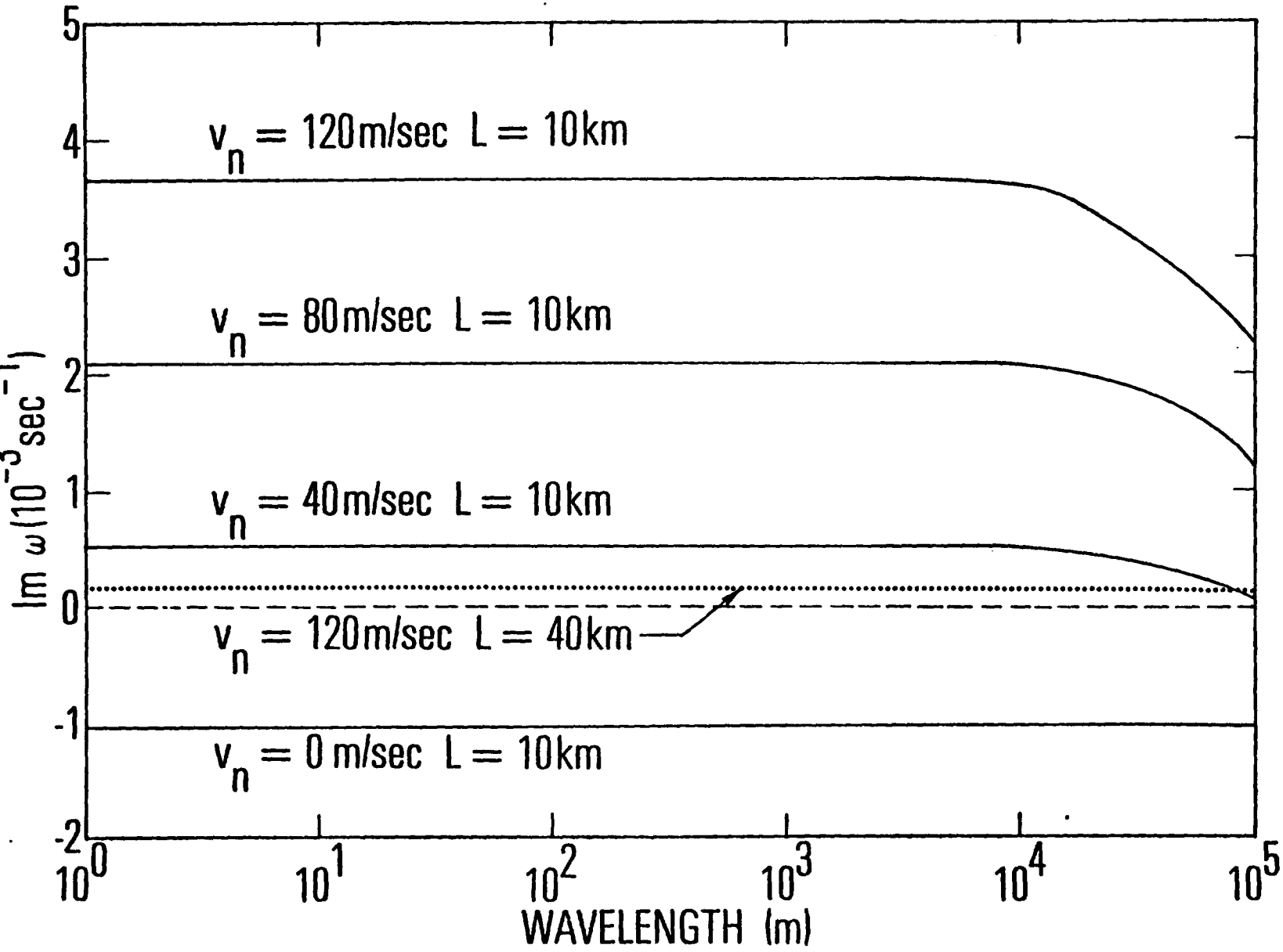
5
4
3
2
1
0
-1
-2
v_n = 120m/sec L = 10km
v_n = 80m/sec L = 10km
v_n = 40m/sec L = 10km
v_n = 120m/sec L = 40km
v_n = 0 m/sec L = 10km
Im $\omega(10^{-3}\text{sec}^{-1})$
10^0
10^1
10^2
10^3
10^4
10^5
WAVELENGTH (m)

Fig 3

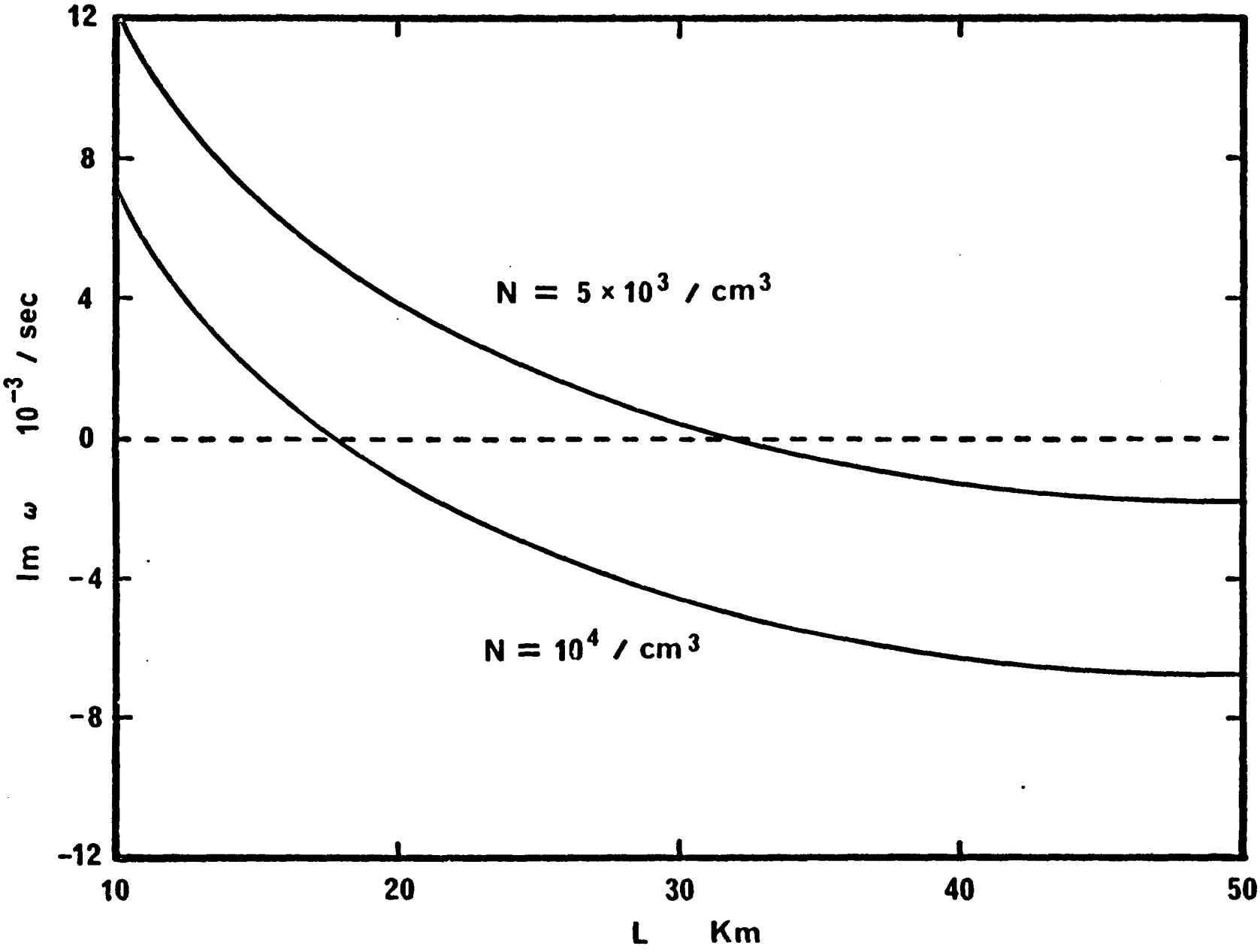

Fig 4

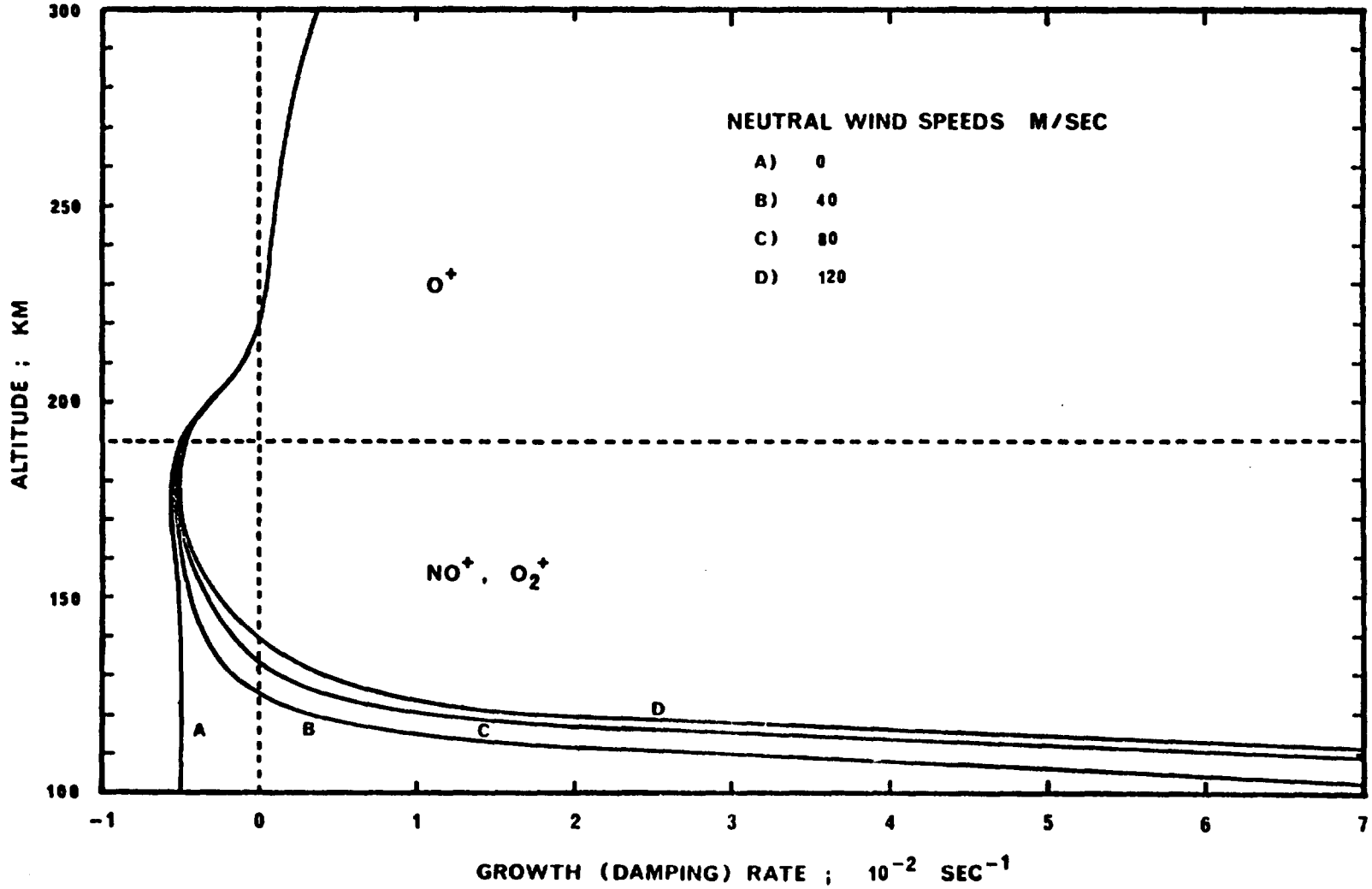
NEUTRAL WIND SPEEDS M/SEC
A) 0
B) 40
C) 80
D) 120
O+
NO+, O2+
A
B
C
D
ALTITUDE ; KM
300
250
200
150
100
-1
0
1
2
3
4
5
6
7
GROWTH (DAMPING) RATE ; 10-2 SEC-1

F18